BABAK POURBOHLOUL

CONTROL AND TRACKING OF CHAOS IN HAMILTONIAN SYSTEMS

Thèse
présentée
à la Faculté des études supérieures
de l'Université Laval
pour l'obtention
du grade de Philosophiae Doctor (Ph.D.)

Département de physique
FACULTÉ DES SCIENCES ET DE GÉNIE
UNIVERSITÉ LAVAL
QUÉBEC

MAI 1999

Contents

List of Figures

List of Tables

Introduction

Au début, tout n'était que CHAOS,
rien que du vide, matière informe
et espace infini.
HESIODE
(Théogonie, 8^{th} century a.C.)

Hamiltonian dynamics is a huge subject with a long history. Although nonlinear dynamics is an interdisciplinary subject today, it was originally a branch of physics. The subject began in the middle of the XVII*th* century, when Newton invented differential equations, discovered his laws of motion and universal gravitation, and combined them to explain Kepler's laws of planetary motion. The success and power of Newton's laws led to a great optimism about our ability to predict the behaviour of mechanical objects and, as a consequence, led to the huge growth in science that we see today. In addition it was accompanied by a deterministic view of nature which is best exemplified in the writings of Laplace[1951]:

> *Given for one instant an intelligence which could comprehend all the forces by which nature is animated and the respective situation of the beings who compose it - an intelligence sufficiently vast to submit these data to analysis - it would embrace in the same formula the movements of the greatest bodies of the universe and those of the lightest atom; for it, nothing would be uncertain and the future, as the past, would be present before its eyes.*

This deterministic view of nature was completely natural given the success of Newton's mechanics and persists almost up to the present day. Specifically, Newton solved the two body problem - the problem of calculating the motion of the earth around the sun given the inverse square law of gravitatinal attraction between them. In a sense Newton was fortunate because the solar system has an amazingly regular behaviour considering its complexity and one can predict its short-time behaviour with fairly

good accuracy [Gutzwiller,1998]. Newton's equations are, indeed, the correct starting point of mechanics, but in general they allow us to determine the long time behaviour of *integrable* mechanical systems, few of which can be found in nature (including the two-body problem). Subsequent generations of mathematicians and physicists tried to extend Newton's analytical methods to the three-body problem(e.g., sun, earth and moon) using *perturbation theory* [Moser,1978]. The problem was so important that it was the subject of a prize question posed by King Oscar II of Sweden in 1885:

> *For an arbitrary system of mass points which attract each other according to Newton's laws, assuming that no two points ever collide, give the coordinates of the individual points for all time as the sum of a unifomly convergent series whose terms are made up of known functions.*

Poincaré won the prize by showing that such series could be expected to diverge and because of this divergence it appears to be impossible to make long-time predictions concerning the evolution of mechanical systems. He developed a powerful geometric approach to analyzing dynamical systems. It was the genius of Poincaré which supplied us with many of our present methods for exploring the unexpected wonder of even simple dynamical systems. In particular, he emphasized the importance of obtaining a global, qualitative understanding of the character of a system's dynamics.

In the first half of this century, Poincaré's geometric methods were being extended to yield a much deeper understanding of classical mechanics, thanks to the work of Birkhoff, Kolmogorov, Arnol'd and Moser. In the 1950s an entirely new tool of analysis came into the scene- the digital computer. The computer allowed one to experiment with equations in a way that was impossible before, and thereby to develop some intuition about nonlinear systems. Such experiments led to Lorenz's discovery [Lorenz, 1969] of *chaos* - the aperiodic behaviour of a deterministic system that depends sensitively on the initial conditions, thereby rendering long-time prediction impossible and making the system inherently unpredictable [Ott, 1993; Ott, Sauer and Yorke, 1994].

The period following 1960 has been particularly rich in new ideas and in the growing application of these ideas to a wide variety of disciplines, such as physics, chemistry, biology, neurology, astronomy, geophysics, meteorology and economics. In addition many new perspectives have been introduced from mathematics, along with the innovative and potentially basic contributions of computer science.

In the present thesis, we would like to study the behaviour of a class of dynamical systems, namely *Hamiltonian systems*. In doing so, we review the theory of the classical Hamiltonian systems in **chapter 1**. We shall introduce a number of Hamiltonian systems including the *Diamagnetic Kepler Problem* which is of our main interest.

One of the fundamental aspects of chaos is that many different possible motions

are simultaneously present in the system. A particular manifestation of this is the fact that there are typically an infinite number of unstable periodic orbits that co-exist with the chaotic motion [Berry, 1978]. By a periodic orbit, we mean an orbit that repeats itself after some time. If the system were precisely on an unstable periodic orbit, it would remain on that orbit forever. These orbits are unstable in the sense that the smallest deviation from the periodic orbit (e.g. due to noise) or to imprecise initial conditions grows exponentially rapidly in time, and the system orbit quickly moves away from the periodic orbit. Thus, although these periodic orbits are present, they are not typically observed. Rather, what one sees is a chaotic trajectory which bounces around in an erratic, seemingly random fashion. Very rarely, the chaotic trajectory may, by chance, closely approach a particular unstable periodic orbit, in which case the chaotic trajectory would approximately follow the periodic cycle for a few periods, but it would then rapidly move away because of the instability of the periodic orbit. In **chapter 2** we shall introduce the algorithms, capable of detecting the unstable periodic orbits in a chaotic system, the orbits which are of extreme importance for understanding the system under study.

The notion of chaos in nonlinear dynamical systems, i.e. extreme sensitivity to the initial conditions, seems to be a cause of despair, because it effectively renders the long-time prediction of these systems impossible. For instance, in a computer simulation a small perturbation may be introduced by numerical round-off, while, in the real world, systems are invariably perturbed by noise. Thus, if a system is chaotic, these small perturbations quickly (indeed, exponentially) grow until they completely change the behaviour of the system. Paradoxically, the cause of the despair is also the reason for hope. Because if a system is so sensitive to small changes, could not small changes be used to control it? This realization led Ott, Grebogi and Yorke [1990] to propose an ingenious and versatile method (now called the *OGY method*) for the control of chaos. We shall discuss this issue in **chapter 3**, where we will apply this method to Hamiltonian systems. We will show for the first time that the successful control can be applied to the chaotic motion of an electron in the presence of a magnetic field as an application of the OGY method in atomic physics.

Control of chaos has recently generated a great deal of research activity in many areas of science. Using model-independent approaches, control of chaos is usually implemented about a fixed parameter. However, one usually needs to examine unstable solutions over a range of parameters, with this range possibly large. If one attempts to use the same control settings over a range of parameter values, control will in general fail. Hence one needs to *track* the unstable states as a function of parameters, while retaining control. We shall discuss this issue in **chapter 4**, where we introduce a new method for tracking the unstable periodic orbits.

Chapter 1

Chaos in Area-Preserving Systems

The classification of CHAOS, nothing less is here essayed.
Hermann Melville
(Moby Dick, chapter 32)

In this chapter we present the elements of chaos theory in Hamiltonian systems which are needed for the rest of the discussion. Moreover we present the models that are used throughout this work. Particular attention is paid to the Diamagnetic Kepler Problem (DKP).

1.1 Survey of Hamiltonian Dynamics

Many aspects of the natural world can be described by differential equations or by variational principles. The simplest differential equations and variational problems can be solved explicitly in terms of standard functions. Even if explicit solutions are lacking, one might feel that having written down the equations governing a system, one has in some sense solved it. One can make further progress by the use of perturbation theory [Goldstein, 1980]. Supposing the motion to be close to that of a known system, one analyses the deviations up to a given order in the size of the deviations or the size of the parameters of the system. In particular, this leads to lowest order to the theory

of the linear stability of the equilibria which is easy to develop and is very powerful. Although perturbation theory often allows one to make reasonable predictions, it is often misleading in that it gives little insight what really happens for moderate or large perturbation sizes, and sometimes even fails for infinitesimal perturbations [Chirikov, 1960].

Hamiltonian mechanics combines the ideas of differential equations and variational principles. As Hamilton realised, many of the systems in mechanics and optics can be put into the special form :

$$\frac{dp_i}{dt} = -\frac{\partial H(\mathbf{p},\mathbf{q},t)}{\partial q_i} \qquad \frac{dq_i}{dt} = \frac{\partial H(\mathbf{p},\mathbf{q},t)}{\partial p_i} \qquad i = 1, ..., n \tag{1.1}$$

or an associated variational form

$$\delta \int \mathbf{p} \cdot d\mathbf{q} - H dt = 0 \tag{1.2}$$

where the p's are the momenta, the q's are the configuration coordinates and H is the scalar Hamiltonian function. The state of the system is given by the canonical coordinates ($\mathbf{p}$,$\mathbf{q}$) in phase space. H is conserved if it does not depend explicitly on time, and in such case the system is then said to be *autonomous*. The search for other conserved quantities led to a new approach for solving Hamiltonian systems [Tabor, 1989]. Instead of finding formulae for the coordinates as a function of time one searches for integrals of the motion. If one can find n integrals $I_i(\mathbf{p},\mathbf{q})$ which are in involution, i.e.

$$\sum_k \frac{\partial I_i}{\partial q_k}\frac{\partial I_j}{\partial p_k} - \frac{\partial I_i}{\partial p_k}\frac{\partial I_j}{\partial q_k} = 0 \qquad i \neq j \tag{1.3}$$

and *independent* (meaning that the vectors ∇I_i are independent (in the sense defined in linear algebra) "almost everywhere"), then associated variables ϕ_i can be derived which evolve linearly in time

$$\frac{d\phi_i}{dt} = \frac{\partial H(I)}{\partial I_i}. \tag{1.4}$$

Such a system is integrable in the sense of Liouville [MacKay and Meiss, 1987]. If the sets $\{I_i = constant\}$ are bounded, the Poincaré - Hopf theorem (sometimes called the

"hairy ball theorem") tells us that phase space can be mapped to an n dimensional torus [Jackson, 1989]. Choosing irreducible cycles, γ_i, on the tori, one can define a preferred set of integrals

$$J_i = \int_{\gamma_i} \mathbf{p} \cdot d\mathbf{q} \tag{1.5}$$

called *action variables*, for which the corresponding ϕ_i are *angle variables* (mod 1) on the torus. The quantities

$$\omega_i(\mathbf{J}) = \frac{\partial H(\mathbf{J})}{\partial J_i} \tag{1.6}$$

are called the *frequencies* of the torus.

Another feature of Hamiltonian systems noticed by Liouville is the preservation of phase space volume $\int dp^n dq^n$. A more general result is that Poincaré 's integral

$$\int \mathbf{p} \cdot d\mathbf{q} = \int \sum p_i dq_i \tag{1.7}$$

is conserved around any loop following the flow. This is the property that really distinguishes Hamiltonian differential equations from general ones [Tabor, 1989]. The infinitesimal version of Poincaré integral invariant is the *symplectic form*:

$$\tau\{(\delta\mathbf{p}, \delta\mathbf{q}), (\delta\mathbf{p}\prime, \delta\mathbf{q}\prime)\} = \delta\mathbf{p} \cdot \delta\mathbf{q}\prime - \delta\mathbf{p}\prime \cdot \delta\mathbf{q} \tag{1.8}$$

which assigns an area to pairs of tangent vectors, and which is conserved along the flow [Ott, 1993]. This conserved symplectic structure is fundamental to Hamiltonian systems. The concept of symplectic structure also allows one to generalize the definition of Hamiltonian systems, and leads to covariance under general coordinate transformations (not just canonical ones).

The simplicity of integrable systems might give the impression that Hamiltonian mechanics is quite easy. However, it is not easy to integrate Hamiltonian systems. The major problem with the notion of integrability is that most systems are *not* integrable. This was first appreciated when Poincaré proved that the circular restricted three-body

problem has no integral analytic in the mass ratio [Gutzwiller, 1990]. The perturbation expansions which gave excellent predictions of the motion of the planets do not converge. The basic reason is that among the invariant tori of integrable systems there is a dense subset on which the frequencies ω are commensurate, i.e. $\mathbf{m}\cdot\omega = 0$ for some non-zero integer vector $\mathbf{m}$; however, most systems have no commensurate tori, because they can be destroyed by an arbitrarily small perturbation.

The key techniques used by Poincaré were geometrical analysis and the idea of surface of section. If Σ is the codimension one surface (i.e. of dimension one less than that of the phase space) transverse to a flow, then the sequence $\mathbf{x}_j$ of successive intersections of an orbit with Σ provides a lot of information about that orbit. The flow induces a mapping of Σ to itself. For Hamiltonian systems, since H is conserved, Σ decomposes into a one parameter family of codimension two surfaces parametrised by the value of energy, a reduction of two dimensions. Furthermore, the return map is symplectic, meaning that it preserves a symplectic form [Tabor, 1989]. So one might as well establish general results for symplectic maps rather than Hamiltonian flows.

For integrable systems, nearby orbits separate linearly in time; however, dynamical systems can have exponentially separating orbits. Let $\delta\mathbf{z}_0$ be a tangent vector at the phase space point $\mathbf{z}_0$ and $\delta\mathbf{z}(t)$ be the evolved vector following the orbit of $\mathbf{z}(t)$. The average rate of the exponentiation of $\delta\mathbf{z}(t)$ is the Lyapunov exponent [Ott, Sauer and Yorke, 1994]:

$$\lambda(\mathbf{z}, \delta\mathbf{z}) = \lim_{t\to\infty} \frac{1}{t} \log \frac{\|\delta\mathbf{z}(t)\|}{\|\delta\mathbf{z}(0)\|}. \tag{1.9}$$

If λ is nonzero, one always has limited precision of observation, the predictions that one can make will be valid for a time only logarithmic in the precision. Examples of complexity of behaviour of typical Hamiltonian systems will be provided later in this chapter.

Despite this complexity, one can get a fair amount of information about the system

by focusing on the simplest aspects of Hamiltonian dynamics: the behaviour of the system near equilibria. An equilibrium of a set of ordinary differential equations d$\mathbf{x}$/dt $= \mathbf{F(x)}$ is a point $\mathbf{x_0}$ where $\mathbf{F}(\mathbf{x_0}) = 0$. From Hamilton's equations, the equilibria are precisely the critical points of the Hamiltonian H, i.e., points $\mathbf{x}$ where the gradient of H is zero. The first step in the general stability analysis is to study the stability of the equilibrium under the linearised equations. It can be shown that as a result of the symplectic structure, the eigenvalues always come in pairs $\pm\sigma$ [MacKay, 1986]. In particular, for linear stability, all the eigenvalues must lie on the imaginary axis and the lost of stability occurs through "collision of the eigenvalues".

Periodic orbits are the next most simple orbits after equilibria. The idea that everything returns eventually to its point of departure has a strong hold on humanity, but the importance of periodic orbits for modern physics has a quite different origin and was first recognized by Poincaré . He found that periodic orbits, i.e., the solutions of the equations of motion that return to their initial conditions, are densely distributed among all possible classical trajectories, and he suggested that the study of periodic orbits would provide the clue to the overall behaviour of any mechanical system [Gutzwiller, 1990]. Poincaré 's suggestion seemed, at first, to be valuable only as a general approach for a better understanding of some difficult problems in classical mechanics. Since the advent of quantum mechanics, however, the periodic orbits have turned out to be of special significance in the transition from classical to quantum regime. This idea is the essence of the Gutzwiller's trace fomula [Gutzwiller, 1990] which relies on the knowledge of the classical periodic orbits in order to understand the quantal spectrum.

Another class of orbits are *quasiperiodic orbits*. An orbit is quasiperiodic when its frequencies do not commensurate. In this case the trajectopry fills up the torus. For integrable systems all orbits lie on invariant tori determined by the constants of motion. The KAM theorem (named after Kolmogorov, Arnol'd and Moser) states

that those invariant tori with sufficiently incommensurate frequencies still persist for sufficiently small perturbations of an integrable system [Arnol'd, 1963]. However when the perturbation from integrability is large enough, each invariant torus is typically destroyed. Chirikov [1960] discovered a practical method for estimating a perturbation amplitude required for the destruction of an invariant surface, the *overlap of resonances*. Roughly speaking, the reason an invariant torus is destroyed is that when a torus with commensurate frequency is perturbed, it becomes a "chain of islands", defined by stable and unstable manifolds of resonant orbits. The width of this chain grows with the perturbation amplitude. Incommensurate tori between two such island chains are squeezed into a smaller space, and can no longer exist when the stable manifold from one island crosses the unstable manifold from the other. Thus one can estimate the amplitude for destruction of an invariant torus by perturbatively calculating the island sizes, and their overlap threshold [Greene, 1979].

Typical Hamiltonian systems have only finitely many equilibria, but they may have infinitely many periodic orbits. By considering return maps of the surface of section, it suffices to ask for the existence of periodic orbits for symplectic maps. Therefore in order to study the behaviour of a Hamiltonian dynamical system, it is important to devise a method to identify the location of periodic orbits via its corresponding symplectic mapping. This task will be done in chapter 2, while for now we will study the area-preserving maps that will be used throughout the rest of the present work.

1.2 Area Preserving Maps

Area preserving maps provide the simplest and most accurate means to visualize and quantify the behaviour of conservative systems with two degrees of freedom. When an integrable map becomes non-integrable by a small perturbation, resonance can occur and degenerate lines of fixed points in the integrable map are changed to finite chains

of alternating hyperbolic and elliptic fixed points surrounded by nonlinear resonance zones. As the strength of the perturbation is increased, the resonance zones grow, can overlap and form a chaotic sea. Chaos appears first in the neighbourhood of hyperbolic fixed points where an incredibly complex dynamics develops. For small variation of the map parameters, resonance zones are separated from one another by *KAM tori*. In area preserving maps on a plane, as in systems with two degrees of freedom, these KAM tori serve to isolate one region of the phase space from another [Berry, 1978]. KAM tori are destroyed by nonlinear resonances. Each KAM torus is labeled by a winding number (see below). Resonance zones form island chains, and each island chain contains a sequence of hyperbolic and elliptic fixed points which have a rational winding number. Greene [1979] has shown that each KAM torus can be approximated by a unique sequence of island chains whose winding numbers are determined by the continued fraction representing the irrational winding number of the KAM torus. Those island chains which approximate a given KAM torus play a dominant role in its destruction. A KAM torus is destroyed suddenly, as the mapping parameter increases, and form a *cantorus* [Meiss, 1992]. A cantorus can still partially block the flow of trajectories in phase space. As the mapping parameter is increased further, the cantorus gradually disappears and trajectories are free to diffuse more or less at random in the chaotic sea [MacKay, Meiss and Percival, 1984]. These properties can be exemplified in the standard map described below.

1.2.1 The Standard Map

As an example, we consider the standard map which results from several physical experiments such as: the motion of an elastic ball bouncing vertically on a plate of velocity $v_p = Vsin(\omega t)$, the relativistic motion of an electron in a microtron accelerator, the Frenkel - Kontorva model of solid state physics which describes the spatial structure of a linear chain of atoms deposited on a spatially periodic force field (a lattice), and

many other situations involving the interplay between translational and some periodic motion, as in magnetic bottles and toroidal magnetic systems (e.g., a stellarator, used in plasma fusion experiments). The common representation of the standard map is [Jackson, 1989]

$$\begin{pmatrix} q_{n+1} \\ \\ p_{n+1} \end{pmatrix} = \begin{pmatrix} q_n + p_{n+1} \qquad (mod 1) \\ \\ p_n - \frac{K}{2\pi}\sin(2\pi q_n) \end{pmatrix} \tag{1.10}$$

Here we are interested particularly in the periodic orbits of the mapping given in equation (1.10). A periodic orbit is a set of finite points that transform among themselves under the iteration of the mapping, and all of which are accessible from any one of the points. We will say that the orbit is of length Q if the orbit closes after Q iterations. When $K = 0$, the standard map is integrable. As K is increased, chaotic regions occupy increasingly large areas, and the original KAM tori of the integrable system are successively destroyed. It is convenient to associate a winding number with the periodic orbits and KAM surfaces of interest [Greene, 1979]. In the integrable limit, $K = 0$, this winding number is $r = 1/p$. For rational $p = P/Q$ with P and Q relative primes, Q is the length of the orbit before it closes, and

$$P \equiv \sum_{n=1}^{Q} p_n = \sum_{n=1}^{Q} (q_n - q_{n-1}) = q_Q - q_0 \tag{1.11}$$

where p_n and q_n are the coordinates of the point of the periodic orbit. Then, from equation (1.10), P and Q, and thus $r \equiv Q/P$ are well-defined and independent of K, and can be used to identify a given periodic orbit. The behaviour of periodic orbits and KAM surfaces are not continuous functions of the winding number, r. It is observed that, in the neighbourhood of a given periodic orbit, KAM surfaces and other longer periodic orbits are strongly perturbed. In perturbation theory, this effect appears to be the *problem of small denominators* [Arnol'd, 1963], where the denominator is the measure of the distance between a perturbing periodic orbit and the region of interest. A good way to take account of this phenomena is to express winding numbers as

continued fractions,

$$r = a_0 + \cfrac{1}{a_1 + \cfrac{1}{a_2 + \cfrac{1}{a_3 + \cdots}}} \tag{1.12}$$

where since $r \geq 1$, the a_n's are positive integers. This will be denoted as $r = [a_0, a_1, a_2, \cdots, a_N]$. Irrational numbers have unique representations as continued fractions, with an infinite number of partial quotients. Thus, these numbers will be denoted r_∞. Successive truncations of the infinite continued fraction yield rational approximations that are called the *convergents of* r. These convergents yield, from among the periodic orbits of the given length or shorter, the one that most nearly approaches the surface of interest. Greene [1979] conjectured that, since the golden mean $r_g = \frac{\sqrt{5}-1}{2}$ is the most irrational number in the sense that it is most slowly approached by cutoffs of its continued fraction expansion,

$$r_g = [1, 1, 1, 1, \cdots] = 1 + \cfrac{1}{1 + \cfrac{1}{1 + \cfrac{1}{1 + \cdots}}} \tag{1.13}$$

the torus with $r = r_g$ will be the last surviving torus as K is increased. Greene finds that $K(r_g) = 0.971635\cdots$. This corresponds to the largest value of K for which there are KAM curves running completely around the (q, p) cylinder. When K increases past the critical value $K \simeq 0.97$ the last invariant tori encircling the cylinder are destroyed, and a chaotic area connecting the two ends of the phase space exists. This can be seen in figure(1.1), where the standard map is shown for four typical values of K.

1.2.2 The Crémona Map

Investigating the Poincaré surface of section for an arbitrary Hamiltonian requires the numerical integration of the trajectories. This is a costly computational task, and if one wants to display the fine structure of the Poincaré map, one may require several thousand integration steps in order to approximate the continuous variation of the

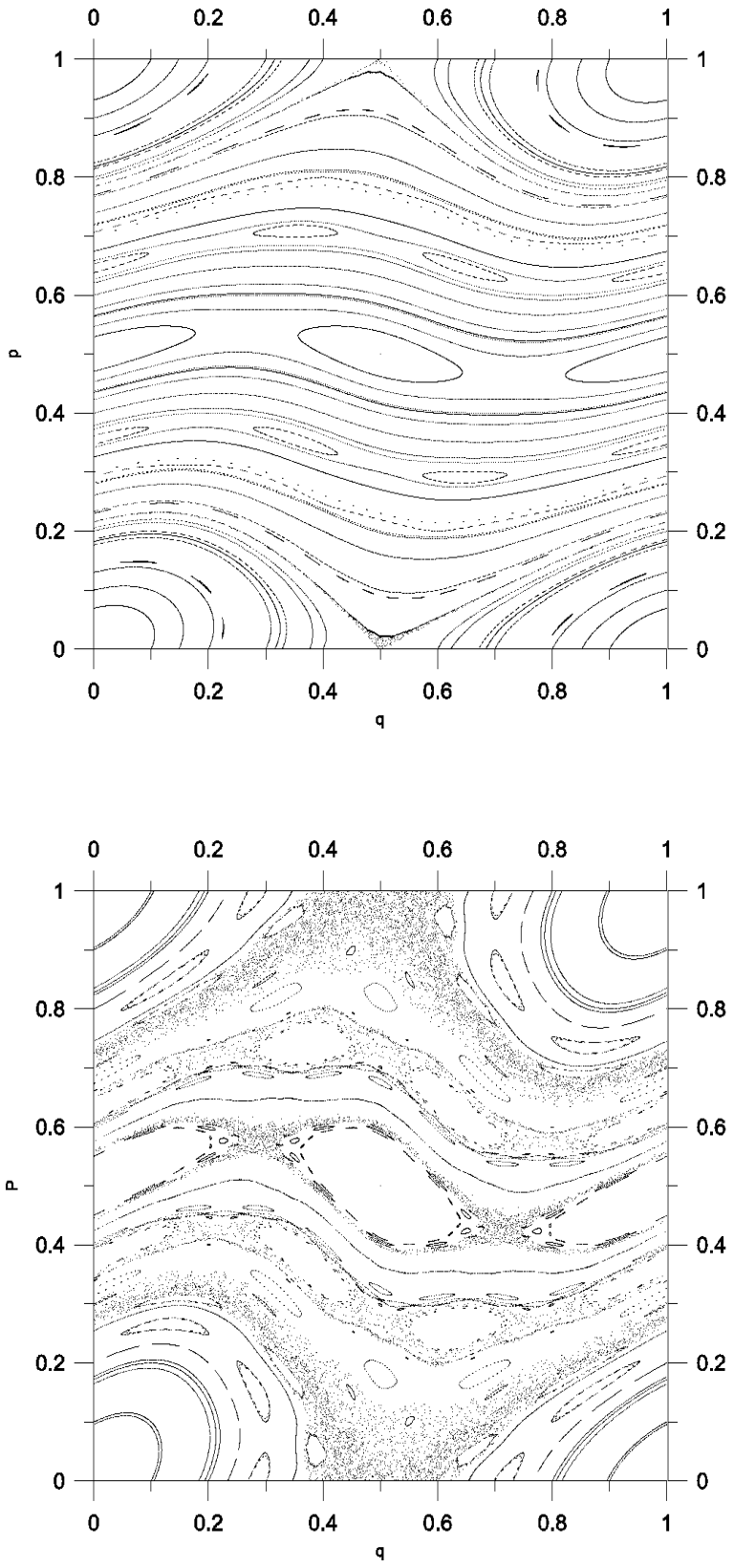

Figure 1.1: (a) **The standard map**. Top: $K = 0.5$; Bottom: $K = 0.975$.

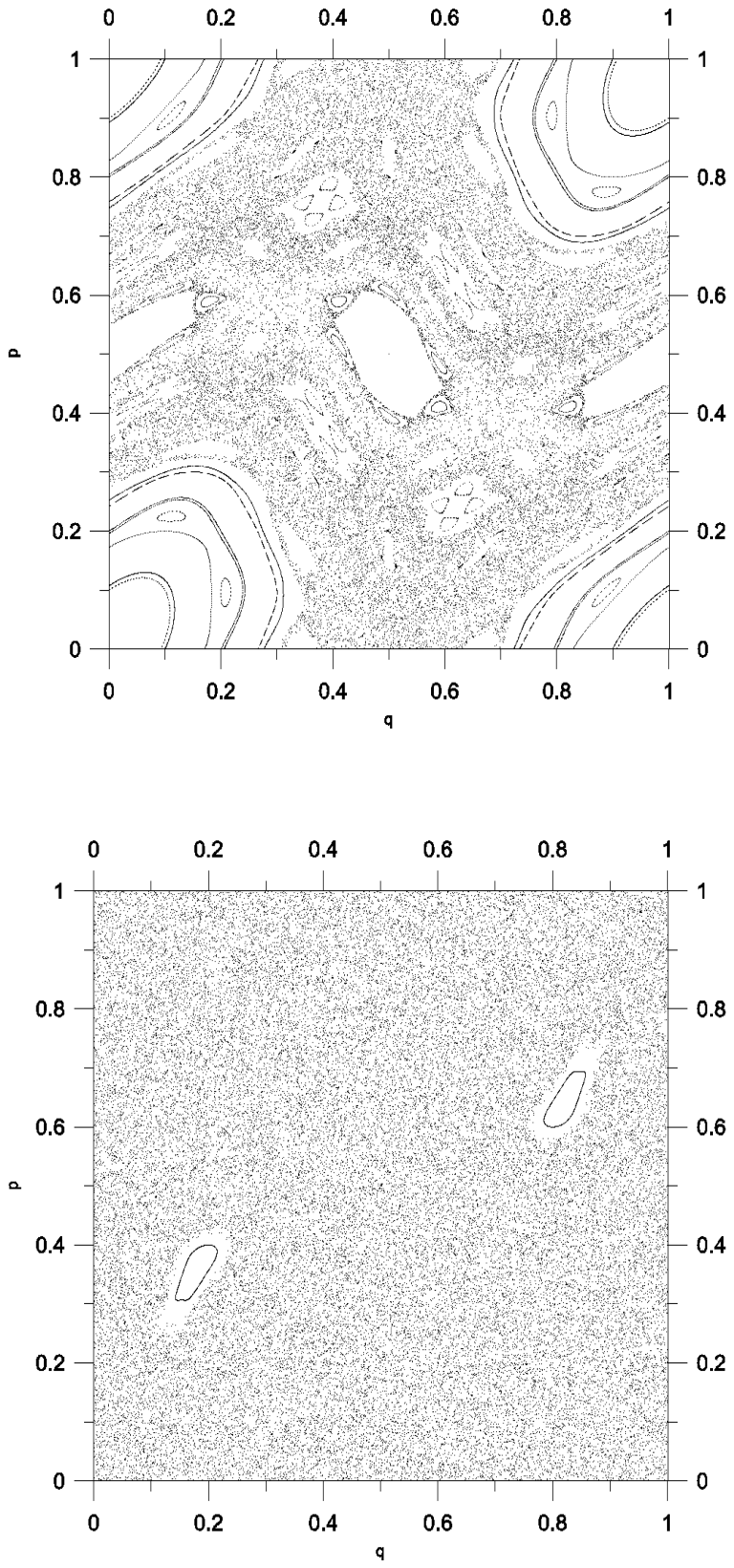

Figure 1.1: (b) **The standard map**. Top: $K = 1.25$, Bottom: $K = 5.0$.

coordinates along the trajectory. In the early days of Hamiltonian dynamics, when high speed computers were not readily available, people started to investigate an artificial transformation from the (x, y) plane into itself, instead of the real trajectories that belong to a given Hamiltonian. Hénon and co-workers [1969] were among the first to try out this strategy to overcome the computational limits of the earlier calculations. The choice of a map $(x, y) \to (x_1, y_1)$ was dictated by the requirement that the element of the area remains invariant, or equivalently that the Jacobian

$$det \frac{\partial(x_1, y_1)}{\partial(x, y)} \equiv det \begin{pmatrix} \frac{\partial x_1}{\partial x} & \frac{\partial y_1}{\partial x} \\ \frac{\partial x_1}{\partial y} & \frac{\partial y_1}{\partial y} \end{pmatrix} = 1. \tag{1.14}$$

Hence, we seek an area preserving mapping of the (x, y) plane onto itself, defined by

$$\begin{pmatrix} x_1 \\ y_1 \end{pmatrix} = \begin{pmatrix} f(x, y) \\ \\ g(x, y) \end{pmatrix}. \tag{1.15}$$

For numerical studies it is simplest to have polynomials for f and g. In that case the mapping is called an *entire Crémona transformation*. Let us choose second degree polynomials for f and g:

$$\begin{pmatrix} x_1 \\ \\ y_1 \end{pmatrix} = \begin{pmatrix} ax + by + cx^2 + dxy + ey^2 \\ \\ a'x + b'y + c'x^2 + d'xy + e'y^2 \end{pmatrix} \tag{1.16}$$

Then, the area preserving condition imposes that

$$\begin{pmatrix} x_1 \\ \\ y_1 \end{pmatrix} = \begin{pmatrix} x\cos\alpha - (y - x^2)\sin\alpha \\ \\ x\sin\alpha + (y - x^2)\cos\alpha \end{pmatrix} \tag{1.17}$$

where α is the only non-trivial parameter left. This map, also called the *Hénon map*, has been investigated intensively during the past three decades in a slightly more general version which was also proposed by Hénon [1976]. This general version has the form [Gutzwiller, 1990]

$$\begin{pmatrix} x_1 \\ \\ y_1 \end{pmatrix} = \begin{pmatrix} -\epsilon y + \mu - x^2 \\ \\ x \end{pmatrix} \tag{1.18}$$

The Jacobian $\frac{\partial(x_1, y_1)}{\partial(x, y)} = \epsilon$, so that this map does not preserve the area unless $\epsilon = 1$; if such is the case, however, the new map (1.18) is the same as (1.17) up to a change of coordinates in the (x, y) plane. The rotation angle α in (1.17) is related to μ in (1.18) through $(1 + \mu)^{1/2} = 2 \sin^2 \alpha/2$. The area-preserving Hénon map (AHM) is shown in figure (1.2) for $\epsilon = 1.0$ and $\mu =$ - 0.4224.

When $\epsilon < 1$, the map is a good model for a dynamical system with dissipation. When the map is iterated, the original area of any portion of phase space becomes smaller by a factor ϵ at each step. The contraction, however, does not lead to a set of points whose diameter decreases indefinitely, but rather to a fractal set with dimension of 1.261. The consecutive points $P_0, P_1, \cdots$ eventually get ever closer to this set and move around this fractal without ever converging to a limit. This set is known as the *Hénon attractor* and is a special case of a *strange attractor* [Eckmann and Ruelle, 1985]. Figure(1.3) shows the typical form of the attractor for the dissipative Hénon map (DHM) ($\epsilon =$ - 0.3, $\mu = 1.4$).

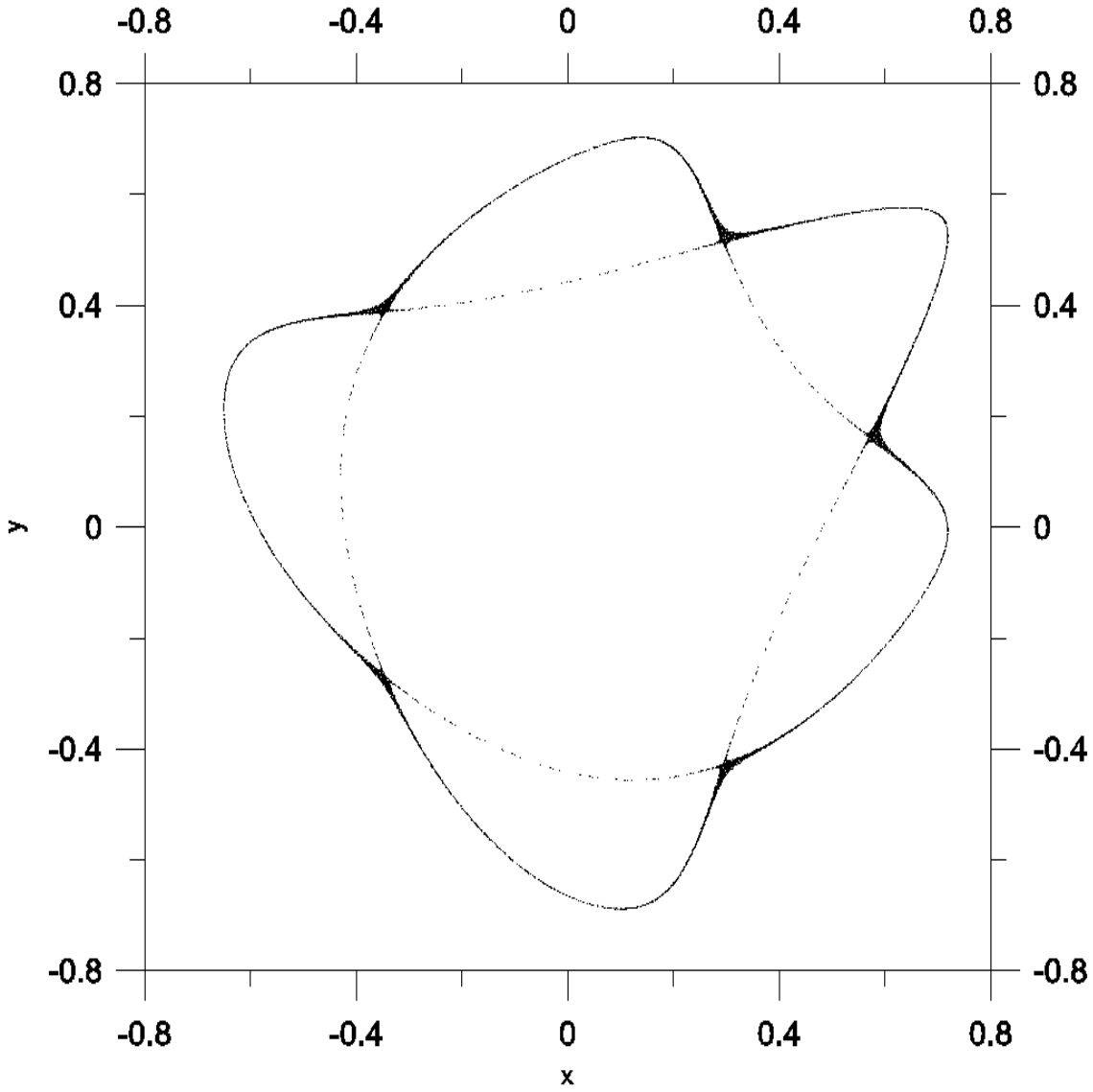

Figure 1.2: **The entire Crémona map** (equation(1.17)): μ = - 0.4224, ϵ = 1.0.

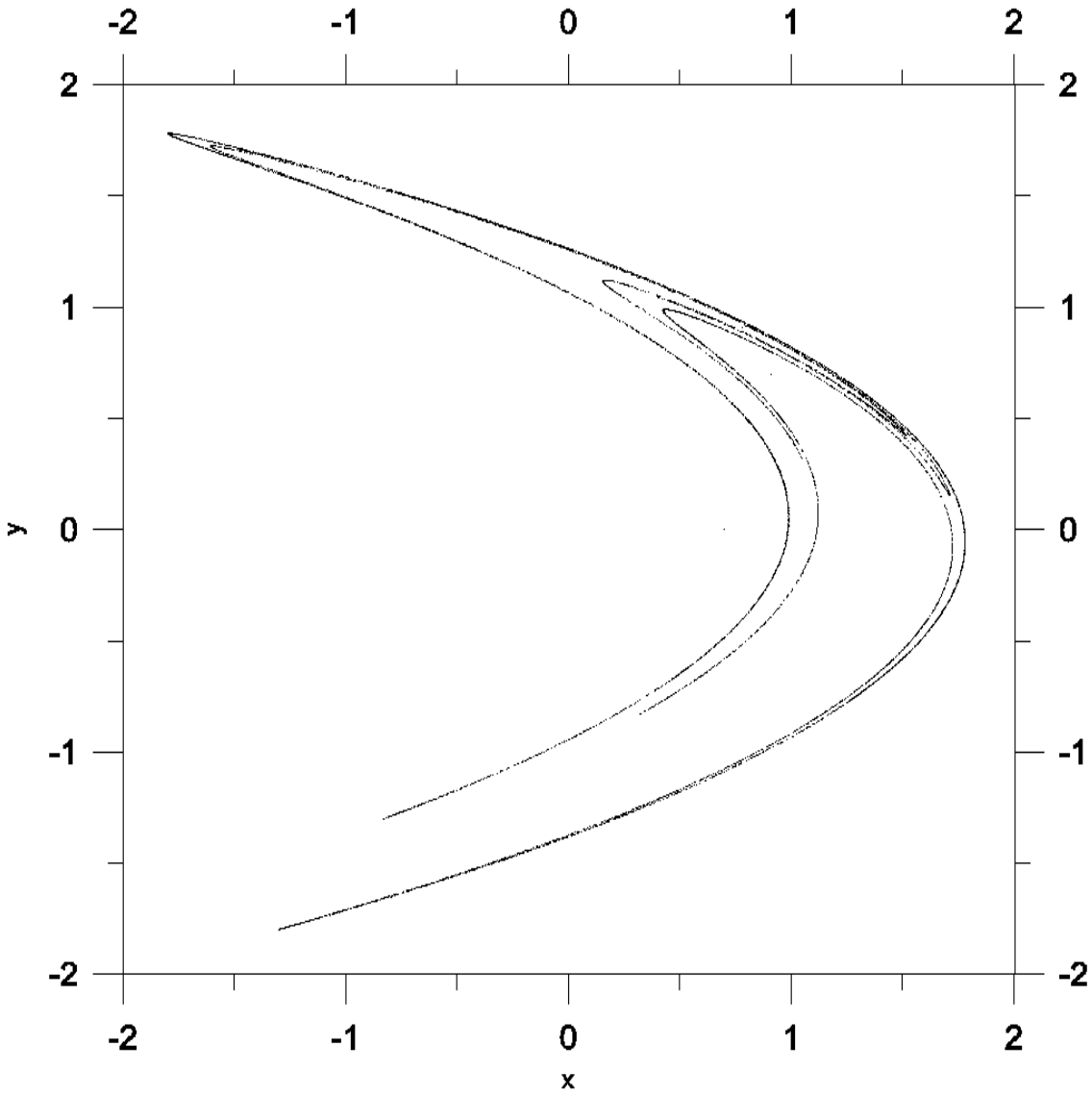

Figure 1.3: **The Dissipative Hénon Map**: $\mu = 1.4$, $\epsilon =$ - 0.3.

1.3 The Poincaré Section of Hamiltonian Flows

In general there is no simple way to tell whether a system is integrable or not. In systems with two degrees of freedom (which is the main theme of the present work), we can verify integrability numerically by constructing a *Poincaré surface of section* [Reichl, 1992]. To see how this works, let us consider a conservative system where the Hamiltonian is an isolating integral of motion. We can write

$$H(p_1, p_2, q_1, q_2) = E \tag{1.19}$$

where the energy, E, is constant and restricts the trajectories to lie on a 3-dimensional surface in the 4-dimensional phase space. One uses equation (1.19) to write $p_2 = p_2(p_1, q_1, q_2; E)$. If the system has a second isolating integral,

$$I_2(p_1, p_2, q_1, q_2) = C_2 \tag{1.20}$$

where C_2 is a constant, it also defines a 3-dimensional surface in the 4-dimensional phase space. Once the initial conditions are given, E and C_2 are fixed and the trajectory is constrained to the intersection of the surfaces defined by equations (1.19) and (1.20); that is, to a 2-dimensional surface in the 4-dimensional phase space. Combining equations (1.19) and (1.20), we also write $p_1 = p_1(q_1, q_2; E, C_2)$. And finally, if we now consider the surface, $q_1 = 0$, the trajectory must lie on a one dimensional curve.

In general if we are given the Hamiltonian (1.19), we do not know if an additional isolating integral, I_2, exists. We can check this numerically by solving Hamilton's equations and then plotting say p_2 and q_2 each time $q_1 = 0$ and $p_1 \geq 0$. If the system is integrable, the trajectory will appear as a series of points (a mapping) which lie on a one dimensional curve. If the system is nonintegrable, the trajectory will appear as a scatter of points limited to a finite area whose boundary is determined by energy conservation. In the following we will see the application of this method in analysing the behaviour of the Hamiltonian system for a) the Hénon - Heiles potential and b)

the Diamagnetic Kepler Problem (DKP). The integrations are performed by using a symplectic integration algorithm with adaptive stepsize [Poulin, 1997; Channell and Scovel, 1990; Casetti, 1995].

1.3.1 The Hénon - Heiles Potential

Poincaré sections were used extensively by Hénon and Heiles [1964] to determine if a third integral existed for the motion of a star in a galaxy which had an axis of symmetry. Such a system has three degrees of freedom and two known isolating integrals of motion, the energy and one component of the angular momentum. It was long thought that such systems do not have a third isolating integral because none had been found analytically. However, the nonexistence of a third integral implies that the dispersion of velocities of stellar objects in the direction of the galactic center is the same as that perpendicular to the galactic plane. What was observed, however, was a 2:1 ratio in these dispersions [Gutzwiller, 1990]. Hénon and Heiles constructed the following Hamiltonian (with no known symmetries that can give rise to a third integral) to model the essential features of the problem

$$H_{HH} = \frac{1}{2}(p_1^2 + p_2^2) + \frac{1}{2}(q_1^2 + q_2^2 + 2q_1^2 q_2 - \frac{2}{3}q_2^3) = E \tag{1.21}$$

and studied its behaviour numerically [Hénon , 1983]. Hamilton's equations for this system are

$$\frac{dp_1}{dt} = -q_1 - 2q_1 q_2 \tag{1.22}$$

$$\frac{dp_2}{dt} = -q_2 - q_1^2 + q_2^2 \tag{1.23}$$

$$\frac{dq_i}{dt} = p_i \tag{1.24}$$

(for i=1,2). The anharmonic terms in the potential energy give rise to nonlinear terms in the equations of motion. The potential term in equation (1.21) has a ternary symmetry,

as is more clearly shown by introducing the polar coordinates $q_1 = r\cos\theta$, $q_2 = r\sin\theta$, in which case the potential energy becomes

$$V_{HH} = \frac{1}{2}r^2 + \frac{1}{3}r^3\sin(3\theta). \tag{1.25}$$

It can be shown that when $V_{HH}(q_1, q_2) = 1/6$

$$(q_2 + \frac{1}{2})(q_2 + \sqrt{3}q_1 - 1)(q_2 - \sqrt{3}q_1 - 1) = 0. \tag{1.26}$$

These three straight lines cross at $(q_1, q_2) = (0, 1), (\pm\frac{\sqrt{3}}{2}, -\frac{1}{2})$. Inside this triangle the motion is bounded, provided that $H_{HH} < \frac{1}{6}$. However, if $H_{HH} > \frac{1}{6}$, or if the motion starts outside of this triangle, the motion is generally unbounded. Figure (1.4) shows Poincaré sections for the Hénon -Heiles potential for $E = 1/12$, $1/8$, and $1/6$. It is clear from the figure that for $E = 1/12$ the system is nearly integrable, while for $E = 1/8$ a large part of the surface of section is clearly ergodic. For $E = 1/6$ almost all of the domain shows ergodic behaviour with the exception of some tiny loops near the centers of the earlier structures of nested tori. It is this ergodic domain that provides us with a useful means of controlling the chaotic behaviour of this system. We will discuss this issue later in chapter 3.

1.3.2 The Diamagnetic Kepler Problem (DKP)

The effect of a magnetic field on an atom has been studied for a long time and has played a crucial role in the understanding of atomic physics. The magnetic fields available in the laboratory are small, however, and their action on the atom used to be well explained by perturbation theory [Waterland, Delos and Du, 1987]. The evidence of strong magnetic field was first found by the astronomers in white dwarfs three decades ago, and extremely strong fields are assumed to exist in neutron stars. This discovery led to laboratory experiments that somehow manage to imitate the extraordinary conditions in these exceptional stars. The main idea is to prepare the atom in a very

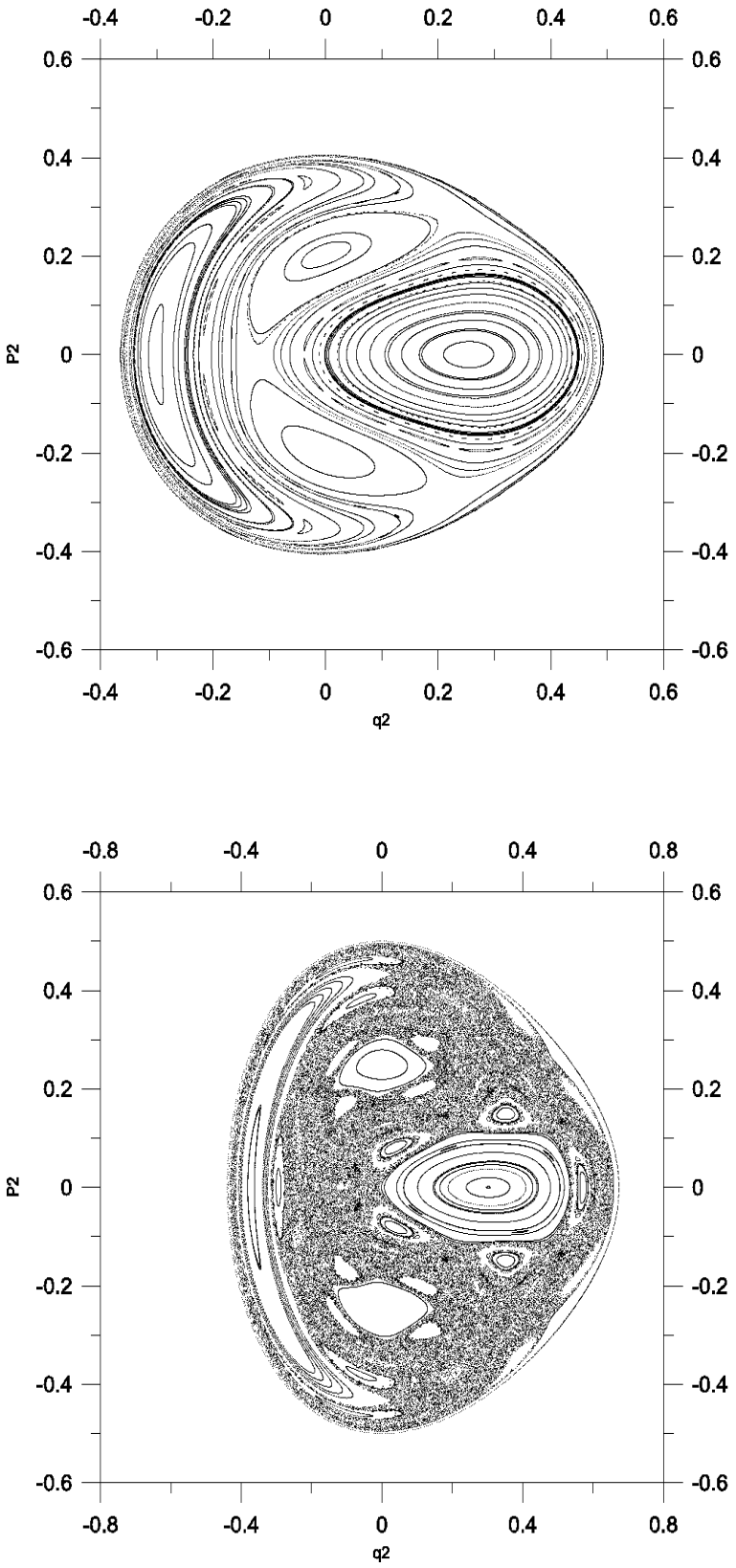

Figure 1.4: (a) **Poincaré sections of the Hénon - Heiles potential.** Top: E=1/12, Bottom: E=1/8.

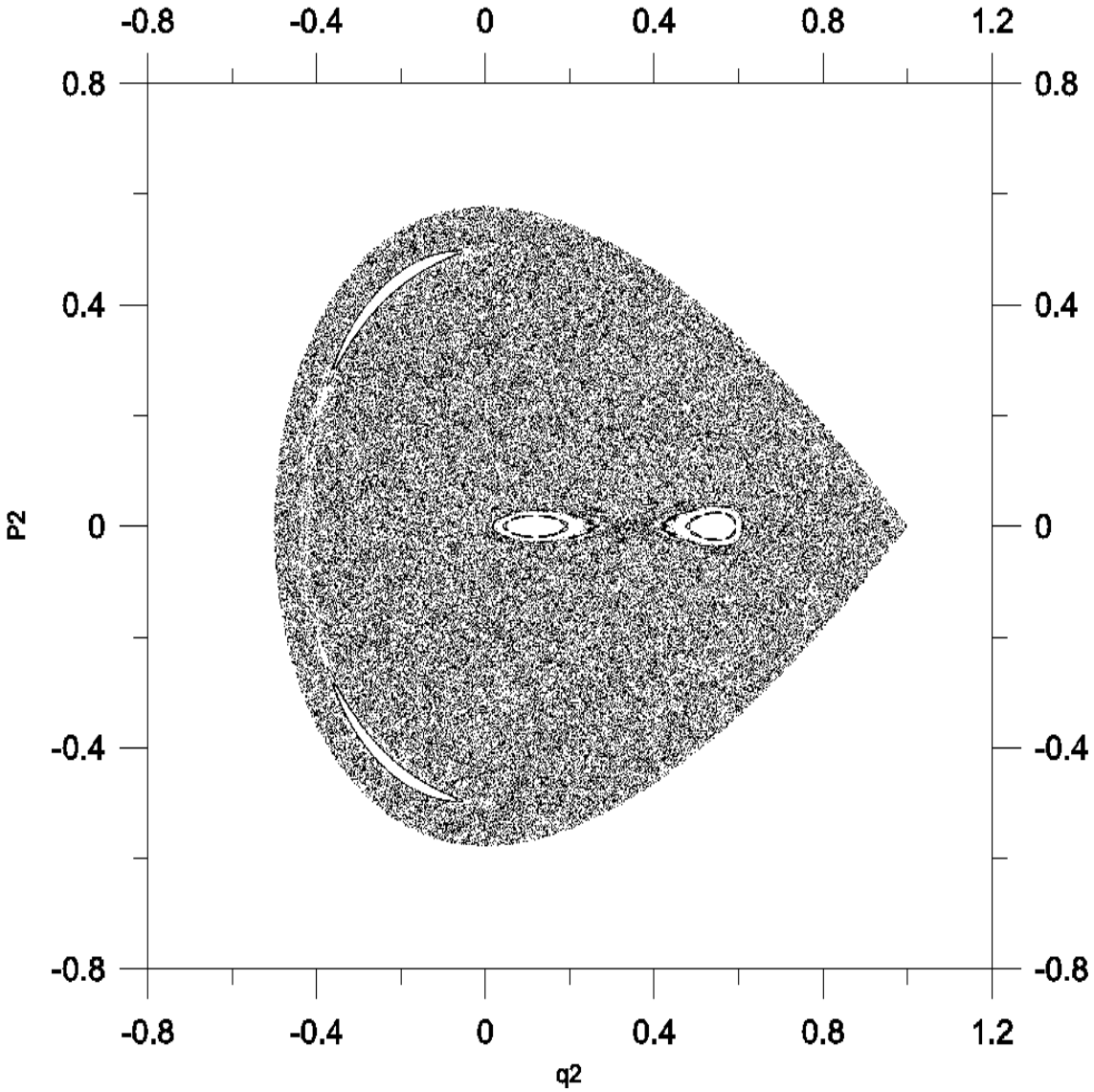

Figure 1.4: (b) **Poincaré section of the Hénon - Heiles potential:** E=1/6.

highly excited, but still bound state, so that the orbit of the electron encloses a large area, and thus a large magnetic flux even in a relatively small field. Perturbation theory is then no longer applicable; the dominant term in the Hamiltonian is no longer the linear one (in the field strenght) giving rise to the ordinary Zeeman effect [Friedrich and Wintgen, 1989]. By contrast, the quadratic term in the Hamiltonian is usually of less importance, because it comes into play only when the atom or molecule does not have a magnetic moment to start with, and it leads to a small negative magnetic susceptibility, called *diamagnetic* rather than the much larger positive *paramagnetic* one. The quadratic, or diamagnetic term, however, is eventually responsible for chaotic classical motion, whereas the linear, or paramagnetic term can be effectively eliminated by using a rotating frame of reference.

The hydrogen atom in a magnetic field is accurately described over a wide range of field strengths B by the simple nonrelativistic single-particle Hamiltonian [Delos, Knudson and Noid, 1983]

$$H_{DK} = \frac{p^2}{2m_e} - \frac{e^2}{r} + \omega L_z + \frac{1}{2} m_e \omega^2 (x^2 + y^2). \tag{1.27}$$

The direction of the field is taken as the z-direction and m_e is the reduced mass of electron and nucleus.The frequency ω is half the cyclotron frequency ω_c

$$\omega = \frac{1}{2}\omega_c = \frac{1}{2}\frac{eB}{m_e c} \tag{1.28}$$

At a field strength of

$$B = B_0 = \frac{m_e^2 e^3 c}{\hbar^3} \approx 2.35 \times 10^9 \ G = 2.35 \times 10^5 \ T, \tag{1.29}$$

the oscillator energy $\hbar\omega$ equals the Rydberg energy $\Re = m_e e^4/(2\hbar^2) \approx 13.6$ eV. In terms of the dimensionless field strength parameter

$$\gamma_0 = \frac{B}{B_0} = \frac{\hbar\omega}{\Re}, \tag{1.30}$$

relativistic corrections to the simple model defined by (1.27) are negligible for fields with $\gamma_0 < 10^4$ [Doman, 1980]. On the other hand, the effects of the spin-orbit coupling

can be neglected for fields with $\gamma_0 n^3 > 10^{-4}$, where n is the principal quantum number [Garstang, 1977]. Effects related to the two body (nucleus and electron) center of mass motion in the presence of an external magnetic field have been investigated by several authors [Herold, Ruder and Wunner, 1981; Vincke and Baye, 1988]. It is possible to separate a generalized field strength dependent momentum, which replaces the center of mass momentum of the field-free two-body system. For fields with $\gamma_0 > 100$ the internal dynamics is considerably influenced by the center of mass motion, but for a vanishing transversal component of the conserved generalized momentum the effect can be accounted for accurately by a constant energy shift which depends only on the magnetic field strength and the azimuthal quantum number m [Herold, Ruder and Wunner, 1981].

The classical dynamics of the hydrogen atom in a uniform magnetic field is described by the Hamiltonian (1.27). In a frame of reference that rotates at the frequency ω about the direction of the magnetic field, z, the Hamiltonian can be written in cylindrical coordinates as [Delos, Knudson and Noid, 1984]

$$H_{DK} = \frac{1}{2m_e}(p_\rho^2 + p_z^2) - \frac{e^2}{(\rho^2+z^2)^{\frac{1}{2}}} + \frac{L_z^2}{2m_e\rho^2} + \lambda\rho^2 \tag{1.31}$$

where $\lambda = e^2B^2/(8m_ec^2)$. The term $-e^2/(\rho^2+z^2)^{1/2}$ is the Coulomb potential energy, $L_z^2/2m_e\rho^2$ is the *centrifugal barrier*, and $\lambda\rho^2$ is the *diamagnetic term*, which is proportional to the square of the magnetic field B. The number of parameters in the above equation can be reduced from four (m_e, e, λ, L_z) to one $(\hat{L})$ with the help of the following scaling law [Delos *et al.*, 1988]. Let us define

$$\hat{\rho} = \frac{\rho}{\alpha}\ , \quad \hat{p}_\rho = \frac{p_\rho}{\beta} \qquad \hat{z} = \frac{z}{\alpha}\ , \quad \hat{p}_z = \frac{p_z}{\beta} \qquad \hat{t} = \frac{t}{\gamma}, \tag{1.32}$$

where

$$\alpha = \left(\frac{e^2}{8\lambda}\right)^{\frac{1}{3}}, \qquad \beta = m_e^{\frac{1}{2}} e^{\frac{2}{3}} (8\lambda)^{\frac{1}{6}}, \qquad \gamma = \left(\frac{m_e}{8\lambda}\right)^{\frac{1}{2}}. \tag{1.33}$$

(The dimensional analysis of this scaling law is presented in the Appendix.) This means that except for a similarity transformation the classical trajectory can be completely

described by the one-parameter scaled Hamiltonian [Delos, Knudson and Noid, 1984]

$$\hat{H}_{DK} = \frac{m_e}{\beta^2} H_{DK} = \frac{1}{2}(\hat{p}_\rho^2 + \hat{p}_z^2) - \frac{1}{(\hat{\rho}^2 + \hat{z}^2)^{\frac{1}{2}}} + \frac{\hat{L}^2}{2\hat{\rho}^2} + \frac{1}{8}\hat{\rho}^2 \tag{1.34}$$

in which the scaled mass, electron charge and diamagnetic coupling constant λ are all equal to unity, and the z component of angular momentum is $\hat{L}$. Then the equations of motion in the scaled variables have the form

$$\frac{d\hat{\rho}}{d\hat{t}} = \hat{p}_\rho, \quad \frac{d\hat{z}}{d\hat{t}} = \hat{p}_z, \quad \frac{d\hat{p}_\rho}{d\hat{t}} = -\frac{\hat{\rho}}{(\hat{\rho}^2 + \hat{z}^2)^{\frac{3}{2}}} - \frac{1}{4}\hat{\rho} + \frac{\hat{L}^2}{\hat{\rho}^3}, \quad \frac{d\hat{p}_z}{d\hat{t}} = -\frac{\hat{z}}{(\hat{\rho}^2 + \hat{z}^2)^{\frac{3}{2}}} \quad . \tag{1.35}$$

These equations of motion contain only one parameter,

$$\hat{L} = \left(\frac{8\lambda}{m_e^3 e^8}\right)^{\frac{1}{6}} L_z = \gamma_0^{\frac{1}{3}} \left(\frac{L_z}{\hbar}\right). \tag{1.36}$$

Study of the Poincaré section of the scaled Hamiltonian shows that the system exhibits various behaviours depending on the values of E and L. The scaled potential energy

$$V_{DK}(\hat{\rho}, \hat{z}) = -\frac{1}{(\hat{\rho}^2 + \hat{z}^2)^{\frac{1}{2}}} + \frac{\hat{L}^2}{2\hat{\rho}^2} + \frac{1}{8}\hat{\rho}^2 \tag{1.37}$$

has a minimum at the point ρ_0 which satisfies

$$\frac{1}{4}\rho_0^4 + \rho_0 - \hat{L}^2 = 0 \tag{1.38}$$

with $z_0 = 0$; the value of V_{DK} at that point is

$$V_{DK}(\rho_0, 0) = -\frac{1}{\rho_0} + \frac{\hat{L}^2}{2\rho_0^2} + \frac{1}{8}\rho_0^2 \equiv \epsilon_{min}(L). \tag{1.39}$$

For each $\hat{L}$, this is the minimum possible value of the energy of the system. V_{DK} also has a *saddle* point at $z = \infty$, $\rho_s = (2\hat{L})^{1/2}$, with

$$V_{DK}(\rho_s, \infty) = \frac{\hat{L}}{2} \equiv \epsilon_s(L). \tag{1.40}$$

ϵ_s is the *classical escape energy*, above which the electron has enough energy to escape from the nucleus (although there are some bound trajectories with $\epsilon > \epsilon_s$). It is convenient to define a dimensionless scaled energy

$$f = \frac{\epsilon - \epsilon_{min}(\hat{L})}{\epsilon_s(\hat{L}) - \epsilon_{min}(\hat{L})} \tag{1.41}$$

where ϵ is the energy of the system (i.e., the value of the scaled Hamiltonian): $f = 0$ for $\epsilon = \epsilon_{min}$ and $f = 1$ for $\epsilon = \epsilon_s$.

For small $\hat{L}$, which corresponds to weak magnetic fields ($\gamma_0 \ll 1$), trajectories are best described as Kepler ellipses with orbital parameters that slowly vary with time. Delos, Knudson and Noid [1983b] showed that many of these trajectories, and their associated quantum states, can be calculated using perturbation theory with the Kepler Hamiltonian $\hat{H}_K^0$ as the starting point, i.e.

$$\hat{H}_{DK} = \hat{H}_K^0 + \hat{H}_D^1 \tag{1.42}$$

with

$$\hat{H}_K^0 = \frac{1}{2}(\hat{p}_\rho^2 + \hat{p}_z^2) - \frac{1}{(\hat{\rho}^2 + \hat{z}^2)^{\frac{1}{2}}} + \frac{\hat{L}^2}{2\hat{\rho}^2} \qquad \text{and} \qquad \hat{H}_D^1 = \frac{1}{8}\hat{\rho}^2. \tag{1.43}$$

The range of ϵ and $\hat{L}$ for which the trajectories have an apparent relationship to Kepler ellipses, is called the *elliptical regime*. Figure (1.5) shows a classical trajectory of DKP for values of ϵ and $\hat{L}$ corresponding to the elliptical regime.

For large $\hat{L}$, corresponding to extraordinarily strong magnetic fields ($\gamma_0 \gg 1$) (such as might exist on the surface of a neutron star), the diamagnetic force on the electron exceeds the Coulomb force, so the electron circles along the magnetic field line, and travels slowly back and forth in the $\hat{z}$ direction. The atom, far from being spherical, has then the shape of a long cylinder or tube. This range of ϵ and $\hat{L}$ is refered to as the *helical regime*. The helical regime may be said to extend to $f > 1$ if $\hat{L}$ is sufficiently large; i.e., even above the escape energy there are bound trajectories with the same helical character. In quantum mechanics these would be quasibound states, or resonances. Figure (1.6) shows a typical trajectory for values of ϵ and $\hat{L}$ corresponding to the helical regime.

Between the elliptical and helical regimes, for f not too small, there is an irregular regime, in which the trajectories are chaotic. This regime extends down to $\hat{L} = 0$. It

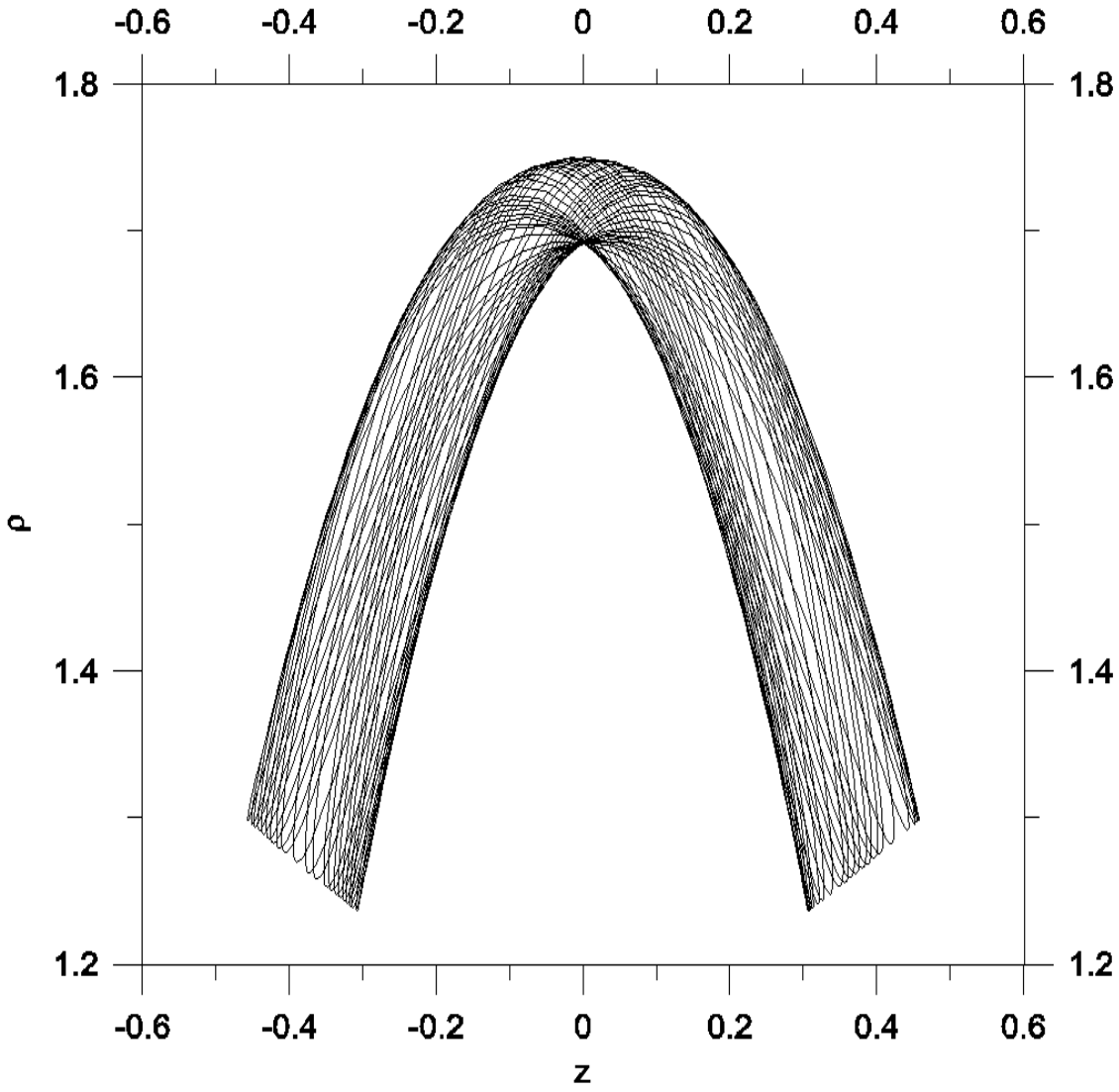

Figure 1.5: **An elliptical trajectory:** $\hat{L} = 1.60$, $f = 0.1$, corresponding to $\epsilon = 0.24376$.

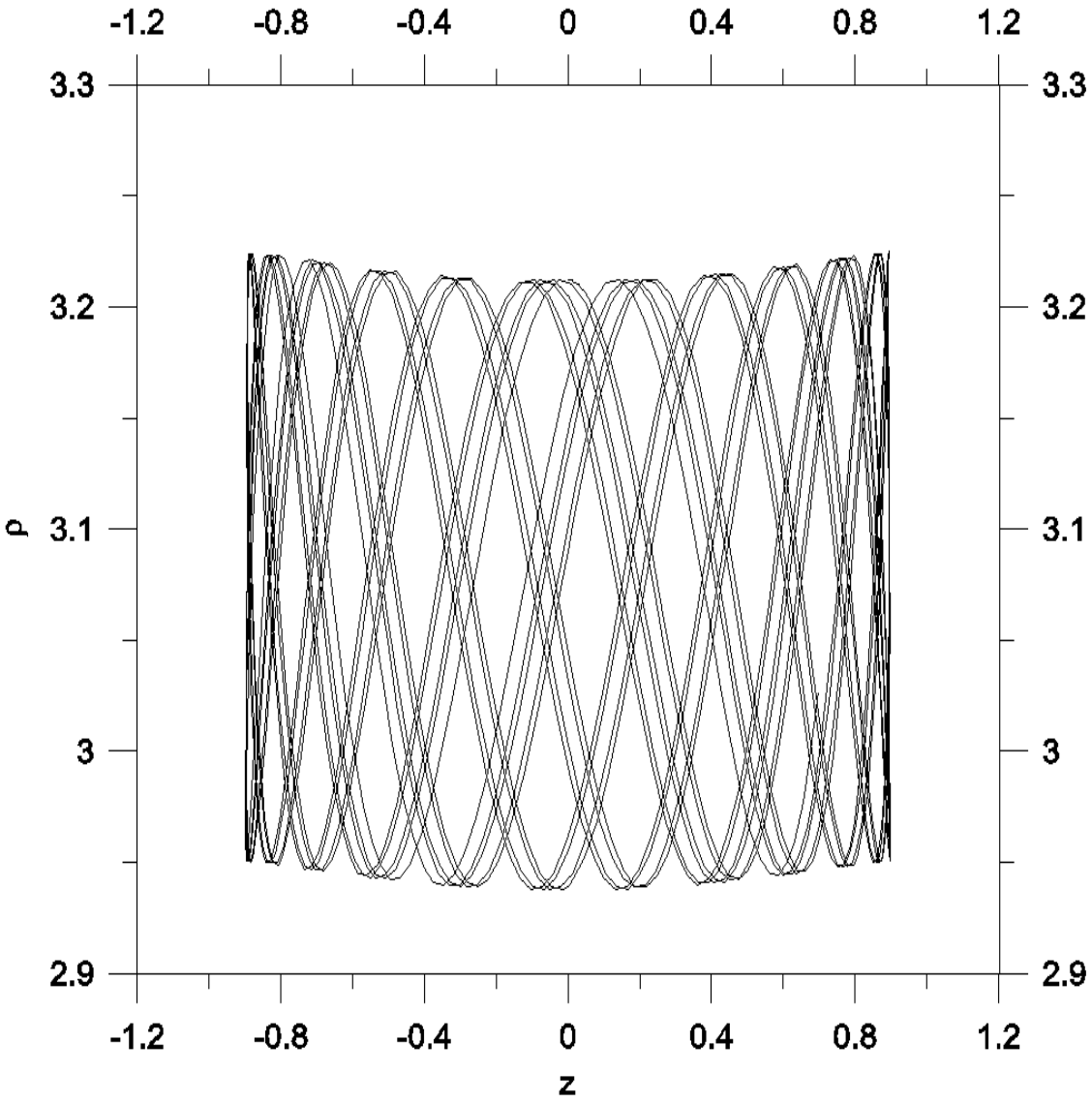

Figure 1.6: **A helical trajectory:** $\hat{L} = 5.035$, $f = 0.1$, corresponding to $\epsilon = 2.22$.

is generally believed that this means that the quantum mechanical spectrum of energy levels will also be irregular in at least part of this region. Irregular orbits are identified by the fact that they show no orderly pattern on the Poincaré surface of section. Figure (1.7) shows the behaviour of the system for different values of ϵ and $\hat{L}$. The regions of scattered points represent chaos.

In order to do a systematic study on trajectories in the chaotic region, we choose a single value for $\hat{L}$ and for the sake of simplicity we choose this value to be $\hat{L} = 0$. One more point is worth mentionning, namely that the Hamiltonian (1.34) has a singularity at $\mathbf{r}$=0, which can be removed, e.g. by the introduction of *semi-parabolic coordinates*. The new generalized coordinates are given by [Friedrich and Wintgen, 1989; Hansen, 1994]

$$\mu^2 = \hat{r}+\hat{z}, \quad \nu^2 = \hat{r}-\hat{z}, \qquad p_\mu = \frac{d\mu}{d\tau}, \quad p_\nu = \frac{d\nu}{d\tau}, \qquad dt = 2\hat{r}d\tau = (\nu^2+\mu^2)d\tau. \tag{1.44}$$

The equations of motion generated by the Hamiltonian $\hat{H}_{DK}$ ($\hat{L} = 0$) in (1.34) at a fixed value of the scaled energy ϵ, are equivalent to the equations of motion generated by the Hamiltonian

$$h_{DK} = \frac{1}{2}p_\nu^2 + \frac{1}{2}p_\mu^2 - \epsilon(\nu^2+\mu^2) + \frac{1}{8}\nu^2\mu^2(\nu^2+\mu^2) \equiv 2, \tag{1.45}$$

at the fixed *pseudo energy* equals to 2. For negative energies $\epsilon < 0$ the Hamiltonian (1.45) represents 2 harmonic oscillators with frequency $\omega = (-2\epsilon)^{1/2}$, coupled by the term $\nu^2\mu^2(\nu^2+\mu^2)$ originating from the diamagnetic interaction. The quadratic potential vanishes at the zero-field threshold $\epsilon = 0$. For positive energies $\epsilon > 0$ the Hamiltonian corresponds to 2 inverted oscillators coupled by the diamagnetic interaction. There is a one-to-one correspondence between the classical trajectories generated by the Hamiltonian $\hat{H}_{DK}$ (1.34) and h_{DK} (1.45), but they are not related by a canonical transformation. Because of the coordinate dependent rescaling of time, two periodic orbits which have the same period in the cylindrical representation may have different periods in the semi-parabolic representation.

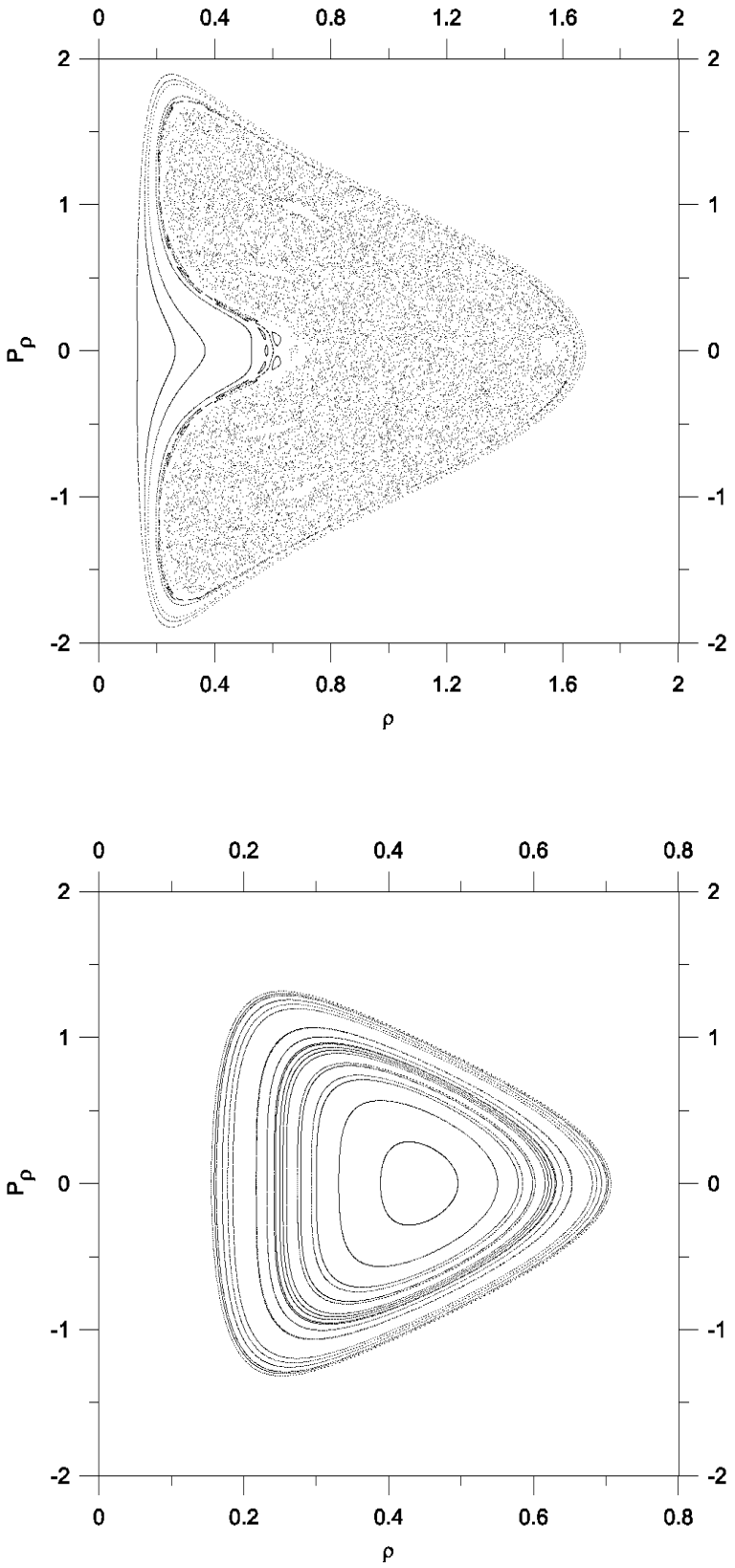

Figure 1.7: (a) **Poincaré sections of the DKP:** ($\hat{z} = 0$ and $\hat{p}_z > 0$) Top: $f = 0.8$, $\hat{L}$ = 0.5 ; Bottom: $f = 0.4$, $\hat{L} = 0.5$.

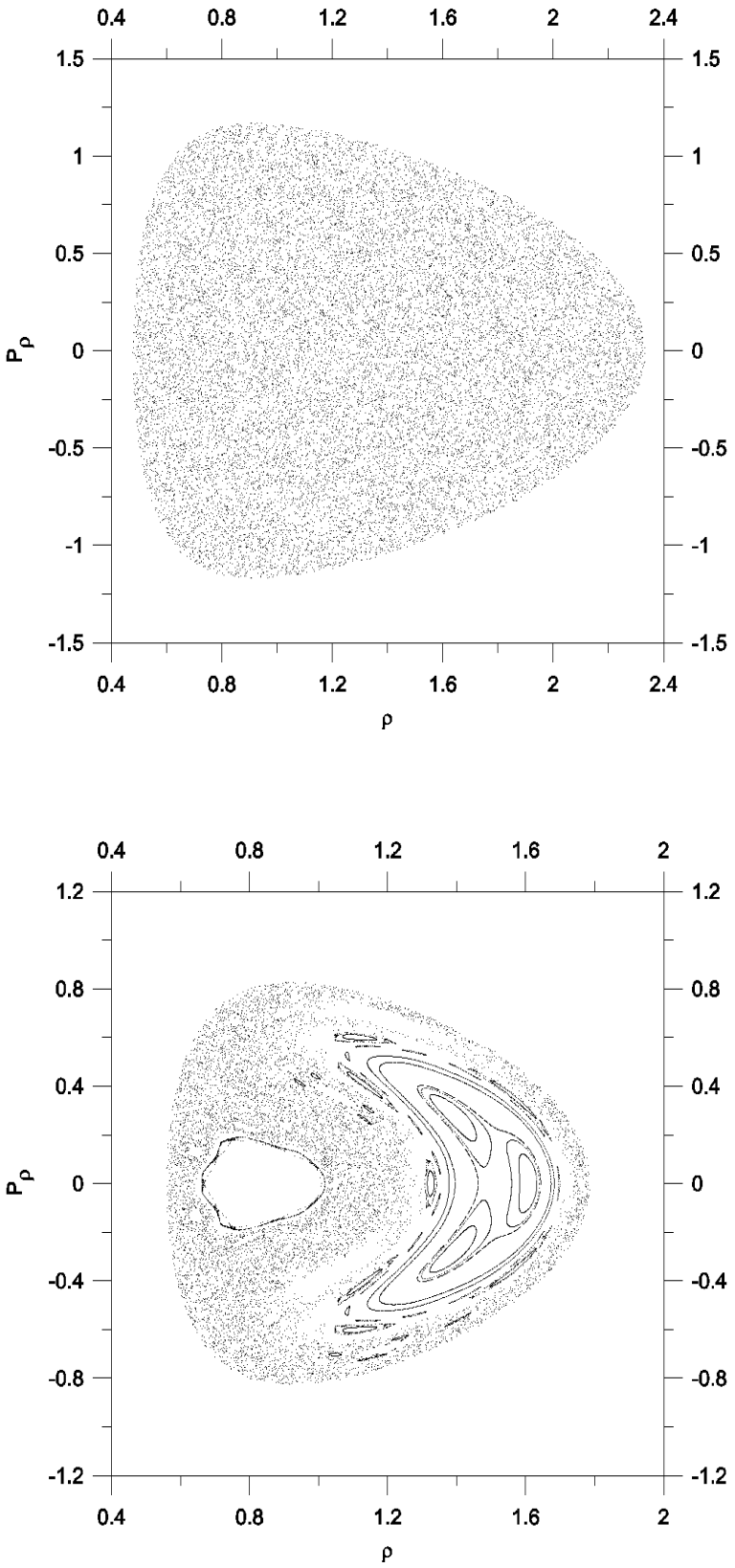

Figure 1.7: (b) **Poincaré sections of the DKP:** ($\hat{z} = 0$ and $\hat{p}_z > 0$) Top: $f = 0.8$, $\hat{L}$ = 1.05; Bottom: $f = 0.4$, $\hat{L} = 1.05$.

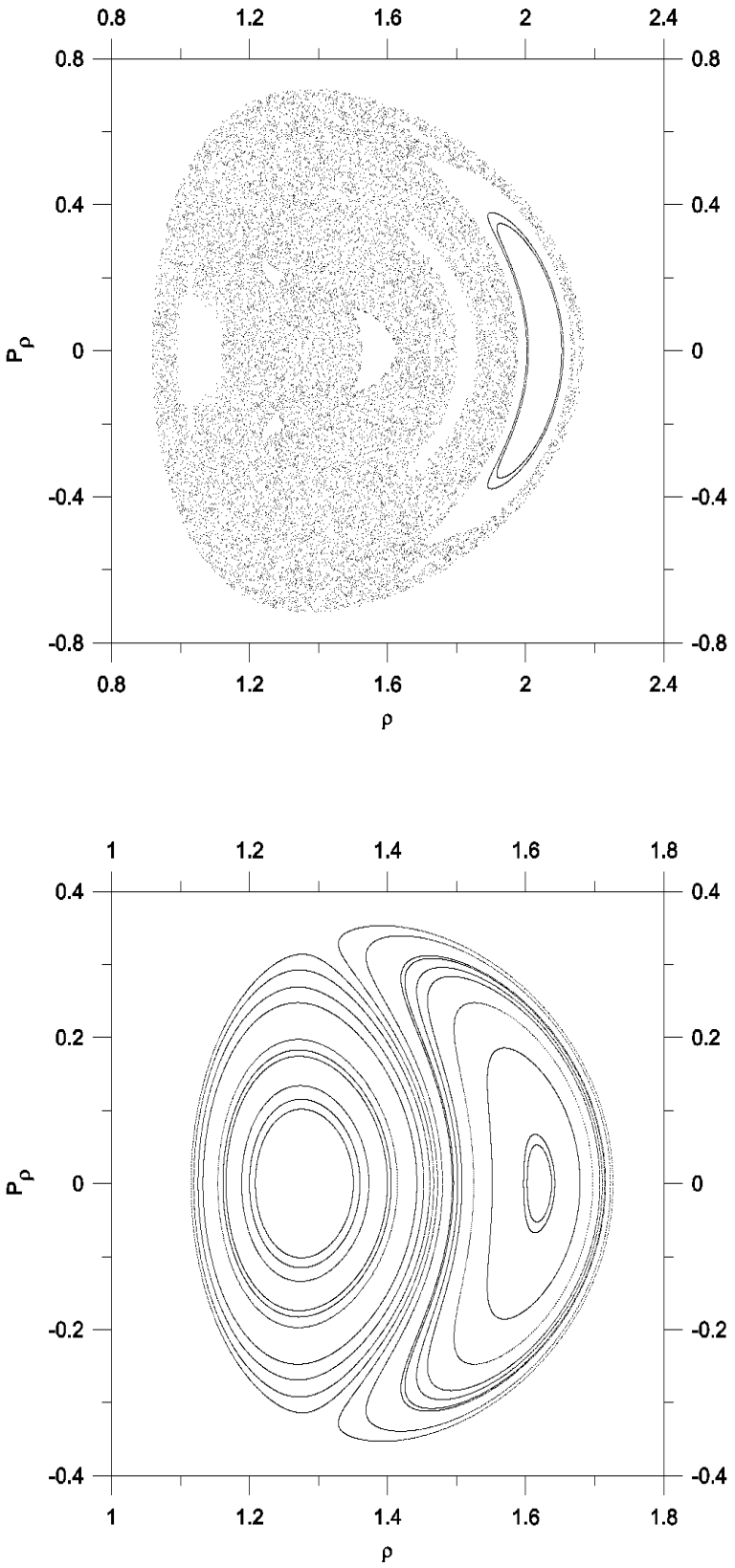

Figure 1.7: (c) **Poincaré sections of the DKP:** ($\hat{z} = 0$ and $\hat{p}_z > 0$) Top: $f = 0.4$, $\hat{L}$ = 1.51; Bottom: $f = 0.1$, $\hat{L} = 1.51$.

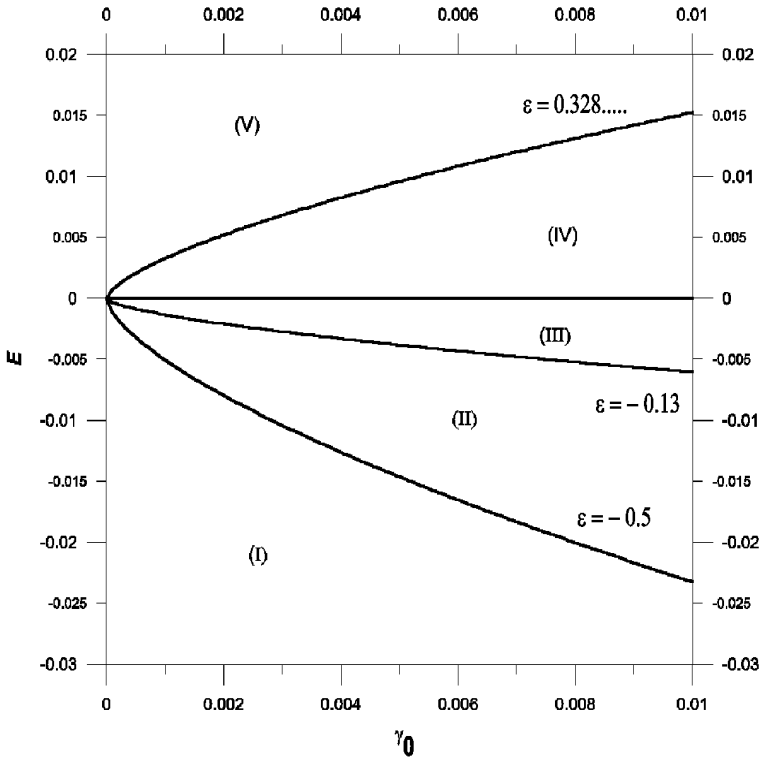

Figure 1.8: **The parameter space of the DKP**: the five main dynamical regions in the $E - \gamma_0$ parameter space.

The structure of the dynamics of the Hamiltonian (1.45) depends on the value of the scaled energy alone. The $E - \gamma_0$ parameter plane can be partitioned into five distinct regions (figure (1.8)) somewhat arbitrarily defined by Tanner, Hansen and Main [1996]:

I. $\epsilon < -0.5$: bounded almost integrable motion;

II. $-0.5 < \epsilon < -0.13$: bounded motion with mixed chaotic and regular motion;

III. $-0.13 < \epsilon < 0.0$: the last large stable island disappear; the dynamics is mostly chaotic;

IV. $0.0 < \epsilon < 0.328782\cdots$: unbounded mostly chaotic motion; the symbolic dynamic is not complete;

V. $0.328782\cdots = \epsilon_c < \epsilon$: unbounded chaotic motion with a complete symbolic description.

In order to illustrate the structure of the classical phase space, one looks at the Poincaré surface of section . At a fixed (scaled) energy the classical motion is confined to the energy shell, which is a three-dinensional subspace of the four-dimensional phase space spanned by (ν, μ, p_ν, p_μ). The Poincaré surface of section is a two-dimensional slice in the three dimensional energy surface. The set of all intersections of a trajectory with this surface (in a certain direction) contains most of the information related to the particular trajectory. Here we choose the surface of section by $\mu = 0$. It can be seen from equation (1.45) that the energy shell for $\mu = 0$ maps into an area bounded by the condition $-2\epsilon\nu^2 + p_\nu^2 = 4$, which defines an ellipse with respect to the coordinates ν and p_ν (see figure (1.9)).

At $\epsilon = -0.8$ the system is still very close to its integrable limit $\epsilon \to -\infty$, which corresponds to the infinitesimally perturbed hydrogen atom. It is important to note that even an infinitesimal perturbation is strong enough to change the phase space structure of the hydrogen atom completely. For a pure hydrogen atom the surface of section would simply give concentric closed curves and each orbit would contribute a fixed point.

As we increase the scaled energy ϵ, irregular motion appears first near the separatrix, as is clearly visible in figure (1.9) for ϵ = -0.5. The separatrix is replaced by a stochastic layer, which fills a finite area in the surface of section. As we further increase the scaled energy, this layer increases in size whereas the large islands related to regular motion become smaller and smaller. Some new island structures embedded in the stochastic layer appear close to the large islands, but they disappear quickly as ϵ is further increased. Finally, for ϵ = -0.1, no regular structure is visible on the surface of section and the classical motion is dominated by global chaos. Some regular motion is

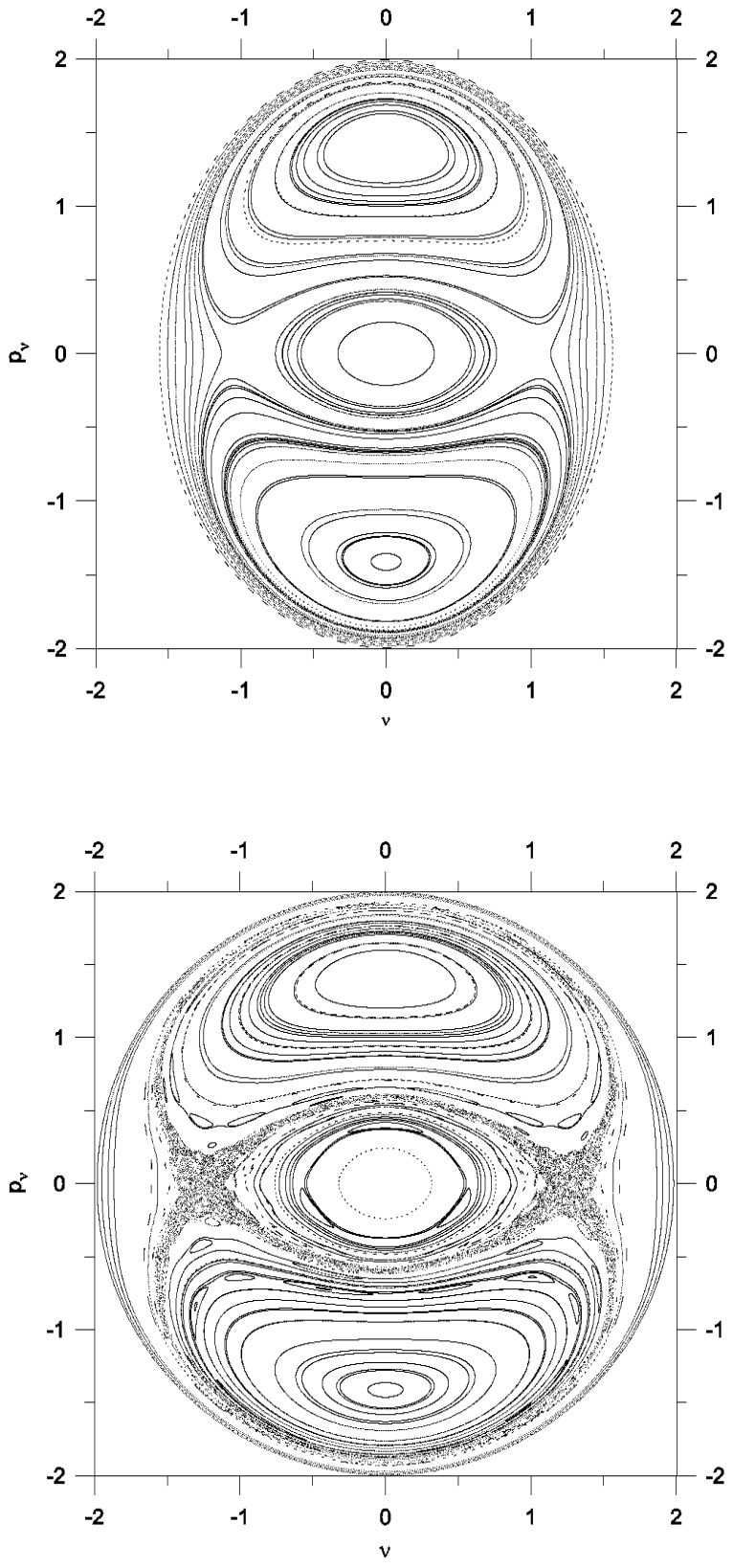

Figure 1.9: (a) **Poincaré sections of the "Pseudo-Hamiltonian" of the DKP:** Top: ϵ = - 0.8; Bottom: ϵ = - 0.5.

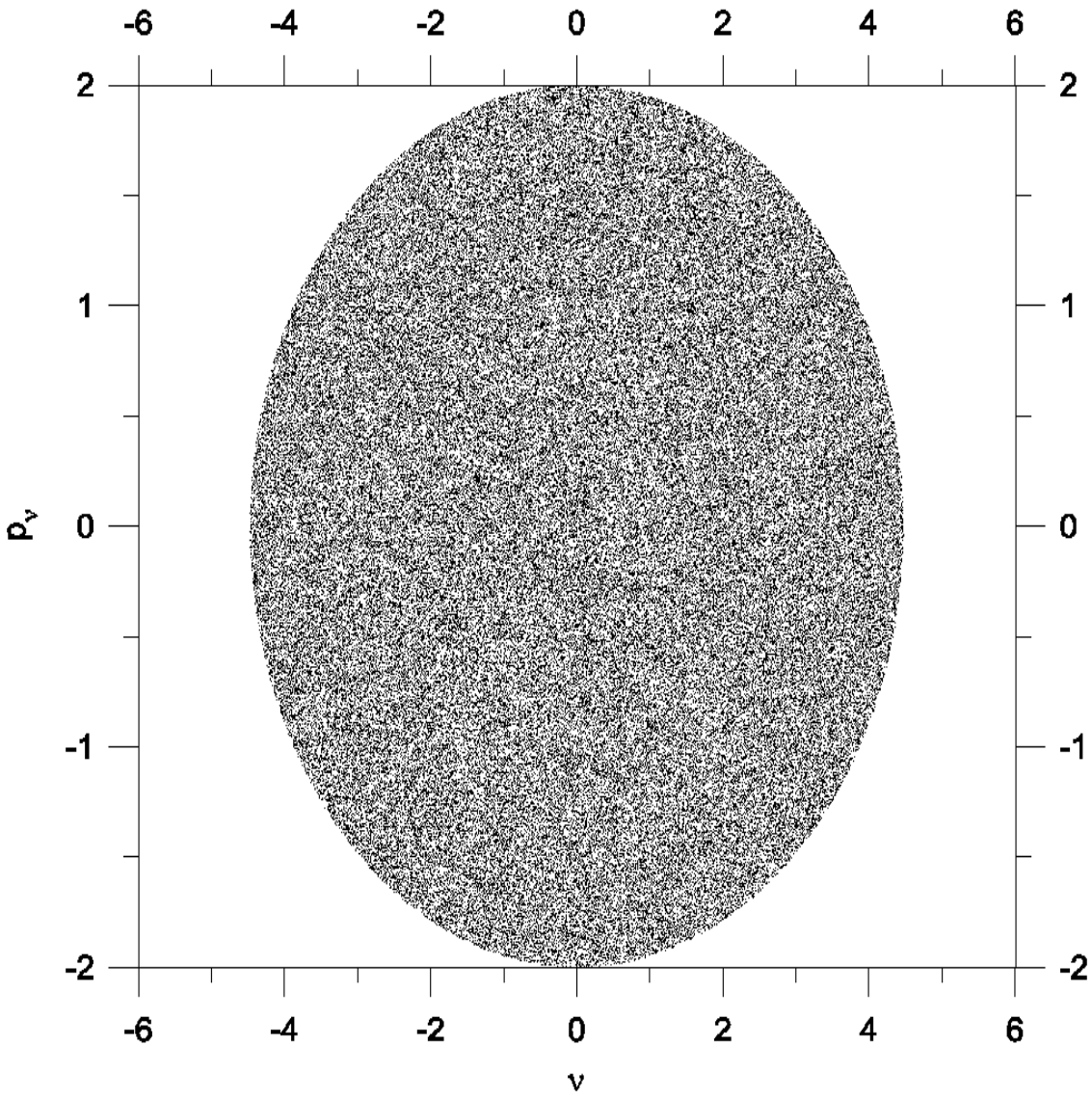

Figure 1.9: (b) **Poincaré section of the "Pseudo - Hamiltonian" of the DKP :** ϵ = - 0.1.

present even for $\epsilon >$ -0.1, but the related elliptic islands are so small that they are not visible on the scale of figure (1.9).

The question that we would like to answer is the following: Is it possible to turn the chaotic behaviour of the electron into regular motion by varying slightly a system parameter (e.g. the magnetic field intensity)? In other words is it possible to stabilize the electron around one of the periodic orbits, embedded in the chaotic region, without changing the system by a large perturbation? In order to answer this question, one must first find the location of periodic orbits embedded in the chaotic sea. This task will be done in chapter 2. Afterwards, one must devise an algorithm to stabilize the electron around one of those periodic orbits; that is the content of chapter 3. Another interesting question that may arise is since in every experiment the system parameters may be allowed to vary, is it possible to maintain the stability of the electron orbit while the system parameters are changing as a function of time? We will address this issue of tracking in chapter 4.

Chapter 2

Detecting Unstable Periodic Orbits

What renders these periodic orbit solutions so precious to us is that they are, so to speak, the only breach through which we may attempt to penetrate an area hithetro deemed inaccessible.
Henri Poincaré
(Les Methodes Nouvelles de la Mécanique Céleste, 1892, Vol 1, §36)

Unstable periodic orbits (UPO) play a fundamental role in the geometrical and dynamical properties of chaotic systems. Their locations are of prime importance in the control of chaos as well as in the calculation of invariant measures. Through the cycle expansion theory, the UPOs provide an essential link between the classical and quantal world. We present two effective methods which provide us with the position of unstable periodic orbits. We discuss the advantages and disadvantages of each method.

2.1 Recurrence Method

Auerbach *et al.*[1987] proposed a recurrence algorithm for extracting periodic orbits from a chaotic time series. In this method one assumes that N elements of the time series $\{\mathbf{X}_i\}_{i=1}^{N}$ are available, with $\mathbf{X}_i$ being points in $\mathcal{R}^2$. If N is sufficiently large, the

time series will visit the neighbourhood of an arbitrary period-n cycle point at some time i, due to the ergodicity of chaotic trajectories. (The Poincaré recurrence theorem which explains this feature of chaotic trajectories is discussed in [Jackson, 1989]). At time $i+1$ the time series will be in the vicinity of another point of that cycle and so on. After n iterations the time series will again visit the neighbourhood of the initial period-n cycle point, under the assumption that n time steps previously the sequence was sufficiently close to it. Obviously this process will not last forever and after few cycles the trajectory will spread over the phase space. This idea is used to locate the periodic orbits by scanning the time series for pairs of points separated by n time steps that are within a small preassigned spatial distance r_1 of one another. At this stage all points in the time series which return after n steps are located and must now be grouped into periodic cycles. Throughout the length of the run, the vicinity of a particular periodic point may have been visited many times. In order to decide whether two nearly periodic orbits in the time series correspond to distinct periodic orbits, their positions relative to each other are verified. If all the corresponding pairs of points of the two orbits are less than a preassigned distance r_2, then they are grouped into the same periodic cycle. Otherwise, they represent distinct periodic cycles. The position of a point belonging to a true unstable n-cycle is then estimated by the center of mass of all points in the time series which were found to correspond to it. It is clear that the resulting point may not belong to the original time series. The two externally assigned parameters r_1 and r_2, used in the process, are chosen by the following criteria: r_1 is chosen large enough to include several sequences corresponding to a particular periodic orbit. The distance between cycles, r_2, is set small enough so as to distinguish between distinct periodic orbits under the condition that $r_2 > r_1$. The correct grouping should not change with an increase in the length of the time series. The advantage of the recurrence method is that it does not need the mathematical form of the map, which is the case for the Poincaré surface of section of a Hamiltonian flow. As was shown in chapter 1, all we know from a Poincaré section, is that all points on this plane come

from the natural evolution of a dynamical system, but we do not have any function that iteratively produces these points on the plane. In order to do a systematic study we start testing this method on the dissipative Hénon map (DHM), then we will extend its application to the Poincaré sections of Hamiltonian flows.

Figure (2.1) shows the location of a fixed point (period-1) for the Hénon map written in the form

$$\begin{pmatrix} x_{n+1} \\ y_{n+1} \end{pmatrix} = \begin{pmatrix} \mu - x_n^2 - \epsilon y_n \\ x_n \end{pmatrix} \tag{2.1}$$

with $\mu = 1.4$ and $\epsilon = -0.3$.
Here we use this mapping only to generate a sequence of data whereafter the mathematical form of the map is no longer used. This map enables us to compare the results from recurrence method with the exact analytical solution. It is clear from the above equations that for the fixed point we must have $x^* = y^* = \frac{-\epsilon - 1}{2} \pm 1/2[(1+\epsilon)^2 + 4\mu]$ which is $x^* = y^* = 0.88389626$ for the chosen constants. This should be compared with $x^* = 0.883892$ and $y^* = 0.884215$ shown in figure (2.1). This shows the limitation of the center of mass estimation, but also indicates that the method can give reliable results.

We have also obtained the periodic orbits for the Hénon - Heiles potential and DKP using the recurrence method. Figure(2.2) shows period-1 and period-3 cycles for the Hénon - Heiles potential and figure (2.3) shows period-2 and period-3 cycles for DKP.

A disadvantage of the recurrence method is that it needs very long time series (N very large). For DHM we used 2×10^5 points. In order to obtain the periodic orbits for Hamiltonian flows we have used over 10^6 points on the Poincaré section to reach the accuracy obtained in figures(2.2) and (2.3). Recalling that between every two consecutive points on the Poincaré surface of section there is a segment of trajectory in the phase space which must be calculated by an integration algorithm, one can see that it is a very CPU intensive task to produce a section with as many points on it. An

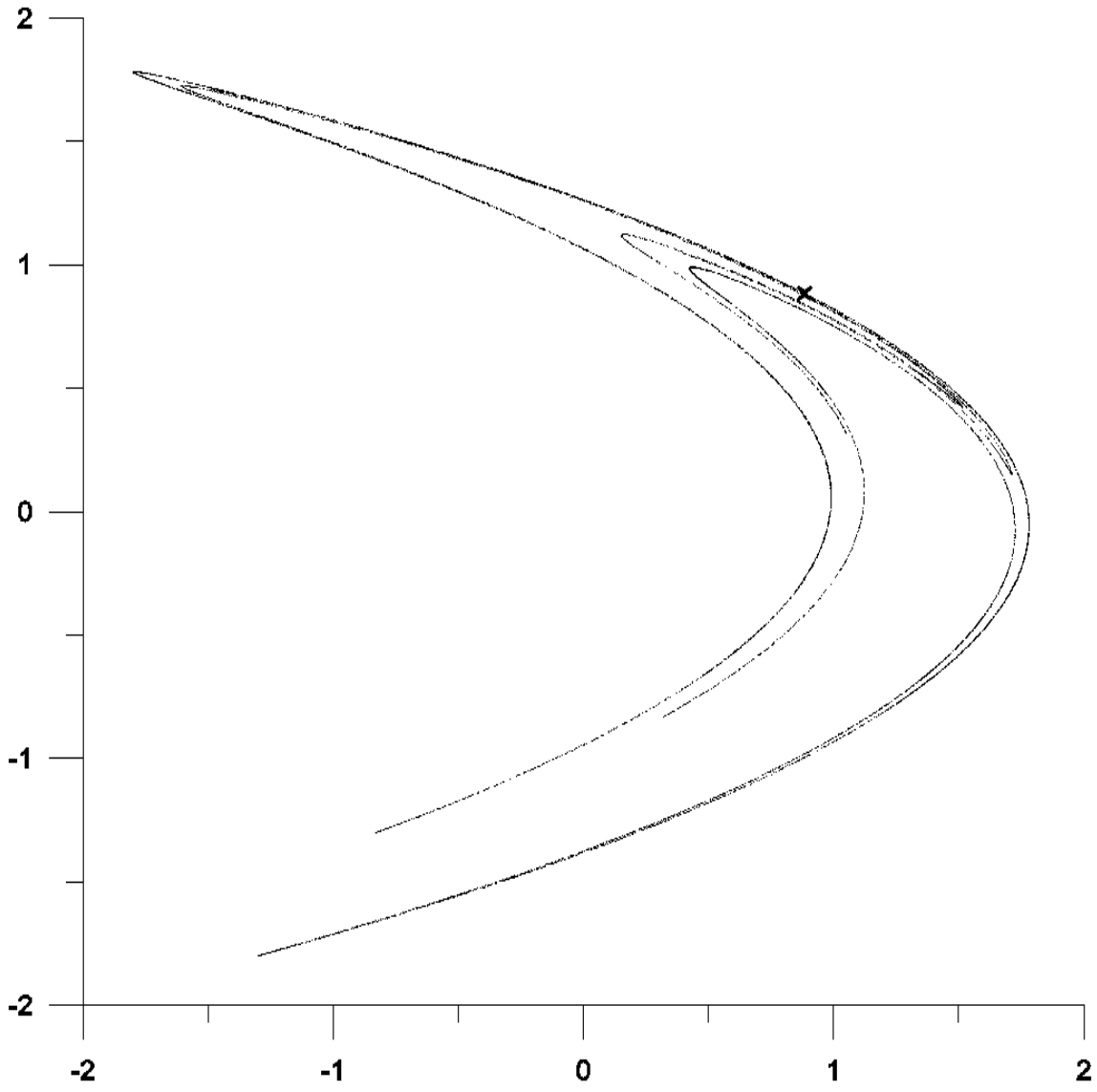

Figure 2.1: **Fixed point of the dissipative Hénon map detected by the recurrence method:** $x^* = 0.883892$, $y^* = 0.884215$, $\mu = 1.4$ and $\epsilon =$ - 0.3 (horizontal axis: x, vertical axis: y).

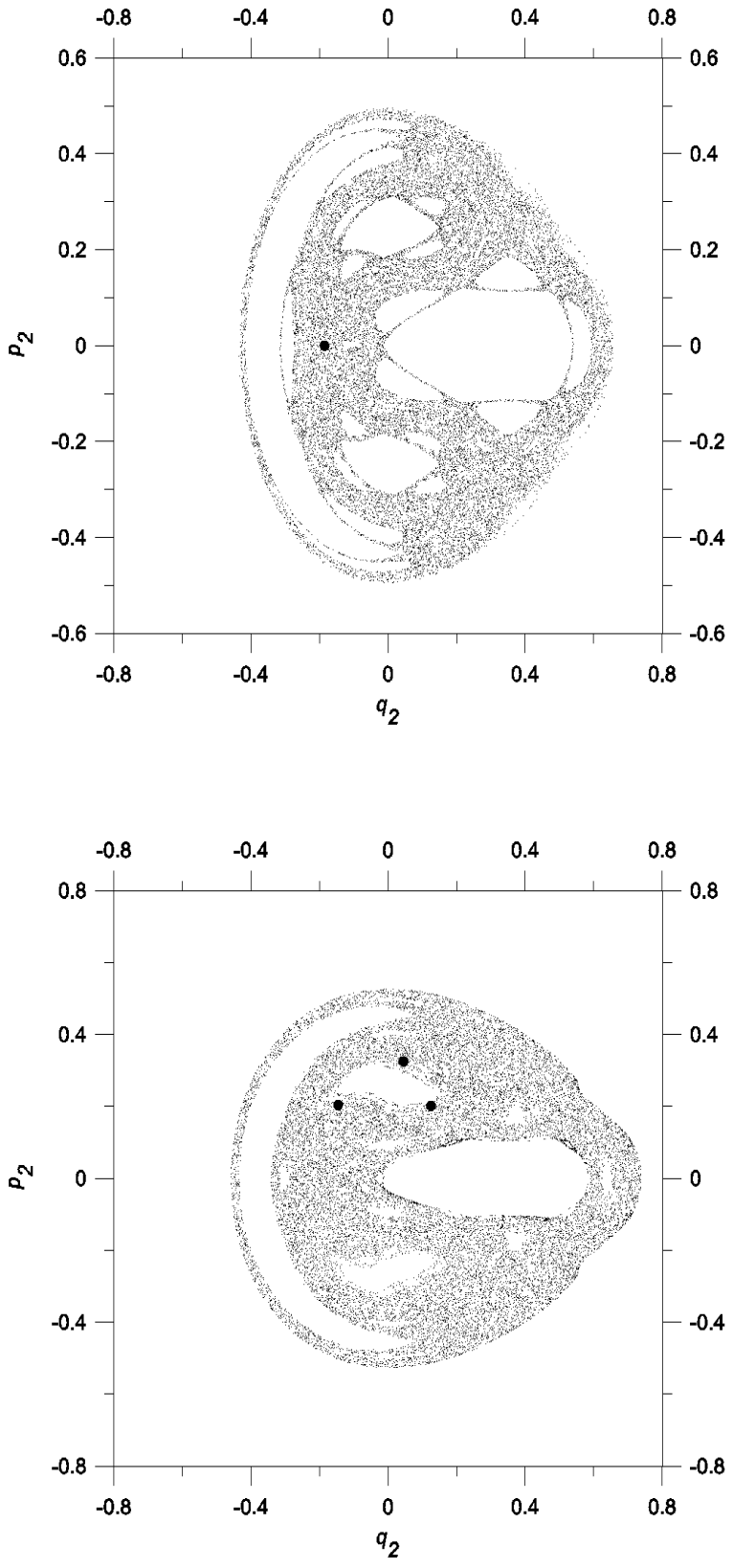

Figure 2.2: **Periodic cycles on the Poincaré section of the Hénon - Heiles potential:** Top: Period - 1 cycle (E = 0.125). $q_2^* = -0.185468$ and $p_2^* = -0.00018723$. Bottom: Period - 3 cycle (E = 0.14). $q_{2_1}^* = 0.1255501$, $p_{2_1}^* = 0.2017429$, $q_{2_2}^* = -0.1458445$, $p_{2_2}^* = 0.204073$, $q_{2_3}^* = 0.04480447$, $p_{2_3}^* = 0.3252957$.

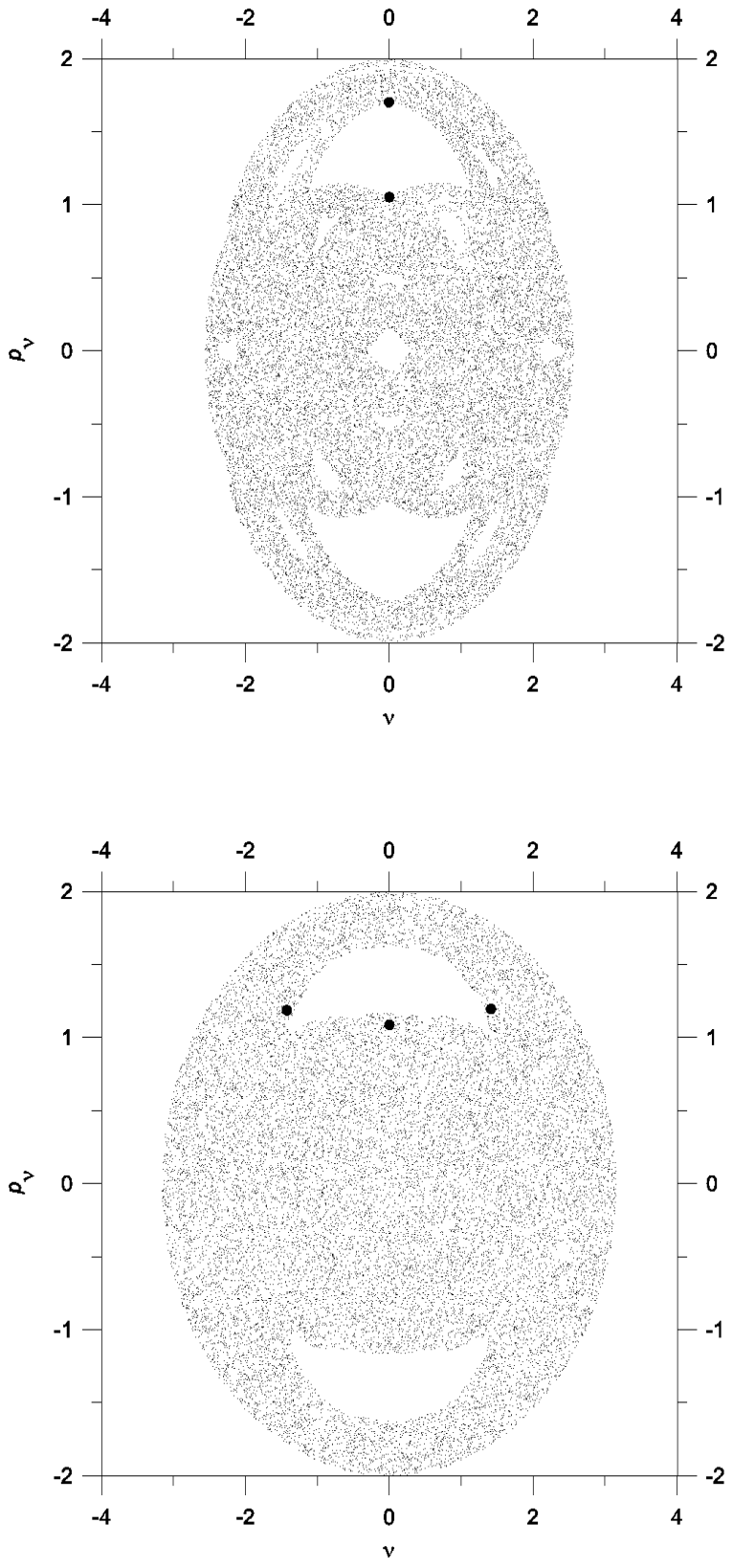

Figure 2.3: **Periodic cycles on the Poincaré section of the DKP:** Top: Period - 2 cycle(ϵ = - 0.3). $\nu_1^* = -0.00334025$, $p_{\nu_1}^* = 1.70168$, $\nu_2^* = 0.001787469$, $p_{\nu_2}^* = 1.051106$. Bottom: Period - 3 cycle (ϵ = - 0.2). $\nu_1^* = -1.42218$, $p_{\nu_1}^* = 1.18476$, $\nu_2^* = 1.415831$, $p_{\nu_2}^* = 1.195062$, $\nu_3^* = 0.003226735$, $p_{\nu_3}^* = 1.086226$.

important improvement over the "brute force" method just described, can be achieved in the following way. We choose M points on the Poincaré section (M relatively large, but much smaller than N) as initial conditions for M trajectories, and start integrating each point until it produces the n^{th} return on the Poincaré section (for period-n). If the initial point is closer to the n^{th} return point than r_1(defined earlier), we accept the initial point as belonging to a period-n cycle, otherwise we reject it and move to the next. As before we group the accepted points to obtain all distinct period-n cycles. If the M initial points are spread densely and uniformly, then ergodicity guarantees that the result from the first algorithm would be the same as the result from the second one. We call this method the "modified reccurence method (MRM)". We can also take advantage of the symmetries on the Poincaré surface of section of the Hamiltonian flows. For example, for DKP one can see from figure (1.9) that the mapping is symmetric with respect to both ν and p_ν axes. Therefore we only need to spread the initial conditions over one quarter of the mapping, which means that we can select a smaller set of initial conditions or provide a denser distribution.

Another improvement is that in order to reach a higher accuracy, instead of executing the above algorithm only once, we can repeat the same algorithm as many times as it is desired. After the first run we collect the accepted points. Then we take any of those points and choose a small box (of size δ on each side) with that particular point at the center of the box. Now, within that box we select a new set of initial points and we run the algorithm for the second time. The results of the second run are more reliable than the first one, because in the former case the probability of closeness of an initial condition to its n^{th} return map (for period-n) is much higher than the latter case, and consequently the center of mass of the points gives a better estimation of the position of a periodic orbit. Our experiments show that usually after four or five applications of the process, no further improvement in the accuracy is observed.

It is important to note that not all the points obtained in this way are unstable. For

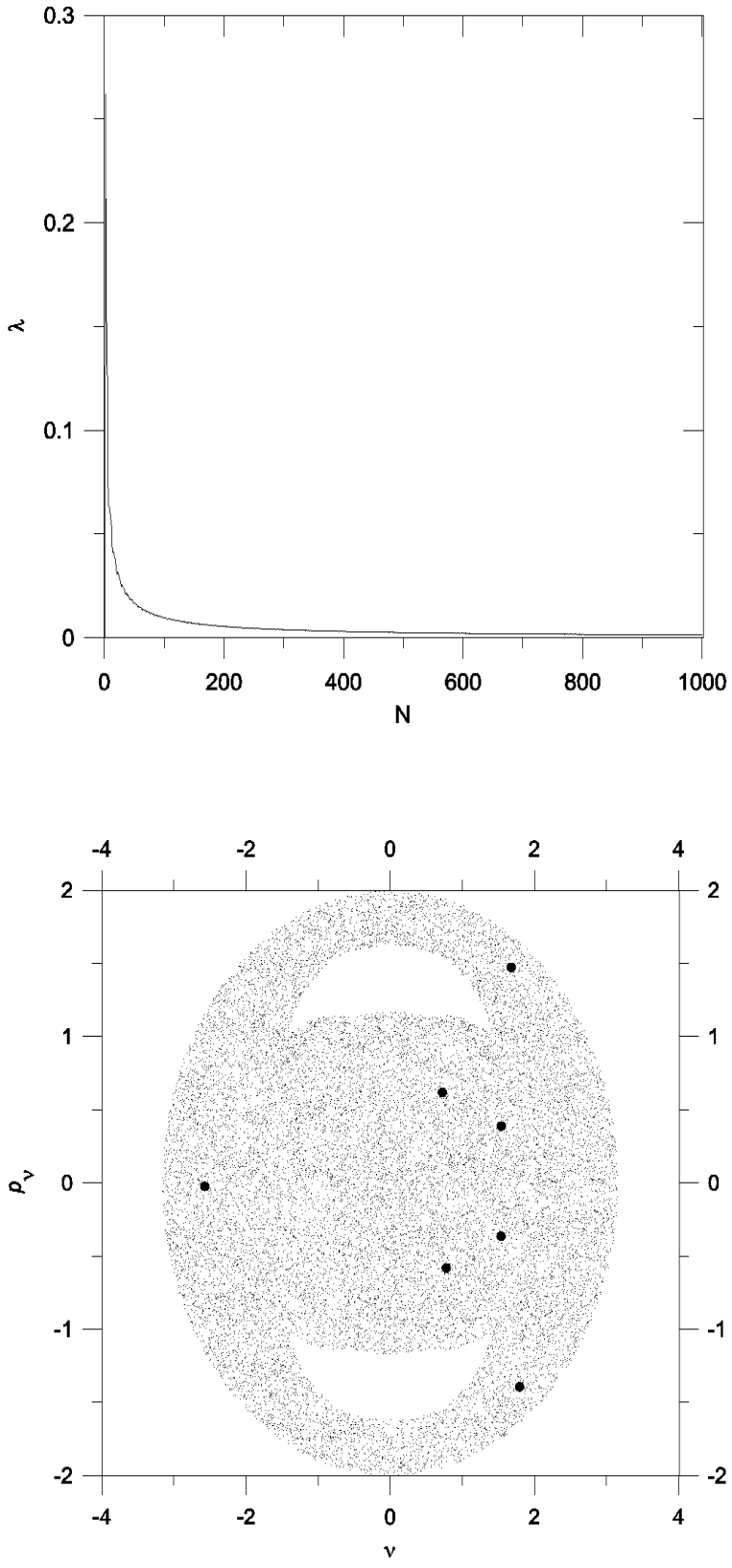

Figure 2.4: **The Poincaré section of the DKP:** A period - 7 stable cycle ($\epsilon = -0.2$, $\nu_1^* = 1.538$, $p_{\nu_1}^* = -0.3656$). For better visibility we mapped these points over the chaotic sea surrounding them. The Lyapunov exponent curve (top) confirms the stability of the trajectory.

example figure(2.4) shows a period-7 orbit for DKP resulting from recurrence method. The Lyapunov exponent for this trajectory is zero indicating a stable orbit. The seven points indicated in figure (2.4), represent 10^4 iterates on the Poincaré section, indeed very stable!

2.2 Stability Transform Algorithm

As mentionned in the previous section, the difficulty with the algorithms based on the return map is that the time series must be very long. So *et al.*[1997], and Schmelcher and Diakonos [1997a, 1997b, 1998] and Diakonos, Schmelcher and Biham [1998] have recently developed two different methods to overcome this difficulty. The first method reported a successful detection of an unstable period-1 for Hénon map using a time series of only 1200 elements and with the relative error of 10^{-3} with respect to the exact value. With the second algorithm it is possible to obtain the same point by using a time series of barely 100 elements and a relative error of 10^{-17} with respect to the exact value! We have successfully extended to area-preserving maps the method of Schmelcher and Diakonos originally developed to treat dissipative dynamics. We call the method the "stability transform algorithm (STA)". The STA can be explained as follows [Schmelcher and Diakonos, 1997a].

Let us consider an N-dimensional discrete chaotic dynamical system given by

$$U : \mathbf{x}_{i+1} = \mathbf{F}(\mathbf{x_i}). \tag{2.2}$$

The goal is to construct from equation (2.2) other dynamical systems S_k with the same number of fixed points, still at their original positions, but having become *stable* through the transformation

$$L_k : U \to S_k. \tag{2.3}$$

The effect of the transformation L_k is therefore to change the stability properties but

not the locations of the fixed points. Because of the stability of the fixed points in the constructed system S_k, every trajectory of S_k converges after a finite number of iterations to a fixed point x^*. Per construction x^* is then also a fixed point of the original system U. To fullfill the requirement of the one to one correspondence between the fixed points of U and S_k, the transformation L_k should in general be linear. Consequently S_k takes the following form

$$S_k : \mathbf{x_{i+1}} = \mathbf{x_i} + \mathbf{\Lambda}_k(\mathbf{F}(\mathbf{x_i}) - \mathbf{x_i}) \tag{2.4}$$

where $\mathbf{\Lambda}_k$ is an invertible constant $N \times N$ matrix. By suitable choices of $\mathbf{\Lambda}_k$ one can stabilize the fixed points of the transformed system S_k. In general, different fixed points are stabilized by different transformed systems S_k corresponding to different matrices $\mathbf{\Lambda}_k$. It turns out that if the absolute values of the elements of the matrices $\mathbf{\Lambda}_k = \lambda \mathbf{C}_k$ $(0 < \lambda \ll 1)$ are sufficiently small, there exists a universal set of very restrictive matrices $\mathbf{C}_k$ such that at least one matrix belonging to this set transforms a given unstable fixed point of U to a stable fixed point to the corresponding S_k.

Schmelcher and Diakonos [1998] showed that these matrices are made of elements $c_{ij} \in \{0, \pm 1\}$ such that each row or column contains only one element which is different from zero. The number of such matrices is $2^N N!$. Thus, for a two-dimensional map there are 8 matrices, namely

$$\begin{pmatrix} \pm 1 & 0 \\ 0 & \pm 1 \end{pmatrix} \qquad \text{and} \qquad \begin{pmatrix} 0 & \pm 1 \\ \pm 1 & 0 \end{pmatrix}. \tag{2.5}$$

The method can easily be extended to find the unstable points of period-n cycles. All one has to do is to replace $\mathbf{F}(\mathbf{x_i})$ in equation (2.4) by its n^{th} iterate $\mathbf{F^{(n)}}(\mathbf{x_i})$.

Figure (2.5) shows the application of the STA to the Hénon map. It clearly shows that the successive iterates converge towards the periodic point. The result is in perfect agreement with the exact value. Note that in this case only 100 iterates were used. Figure (2.6) shows a period-2(stars) and a period-7 cycle (circles) for the same mapping. The method is implemented in the following way.

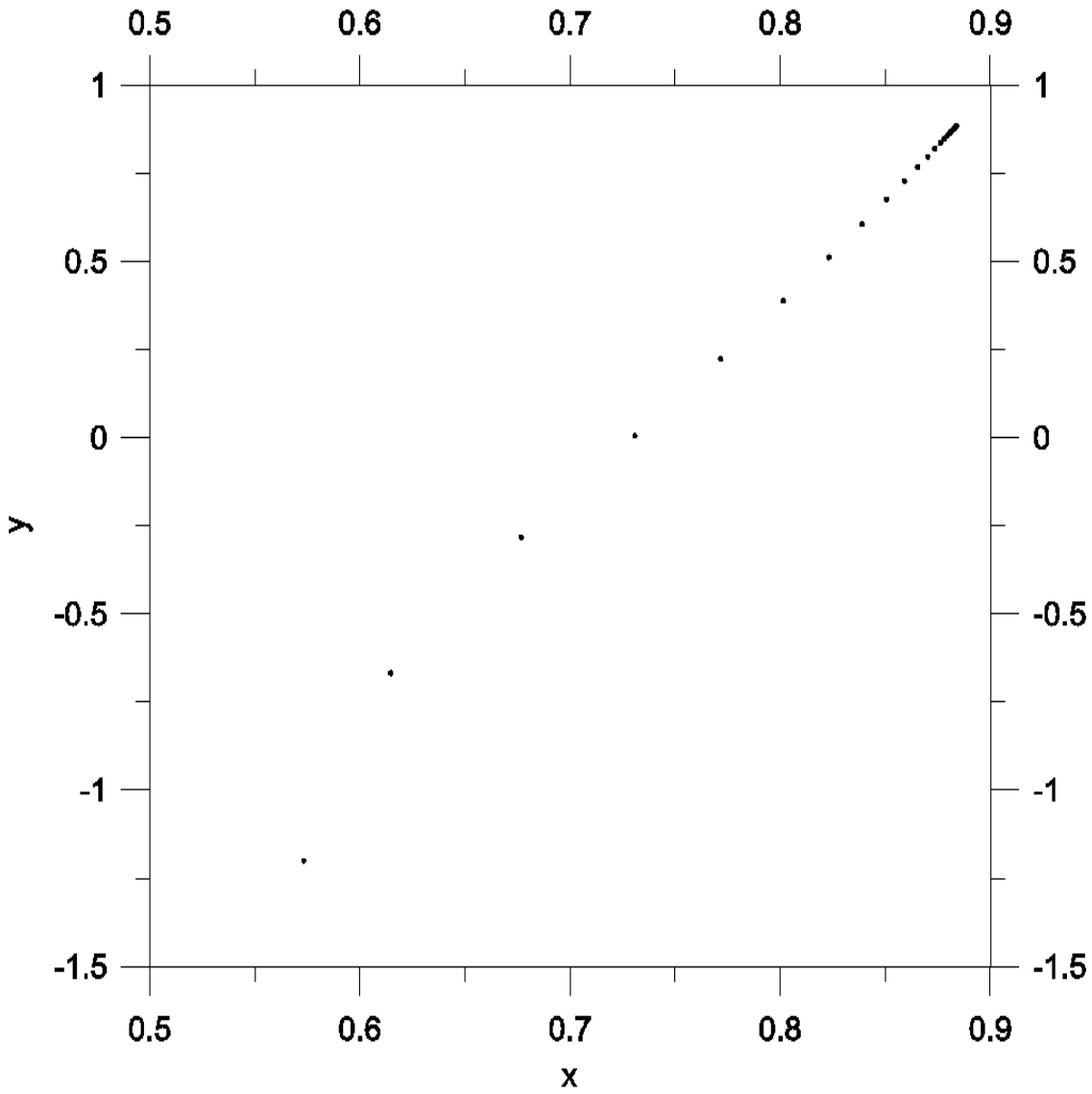

Figure 2.5: **A fixed point for dissipative Hénon map obtained by STA.** $\lambda = 0.3$, $x^* = y^* = 0.883896$. The initial point is at the bottom left corner of the graph and after 100 iterations using STA the points converge towards the fixed point at the top right corner of the graph ($\epsilon = -0.3, \mu = 1.4$).

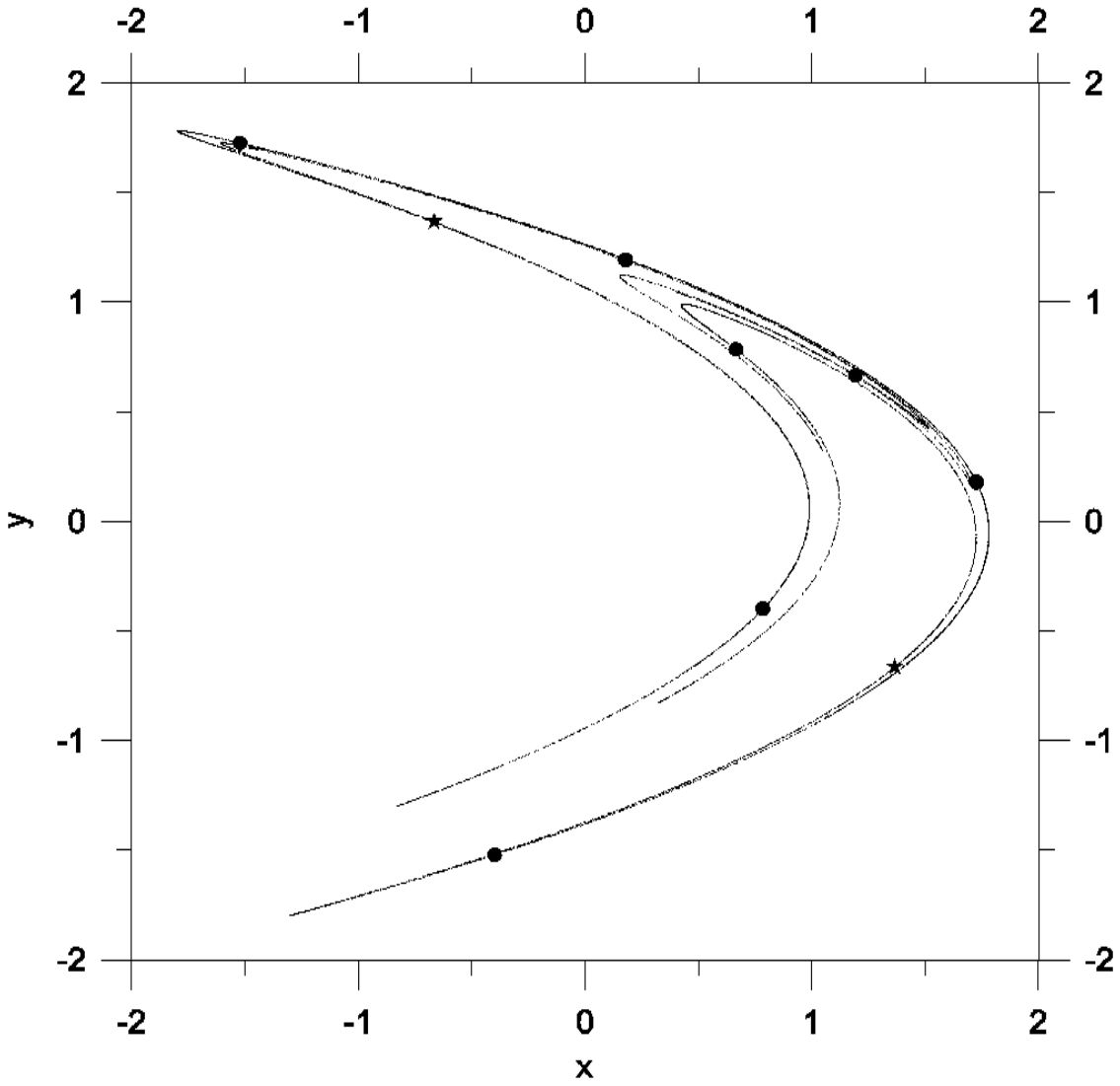

Figure 2.6: **The Dissipative Hénon Map:** Periodic orbits obtained by STA. A period - 2 cycle (stars) and a period - 7 cycle(circles) ($\epsilon = -0.3, \mu = 1.4$).

We choose a starting point $\mathbf{x_0}$, one of the matrices $\{\mathbf{C_k}\}$ and a value for λ. Using equation (2.4) we obtain the successive values $\mathbf{x_1}, \mathbf{x_2}, \cdots$. This sequence either converges to a point $\mathbf{x}^*$ or it escapes to infinity. In the former case we accept the result as a fixed point or a period-n point. We then take another matrix from the set $\{\mathbf{C_k}\}$ and repeat the process. After testing all 8 matrices, we choose another starting point and repeat the procedure. By choosing a uniformly distributed array of points as initial conditions, one can make sure that all the periodic orbits are captured.

As the first case for area-preserving maps, we apply the STA to the standard map. Figure (2.7) shows the points obtained for period-2 ($K = 1.25$). It is important to mention that while the stability transform changes the stability properties of unstable fixed points, it does not alter originally stable points. Therefore among the points obtained by this method, some are stable and others are unstable.

As the second application we applied the STA to the Crémona map. Figure(2.8) shows a period-5 cycle for the Crémona map ($\epsilon = 1$ and $\mu =$ - 0.4224).

When we apply the STA to the Poincaré section of a Hamiltonian flow, we encounter a serious limitation. In this case the only periodic orbits that have been detected so far were period-1 (fixed points). For higher periodic orbits the method fails to detect the orbits other than period-1, which is obviously the correct answer to any period-n otbit. It remains an open question why the STA cannot detect the period-n cycles ($n \neq 1$) on the Poincaré section of Hamiltonian flows. Nevertheless the method maintains its efficiency for $n = 1$. In this case only after 250 iterates, the fixed points are detected which is remarkable if one compares with the computational effort necessary in the case of the recurrence method. Figures (2.9) and (2.10) show the fixed points obtained by the STA for the Hénon - Heiles potential and the DKP respectively.

It is worth mentionning that we have collected a wealth of information on the

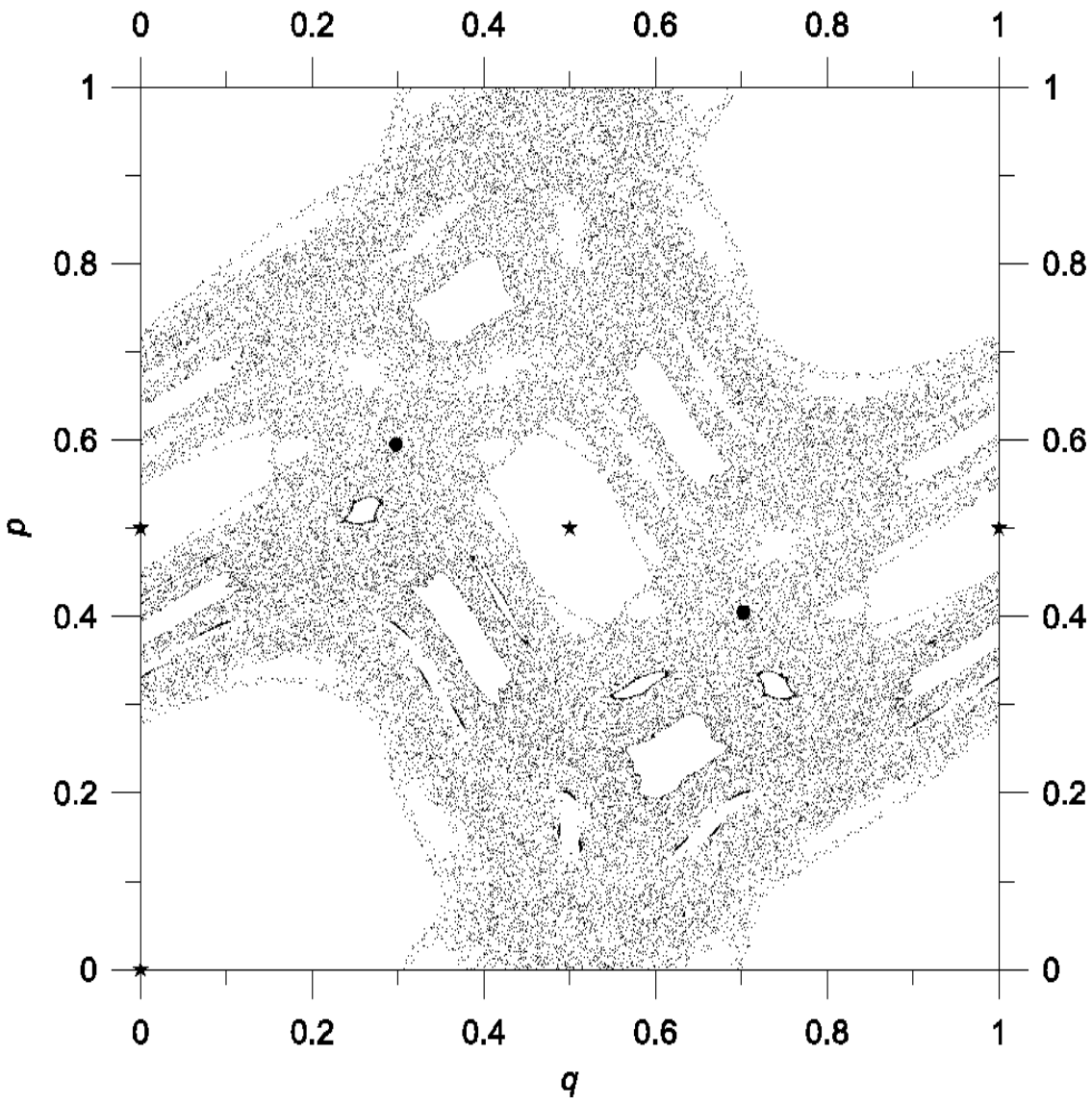

Figure 2.7: **A set of period-2 cycles of the standard map ($K = 1.25$) obtained by STA:** Circles represent the unstable orbit while stars show the stable orbits($\lambda = 0.3$).

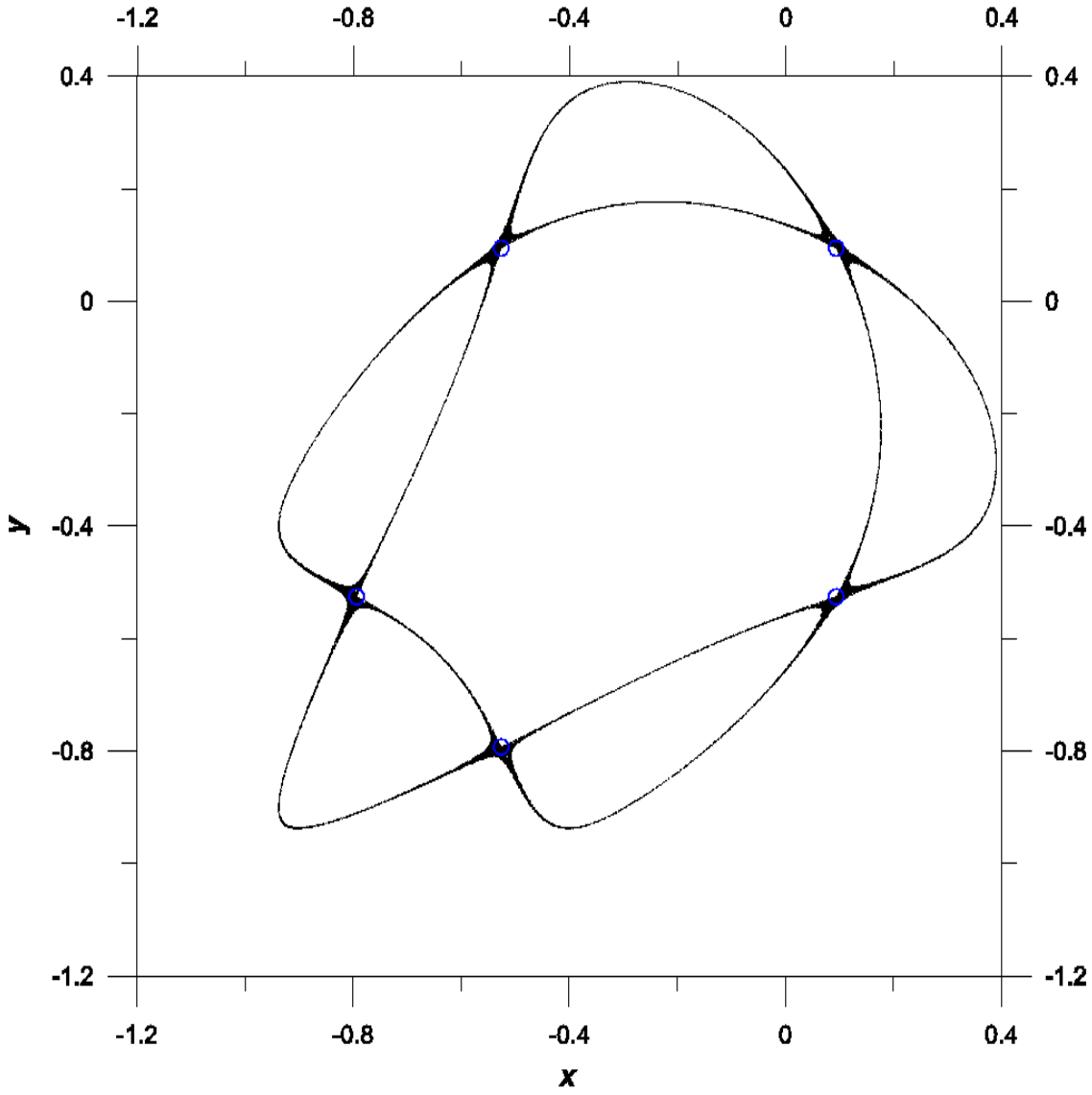

Figure 2.8: **A period - 5 cycle for the Crémona map obtained by STA.** Only 100 iterates were used to detect one of the periodic points.

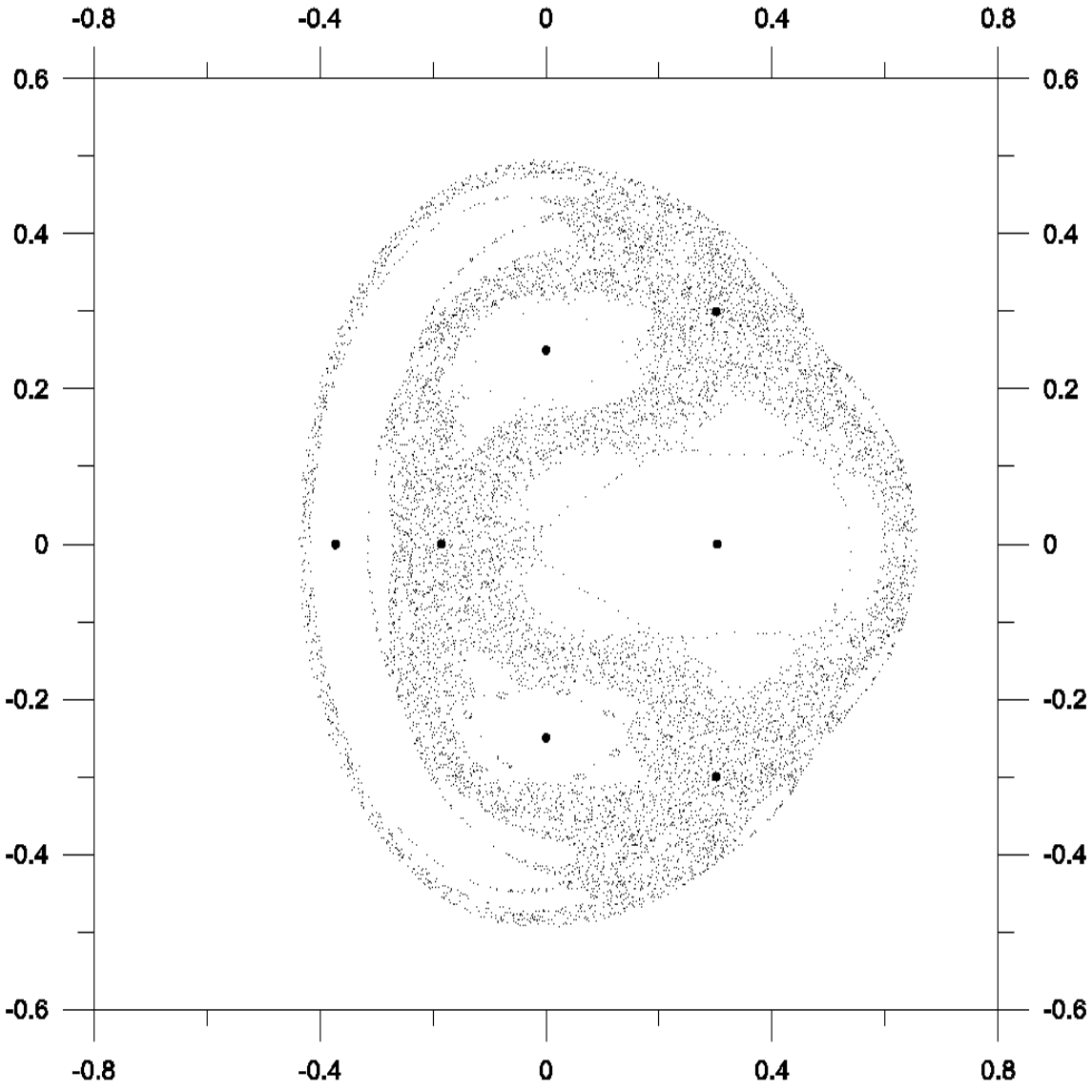

Figure 2.9: **Fixed points for the Hénon - Heiles potential:** A set of period-1 cycles for $E = 0.125$. In order to detect these points 1000 initial conditions were used, each of which was iterated 250 times. The same calculation was repeated for every $\mathbf{C}_k$.

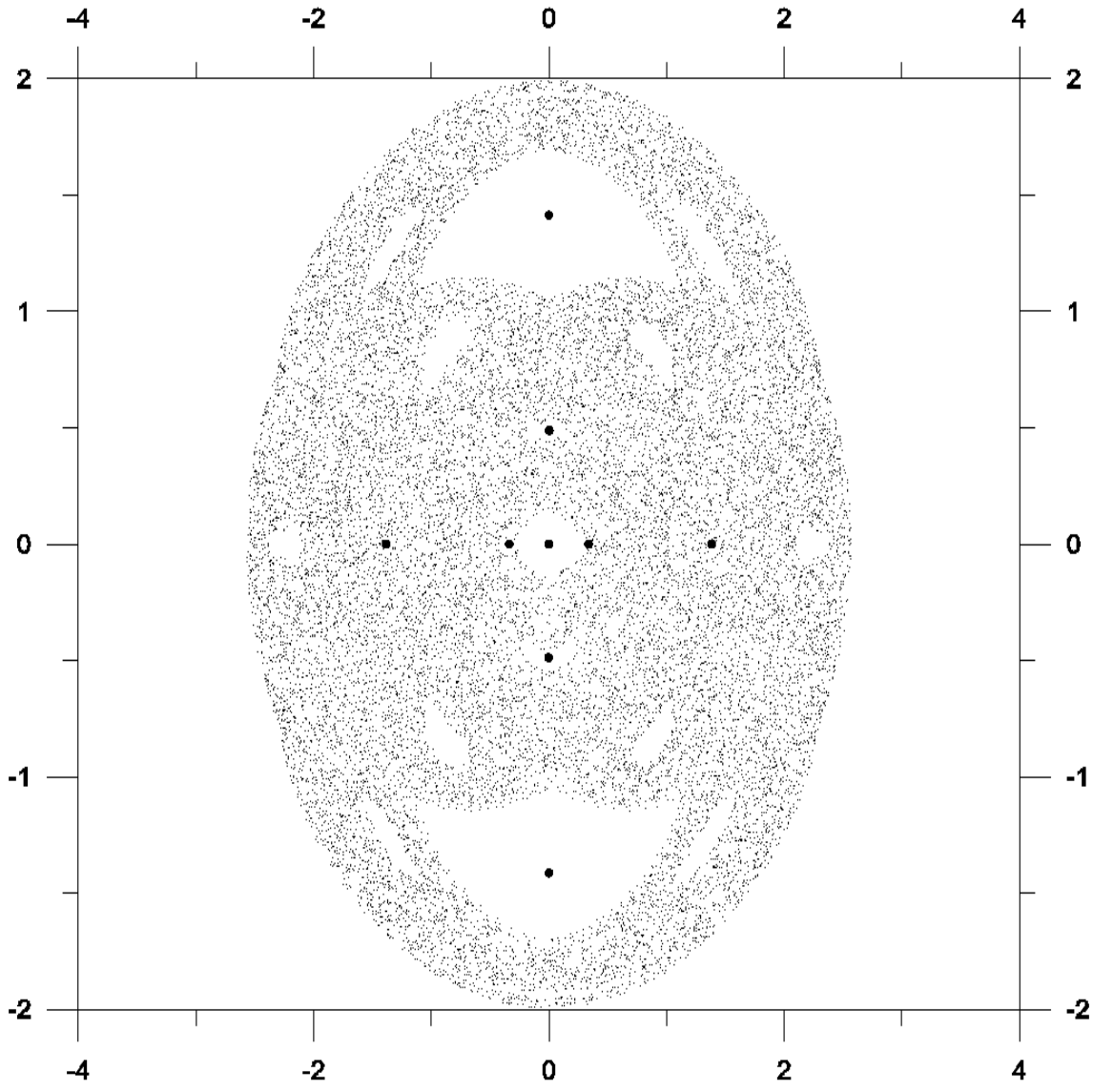

Figure 2.10: **Fixed points of the DKP obtained by STA:** A set of period-1 cycles for ϵ = - 0.3. In order to detect these points 1000 initial conditions were used, each of which was iterated 250 times. The same calculation was repeated for every $\mathbf{C}_k$.

Map	Parameter(s)	Period	x^*	y^*
DHM	$\epsilon = -0.3$, $\mu = 1.4$	1	-1.58389	-1.58389
DHM	$\epsilon = -0.3$, $\mu = 1.4$	2	-0.66612	1.36612
DHM	$\epsilon = -0.3$, $\mu = 1.4$	7	-1.46535	1.65652
DHM	$\epsilon = -0.3$, $\mu = 1.4$	11	-1.42604	1.64998
Standard	K = 1.25	2	0.297534	0.595068
Standard	K = 1.25	5	0.17033	0.67033
Standard	K = 1.25	7	0.418255	0.836511
Standard	K = 1.25	11	0.502424	0.954342
Crémona	$\epsilon = 1$, $\mu = -0.4224$	5	-0.525669	0.0943363
Hénon -Heiles	$E = 0.125$	1	-0.185468	-1.87239810^{-4}
Hénon -Heiles	$E = 0.14$	3	0.1255501	0.2017429
DKP	$\epsilon = -0.3$	2	-3.34025×10^{-3}	1.70168
DKP	$\epsilon = -0.2$	3	-1.42218	1.18476
DKP	$\epsilon = -0.1$	1	-1.050112×10^{-4}	1.41422

Table 2.1: **Position of periodic cycles for different maps**: Numerical values of the position of a number of periodic orbits belonging to different maps. Only one member of a periodic cycle represents its cycle in this table.

position of unstable fixed points as well as the control parameters (will be discussed later) for different parameter values of the systems discussed earlier. In this chapter we selected only a small subset of those points which are representative for the behaviour of those systems. The numerical data corresponding to this subset are summarized in table (2.1).

In summary, we have developed a reliable and robust method for the detection of UPOs in area-preserving maps. For Hamiltonian flows obtained from Poincaré sections a mixture of modified recurrence method (MRM) and STA is, at present, necessary to detect orbits of period higher than one. As we will see shortly, the unstable periodic orbits are essential for a successful control of the dynamics in the chaotic regime. How this can be achieved is explained in the next chapter.

Chapter 3

Controlling Hamiltonian Systems

Chaos often breeds life, when order breeds habit.
Henry Brooks Adams
(The Education of Henry Adams)

In this chapter we will discuss the algorithm proposed by Ott, Grebogi and Yorke [1990] whose aim is to stabilize the chaotic behaviour of a nonlinear system around one of the selected periodic orbits embedded in the chaotic region of its phase space. We report *for the first time* the successful control of the chaotic behaviour of the Hénon - Heiles Hamiltonian as well as the diamagnetic Kepler problem (DKP).

The hallmark of deterministic chaos, an extreme sensitivity to initial conditions, suggests that chaotic systems might be difficult if not impossible to control, since any perturbations used to control would grow exponentially in time. Indeed, this quite reasonable view was widely held until only a few years ago. Surprisingly, the basis for controlling chaos is provided by just this property, which allows carefully chosen, tiny perturbations to be used for stabilizing virtually any of the unstable periodic orbits

making up a strange attractor. Ergodicity [Eckmann and Ruelle, 1985] is another property of chaotic systems that makes them particularly amenable to control, since most points of interest are eventually visited in the evolution of the system.

Research on controlling chaotic systems has experienced a remarkable growth in a short time span, with the first studies in the field appearing only ten years ago. In the late 1980s, Hübler and co-workers [1988] carried out a series of studies on manipulating chaotic systems to achieve a desired "goal dynamics" with forcing terms appropriately incorporated into the corresponding governing equations. In 1990, Ott, Grebogi and Yorke introduced a linear feedback method (called hereafter the OGY method) for stabilizing unstable periodic orbits in chaotic systems, which did not require a knowledge of the governing equations [Ott, Grebogi and Yorke, 1990; Auerbach *et al.*, 1992; Ditto, Spano and Lindher, 1995].

The OGY method is based on the idea of stabilization of a periodic orbit embedded in a chaotic system. In this method we linearize the system in a neighbourhood of a target orbit and apply a small perturbation to the system such that when a trajectory enters the neighbourhood it can be made to converge to the target. The OGY method has generated widespread interest, and various modifications and reductions of the scheme soon followed [Shinbrot *et al.*, 1993; Alsing, Gavrielides and Kovanis, 1994a, 1994b; Epureanu and Dowell, 1998; Yagasaki and Uozumi, 1998a, 1998b] as well as alternative approaches [Pyragas, 1992; Rollins, Parmanada and Sherard, 1993; Kittel, Pyragas and Richter, 1994; Bielawski, Derozier and Glorieux, 1994; Jackson, 1997; Feudel and Grebogi, 1997; Fouladi and Valdivia, 1997; Löcher, Johnson and Hunt, 1997; Mascolo and Grassi, 1997; Schuster and Stemmler, 1997; Chau, 1998; Ushio and Yamamoto, 1998; Osipov, Kozlov and Shalfeev, 1998; Yang, 1998; Góra and Boyarsky, 1998; Just *et al.*, 1998; Pisarchik, Kuntsevich and Corbalán, 1998; Sinha and Gupte, 1998; Bolotin *et al.*, 1999]. Soon after OGY method was published, strikingly successful applications of the method in the experimental systems began to appear. Ditto, Rauseo

and Spano [1990] reported the first example of experimental chaos control in which the unstable period-1 and period-2 orbits of a chaotically oscillating magnetoelastic ribbon were stabilized. Other demonstrations of experimental chaos quickly followed, including the stabilization of unstable periodic orbits in a driven diode circuit [Hunt, 1991], a multimode laser with an intracavity crystal [Roy *et al.*, 1992], a thermal convection loop [Singer, Wang and Bau, 1991] and the Belousov-Zhabotinsky reaction [Petrov *et al.*, 1993, 1994] (a collection of articles about the control of chaos and its applications can be found in **Chaos, 7(4), 1997**).

We report for the first time the successful control of two Hamiltonian systems: the Hénon - Heiles potential and the diamagnetic Kepler problem (DKP). We have also extended the controlability of area-preserving maps to include the Crémona map. In the following, we first review the OGY method. Our goal is to stabilize a chaotic orbit around some desired periodic orbit (which we obtained in the previous chapter) for two-dimensional Hamiltonian maps. These maps may arise from a surface of section of a two-degree-of-freedom time-independent Hamiltonian system or from an experimental time series originating from a conservative process. It is important to note that due to the existence of complex conjugate eigenvalues along an unstable orbit, characteristic of area-preserving maps, the original OGY method, which is expressed in terms of real eigenvalues and eigenvectors along the periodic orbit, fails to apply. We follow and implement the algorithm proposed by Lai, Ding and Grebogi [1993] which is a modified version of the OGY method suitable for area-preserving mappings.

3.1 The Control Method

We consider the following discrete time dynamical system

$$\mathbf{X}_{n+1} = \mathbf{F}(\mathbf{X}_n, p), \tag{3.1}$$

where $\mathbf{X}_i \in \mathcal{R}^2$, p$\in \mathcal{R}$ is a control parameter, and $\mathbf{F}$ is a smooth vector valued function of both variables. Since we do not want to change the dynamics substantially, we restrict our parameter perturbation to be small. In other words we require $|p - p_0| < \delta p$, where p_0 is some nominal parameter value and δp is a small number defining the range of parameter variation. Our objective is to tune the parameter p in such a way that a typical trajectory in the chaotic region is stabilized around some desirable unstable periodic orbit after an initial chaotic transient. The procedure is as follows.

First we choose the periodic orbit that yields the best system performance (this was done in the previous chapter). Next, we define a small region of size ϵ_c around each of the periodic orbit points whose size is proportional to δp. We then start the trajectory with some initial condition in the chaotic region. Due to the ergodicity, there is a finite probability that the particle enters the small region around one of the periodic-orbit points. Once the particle is inside the small region, p will be judicously changed to keep the trajectory around the periodic orbit.

In contrast to dissipative systems, the initial transient, for a typical Hamiltonian system, can be very long [Grebogi, Ott and Yorke, 1983] due to the presence of KAM islands that act as barriers for the "transport" of a chaotic trajectory from one region of phase space to another. This problem has been successfully addressed recently by Bolt and Meiss [1995] and by Schroer and Ott [1997]. The solution is now called *targeting* and can be used at will to accelerate the transport of the trajectory to the desired "target".

Specifically, assume that the unstable orbit of period m to be controlled is

$$\mathbf{X}_{01}(p_0) \longrightarrow \mathbf{X}_{02}(p_0) \longrightarrow \cdots \mathbf{X}_{0m}(p_0) \longrightarrow \mathbf{X}_{0(m+1)}(p_0) = \mathbf{X}_{01}(p_0). \tag{3.2}$$

The linearized dynamics in the neighborhood of the period-m orbit is

$$\mathbf{X}_{n+1} - \mathbf{X}_{0(n+1)}(p_n) = \mathbf{M} \cdot [\mathbf{X}_n - \mathbf{X}_{0n}(p_n)], \tag{3.3}$$

where $\mathbf{M}$ is the two-dimensional Jacobian matrix whose elements (ij) are the partial derivatives of the i^{th} component of $\mathbf{F}$ with respect to the j^{th} component of $\mathbf{X}$, i.e., $\partial F_i/\partial X_j$ evaluated at the unperturbed periodic-orbit point $\mathbf{X}_{0n}(p_0)$. The adjustment of the parameter, $p_n = p_0 + (\Delta p)_n$, with $\mid (\Delta p)_n \mid \leq \delta p$ will result in the following shift of the periodic-orbit points according to

$$\mathbf{X}_{0n}(p_n) - \mathbf{X}_{0n}(p_0) \simeq \mathbf{g}_n (\Delta p)_n, \tag{3.4}$$

where

$$\mathbf{g}_n = \left. \frac{\partial \mathbf{X}_{0n}(p)}{\partial p} \right|_{p_0}. \tag{3.5}$$

In equation (3.3), we will not express the Jacobian matrix $\mathbf{M}$ in terms of its eigenvalues and eigenvectors because there may exist complex-conjugate eigenvalues on the unit circle for some of the periodic points. Instead we explore the stable and unstable directions associated with these points. The stable and unstable directions do not necessarily coincide with the eigenvectors at a given periodic point if $m \neq 1$ [Lai, Grebogi, Yorke and Kan, 1993]. In the case of complex-conjugate eigenvalues, those eigenvectors are not even defined in the real plane.

The existence of both stable and unstable directions around each orbit point can be seen as follows. Let us choose a small circle of radius ϵ at some orbit point $\mathbf{X}_{0n}$. In a Cartesian coordinate system with the origin at $\mathbf{X}_{0n}$, the circle can be expressed as $dx^2 + dy^2 = \epsilon^2$. The image of the circle under $\mathbf{F}^{-1}$ centered at $\mathbf{X}_{0(n-1)}$ can be expressed by $A(dx\prime)^2 + B(dx\prime)(dy\prime) + C(dy\prime)^2 = 1$, which is typically an ellipse. Here A, B and C are functions of the entries of the inverse Jacobian matrix at $\mathbf{X}_{0n}$. This deformation from a circle to an ellipse means that the distance along the major axis of the ellipse at $\mathbf{X}_{0(n-1)}$ contracts as a result of the map. Similarly, the image of a circle at $\mathbf{X}_{0(n-1)}$ under $\mathbf{F}$ is typically an ellipse at $\mathbf{X}_{0n}$. This means that the distance along the inverse image of the major axis of the ellipse at $\mathbf{X}_{0n}$ expands under $\mathbf{F}$. Thus the major axis of the ellipse at $\mathbf{X}_{0(n-1)}$ and the inverse image of the major axis of the ellipse at $\mathbf{X}_{0n}$

approximate the stable and unstable directions at $\mathbf{X}_{0(n-1)}$.

Let $\mathbf{e}_{s(n)}$ and $\mathbf{e}_{u(n)}$ be the stable and unstable directions at $\mathbf{X}_{0n}$, and let $\mathbf{f}_{s(n)}$ and $\mathbf{f}_{u(n)}$ be two vectors that satisfy $\mathbf{f}_{u(n)} \cdot \mathbf{e}_{u(n)} = \mathbf{f}_{s(n)} \cdot \mathbf{e}_{s(n)} = 1$ and $\mathbf{f}_{u(n)} \cdot \mathbf{e}_{s(n)} = \mathbf{f}_{s(n)} \cdot \mathbf{e}_{u(n)} = 0$. To control the orbit, we require that the next iteration of a trajectory point after falling into one of the small neighbourhoods around $\mathbf{X}_{0n}$ lies on the *stable direction* at $\mathbf{X}_{0(n+1)}(p_0)$, i.e.

$$[\mathbf{X}_{n+1} - \mathbf{X}_{0(n+1)}(p_0)] \cdot \mathbf{f}_{u(n+1)} = 0. \tag{3.6}$$

This defines the control strategy. Substituting equations (3.3) and (3.4) into equation (3.6), we obtain the following expression for the parameter perturbations [Lai, Ding and Grebogi, 1993]:

$$(\Delta p)_n = \frac{\{\mathbf{M} \cdot [\mathbf{X}_n - \mathbf{X}_{0n}(p_0)]\} \cdot \mathbf{f}_{u(n+1)}}{[(\mathbf{M} \cdot \mathbf{g}_n) - \mathbf{g}_{n+1}] \cdot \mathbf{f}_{u(n+1)}}, \tag{3.7}$$

where $\mathbf{M}$ is evaluated at $\mathbf{X}_{0n}(p_0)$. The quantities in equation (3.7) are all numerically accessible, so this method is suitable to control the system *without* a knowledge of the governing equations.

3.2 Calculating the Jacobian Matrix and the Manifolds

Once we have selected the desired periodic orbit, the next task before us is to obtain the Jacobian matrix for each periodic point. Since we assume no knowledge of the governing equations of the system, this task must be done numerically. In order to calculate the four elements of the Jacobian matrix, we use equation (3.3) for an unperturbed trajectory (i.e. $p_n = p_0$). However, this equation gives us two equations with four unknowns. To complement this information, we choose a small neighbourhood around each periodic point. In this region, the system is assumed to behave linearly. The following steps are then performed:

1. take one of the periodic points

2. choose a small linear neighborhood around that point

3. select M neighbouring points as initial conditions within that neighbourhood

4. iterate each of the M trajectories to get the next return map

5. write equation (3.3) for each of the M points

6. solve all the 2M equations simultaneously [Press *et al.*, 1992].

   [If the M points are chosen uniformly around the periodic point, the solution to the above equations will give the optimised values for the elements of the Jacobian matrix. Note that due to the limitations of the simultaneous equations solver algorithm, choosing a larger number of neighboring points does not necessarily increase the accuracy of the results. By choosing 1500< M < 2000 points within a box of the order 10^{-4} around the periodic point we obtained the best results for the elements of the Jacobian matrix.]

7. repeat the procedure for the next periodic point.

Table (3.1) compares the exact value of the determinant of the Jacobian matrix with the one obtained numerically for different maps. The numbers are characteristic of the accuracy of the procedure.

Map	Jacobian (exact value)	Absolute numerical error (max.)
DHM	ϵ = - 0.3	$\pm 6.5 \times 10^{-4}$
Standard	1	$\pm 5.5 \times 10^{-4}$
Cremona	1	$\pm 5.0 \times 10^{-4}$
Hénon - Heiles	1	± 0.001
DKP	1	± 0.003

Table 3.1: **The Jacobian**: comparison between exact values and numerical results

Once we know the Jacobian matrices, the stable ($\mathbf{e}_s$) and unstable ($\mathbf{e}_u$) directions at each point must be obtained and the vector $\mathbf{f}_{u(n+1)}$ calculated for its use in equation(3.7). This second task is performed by the following algorithm. This algorithm can be applied to cases where the period of the orbit is arbitrarily large.

To find a stable direction at a point $\mathbf{X}$ [Lai *et al*, 1993], we first iterate this point forward N times under the map $\mathbf{F} : \mathbf{F}^1(\mathbf{X}), \mathbf{F}^2(\mathbf{X}), \cdots, \mathbf{F}^N(\mathbf{X})$. Now imagine that we put a circle of arbitrarily small radius ϵ at the point $\mathbf{F}^N(\mathbf{X})$. If we iterate this circle backward once, the circle will become an ellipse at the point $\mathbf{F}^{N-1}(\mathbf{X})$. We continue iterating this ellipse backwards, keeping the ellipse's major axis of order ϵ by a simple normalization procedure. By iterating the ellipse all the way back to the point $\mathbf{X}$, the ellipse becomes very thin, with its major axis pointing along the stable direction at point $\mathbf{X}$ provided that N is large enough. In practice, instead of using a small circle, we take a unit vector at the point $\mathbf{F}^N(\mathbf{X})$, since the Jacobian matrices of the inverse map $\mathbf{F}^{-1}$ rotates the vector in the tangent space of $\mathbf{F}$ towards the stable direction. Thus we iterate a unit vector backward to the point $\mathbf{X}$ by multiplying the Jacobian matrices of the inverse map at each point on the already existing orbit.

An important practical point in the calculation is that we never actually calculate the Jacobian matrix of the inverse map along the trajectory. The reason is that, the trajectory is very sensitive and will usually diverge from the original trajectory $\mathbf{F}^N(\mathbf{X}), \mathbf{F}^{N-1}(\mathbf{X}) \cdots \mathbf{F}^1(\mathbf{X})$ after only a few backward iterations. Instead we store the inverse Jacobian matrix ($\mathbf{J^{-1}}(\mathbf{X_i}) \equiv \mathbf{J_i^{-1}}, \{\mathbf{X_i}\}_{i=1,\cdots,m}$) at every point of the orbit $\mathbf{F}^i(\mathbf{X})(i = 1, \cdots, N)$ when we iterate forward the point $\mathbf{X}$ beforehand. We normalize the vector after each multiplication to the unit length. For sufficiently large N, the unit vector we get at $\mathbf{X}$ is a good approximation of the stable direction at $\mathbf{X}$. The procedure can be illustrated schematically as follows ($\boldsymbol{s}$ is a unit vector):

$$\mathbf{s_0(X_i)} \longrightarrow \mathbf{\hat{s}_{-1} = J_i^{-1} s_0} \longrightarrow \mathbf{s_{-1}} = \frac{\mathbf{\hat{s}_{-1}}}{|\mathbf{\hat{s}_{-1}}|} \longrightarrow \mathbf{\hat{s}_{-2} = J_{i-1}^{-1} s_{-1}} \longrightarrow \mathbf{s_{-2}} = \frac{\mathbf{\hat{s}_{-2}}}{|\mathbf{\hat{s}_{-2}}|}$$
$$\longrightarrow \cdots\cdots \longrightarrow \mathbf{\hat{s}_{-N} = J_{i-N}^{-1} s_{-N+1}} \longrightarrow \mathbf{s_{-N}} = \frac{\mathbf{\hat{s}_{-N}}}{|\mathbf{\hat{s}_{-N}}|} \sim \mathbf{e_s(X_i)}$$

Similarly, *to find the unstable direction* at point $\mathbf{X}$, we first iterate $\mathbf{X}$ backward under the inverse map N times to get a backward orbit $\mathbf{F}^{-j}(\mathbf{X})(j = N, \cdots, 1)$. We then choose a unit vector at point $\mathbf{F}^{-N}(\mathbf{X})$ and iterate this unit vector forward to the point $\mathbf{X}$ along the already existing orbit by multiplying by the Jacobian matrix of the map N times since the Jacobian matrix of the forward map $(\mathbf{J(X_i)} \equiv \mathbf{J_i}, \{\mathbf{X_i}\}_{i=1,\cdots,m})$ rotates a vector towards the unstable direction normalizing to unit length at each step. The final vector at point $\mathbf{X}$ is a good approximation of the unstable direction at that point if N is sufficiently large. Again, to avoid divergence from the original trajectory, we do not actually iterate the inverse map. What we do in this case is to choose $\mathbf{X}$ to be the end point of a forward orbit, all the points before $\mathbf{X}$ are the inverse images of $\mathbf{X}$, and we store the Jacobian matrices of the forward map at those points. [An illustration of the procedure is shown in figure (3.1) for a period-2 orbit of the dissipative Hénon map ($\mu = 1.4$ and $\epsilon = -0.3$).] The procedure can be illustrated schematically as follows (u is a unit vector):

$$\mathbf{u_0(X_i)} \longrightarrow \mathbf{\hat{u}_1 = J_i u_0} \longrightarrow \mathbf{u_1} = \frac{\mathbf{\hat{u}_1}}{|\mathbf{\hat{u}_1}|} \longrightarrow \mathbf{\hat{u}_2 = J_{i+1} u_1} \longrightarrow \mathbf{u_2} = \frac{\mathbf{\hat{u}_2}}{|\mathbf{\hat{u}_2}|}$$
$$\longrightarrow \cdots\cdots \longrightarrow \mathbf{\hat{u}_N = J_{i+N-1} u_{N-1}} \longrightarrow \mathbf{u_N} = \frac{\mathbf{\hat{u}_N}}{|\mathbf{\hat{u}_N}|} \sim \mathbf{e_u(X_i)}$$

Once we have obtained the Jacobian matrix and the unstable direction at the position of each periodic point, we are able to apply control using small parameter perturbations calculated from equation (3.7). We wait until the trajectory gets close enough to one of the periodic points and at that moment we change the parameter by $(\Delta p)_n$. Therefore for the next iteration the trajectory will land on the stable direction of the successive periodic point. As long as we repeat this procedure, we can maintain the system under

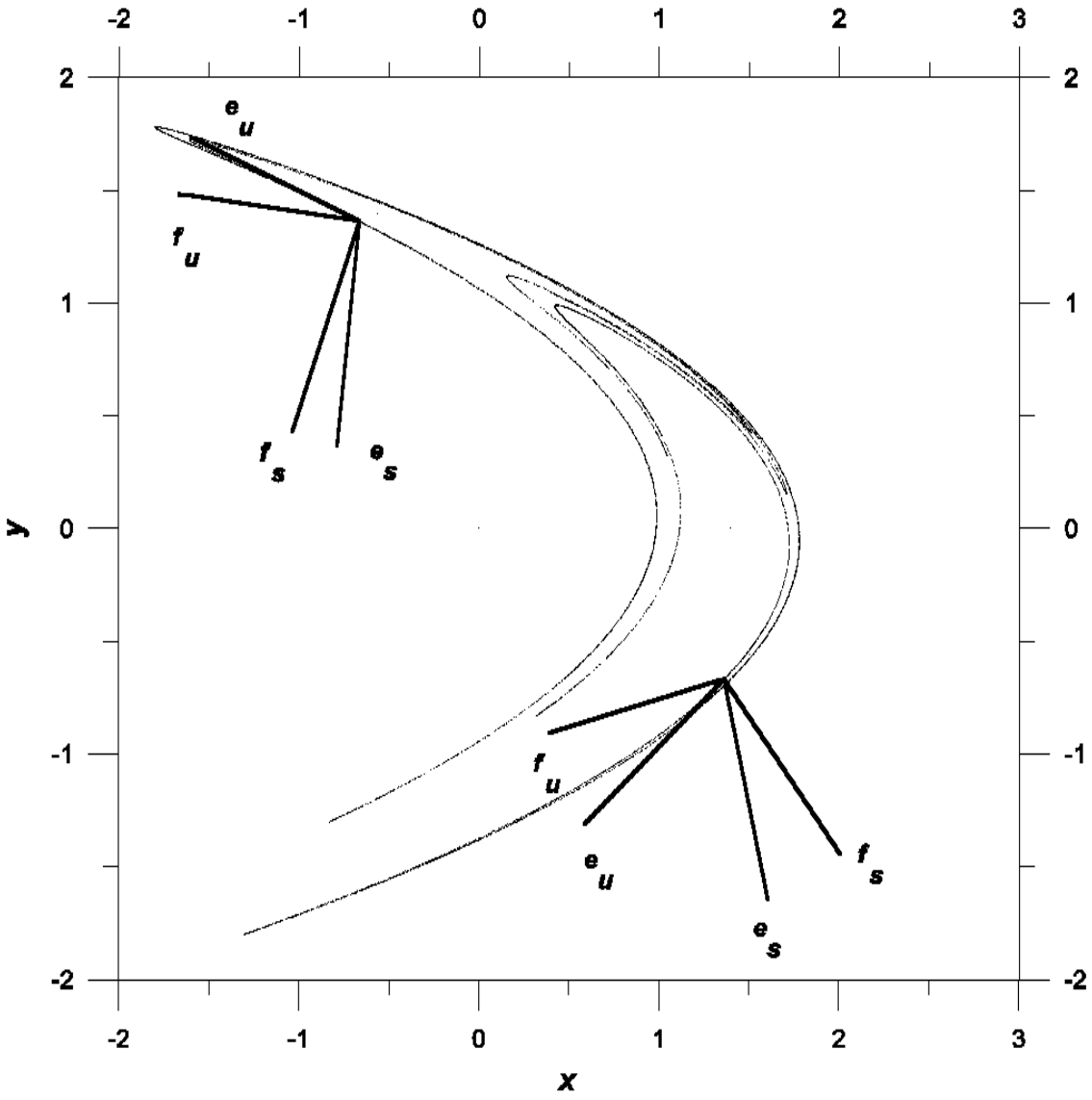

Figure 3.1: **Stable and unstable directions for the dissipative Hénon map**: The direction of vectors e_s, e_u, f_s and f_u for a period-2 orbit of the dissipative Hénon map ($\mu = 1.4$ and $\epsilon = -0.3$).

control. In other words we can bring the system to order by applying small parameter perturbations at each step.

3.3 Numerical results

We have successfully controlled a large number of unstable periodic orbits for the dissipative Hénon map, the standard map, the Crémona map, the Hénon - Heiles potential and the DKP using the procedure just described. As mentionned in the previous chapter we present only a small set of controlled periodic orbits which are representative of the behaviour of these systems under our control algorithm. It is again to emphasize that no prior knowledge of the analytic form of the map is assumed nor used. In the two cases of Hamiltonian flow, only the existence of a mapping on the Poincaré section is assumed. (For convenience, we rewrite the expression for each mapping in this section.)

3.3.1 The Iterative Mappings

We have successfully controlled period-1,2,7 and 11 cycles for the dissipative Hénon map

$$\begin{pmatrix} x_{n+1} \\ \\ y_{n+1} \end{pmatrix} = \begin{pmatrix} -\epsilon y_n + \mu - x_n^2 \\ \\ x_n \end{pmatrix} \quad . \tag{3.8}$$

Figure(3.2) shows the set of periodic orbits as well as the controlled trajectories.

As the first application of OGY method on area-preserving maps, we consider the standard map

$$\begin{pmatrix} q_{n+1} \\ \\ p_{n+1} \end{pmatrix} = \begin{pmatrix} q_n + p_{n+1} \qquad (mod 1) \\ \\ p_n - \frac{K}{2\pi}\sin(2\pi q_n) \end{pmatrix} \quad . \tag{3.9}$$

The results that we obtain confirm the earlier results by Lai, Ding and Grebogi [1993]. We successfully controlled chaos around period-2,5,7 and 11 cycles. Figure(3.3) shows

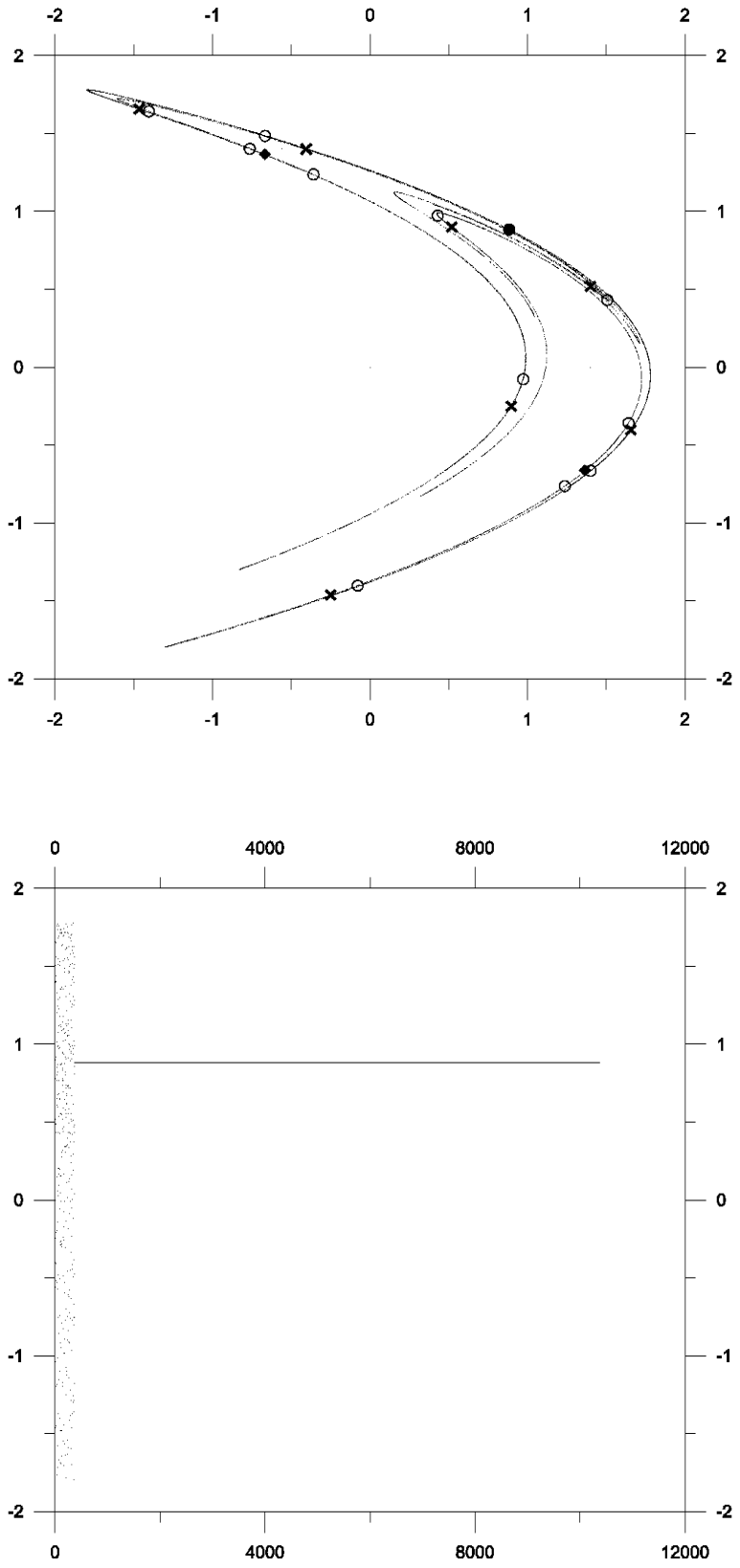

Figure 3.2: (a) **The Dissipative Hénon Map:** Top: The set of periodic orbits of Hénon map selected for the control algorithm. Filled circle: Period-1, Diamonds: Period-2, **x**: Period-7, Circles: Period-11. Bottom: Period-1 controlled trajectory (as can be seen from equation (3.8) the vertical axis represents both x and y axes).

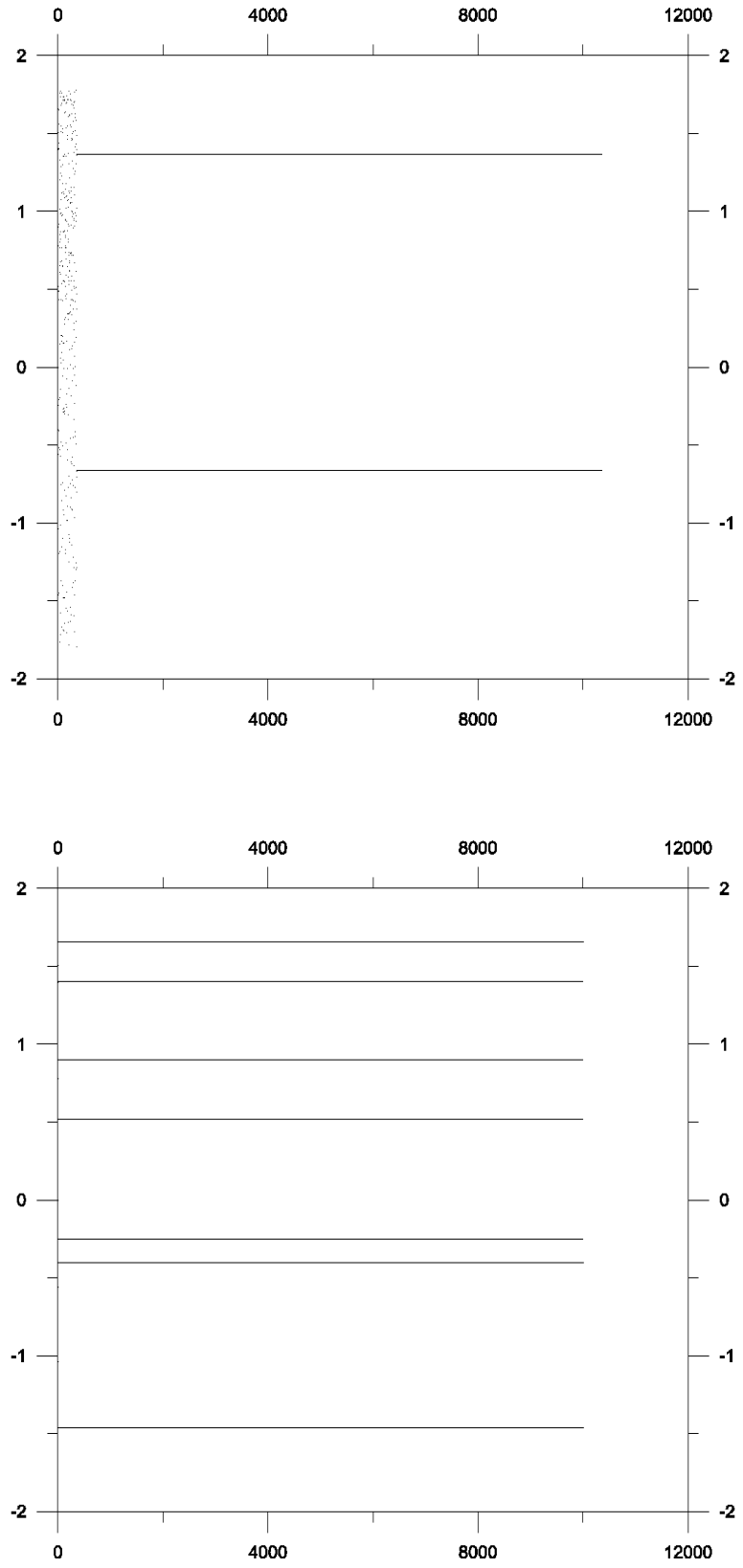

Figure 3.2: (b) **Controlled Trajectories for the Dissipative Hénon Map:** Top: Period-2; Bottom: Period-7 (as can be seen from equation (3.8) the vertical axis represents both x and y axes).

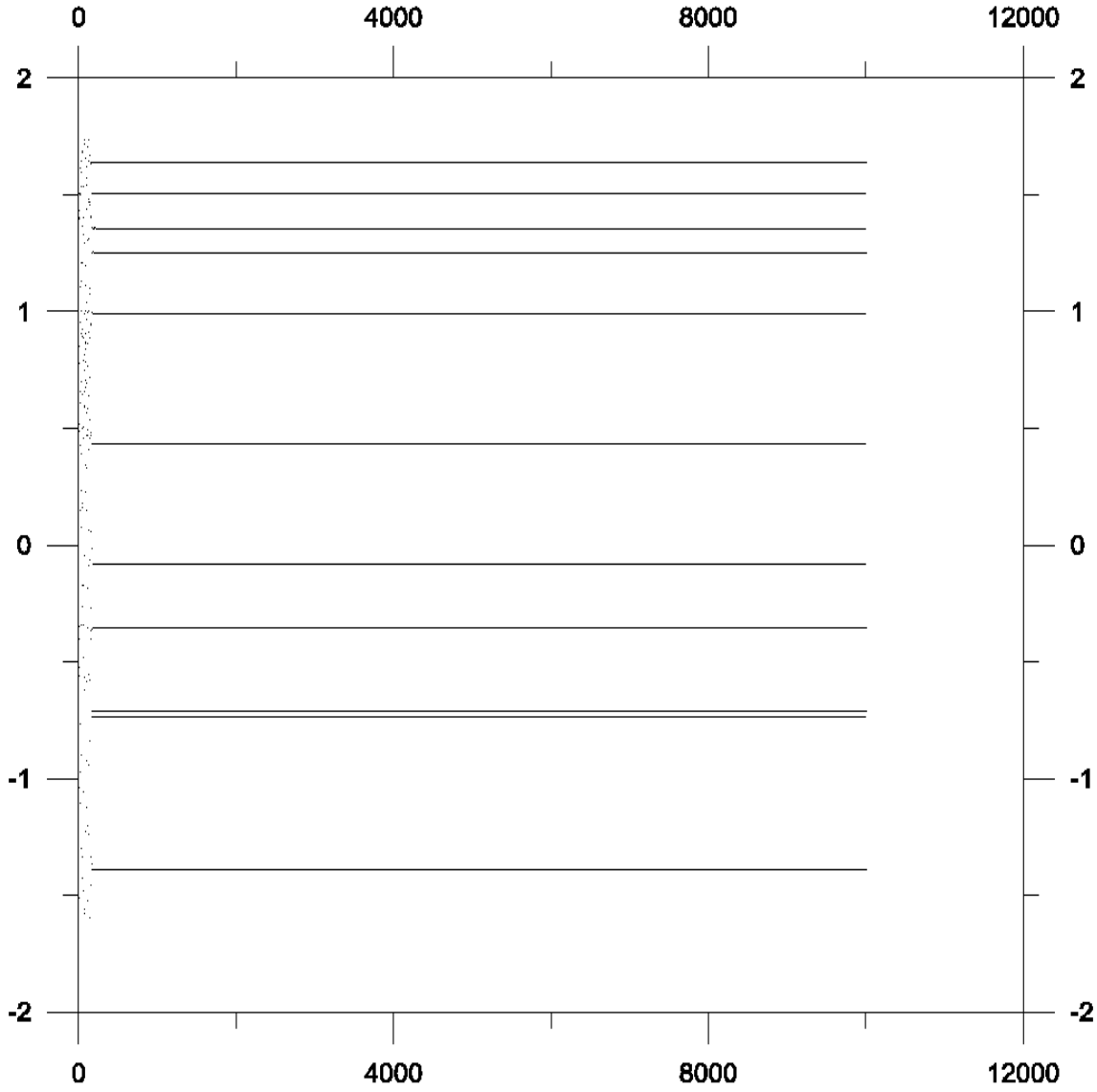

Figure 3.2: (c) **Controlled Trajectory for the Dissipative Hénon Map**: Period-11 (as can be seen from equation (3.8) the vertical axis represents both x and y axes).

the control for the standard map.

An important feature of controlling chaos is that one can make a system work as a multimode system only at the expense of small perturbations. For instance, one can choose the system to be controlled around the period-n orbit and sometime later decide to stabilize the system around another period-m orbit ($m \neq n$) and so on. Figure(3.4) shows the response of the standard map to this multimode control scheme.

We also report the control of the Crémona map around a period - 5 orbit ($\epsilon = 1$ and $\mu = -0.4224$ in(3.8)). Figure (3.5) shows the location of the periodic points on the map as well as the controlled trajectory.

3.3.2 The Hénon -Heiles Potential

We report for the first time the successful control of the Hénon - Heiles Hamiltonian using OGY method. We stabilize the system around period-1 and period-3 cycles. Figures (3.6) and (3.7) show the controlled trajectories for period-1 and period-3 respectively.

3.3.3 The Diamagnetic Kepler Problem

We report for the first time the successful control of the DKP. Although the Poincaré section of DKP is of rich complexity and the system is very sensitive even to small perturbations, the results show a robust control. Although a small variation of the system parameter does not affect the global behavior of DKP drastically, it may change the local behavior of the phase space completely. In order to demonstrate this fact, in figure(3.8) we show a small region of the Poincaré section for three different but close values of the scaled energy ϵ. By varying ϵ, the pairs of stable and unstable periodic orbits appear and disappear. This might seem to be a serious obstacle to

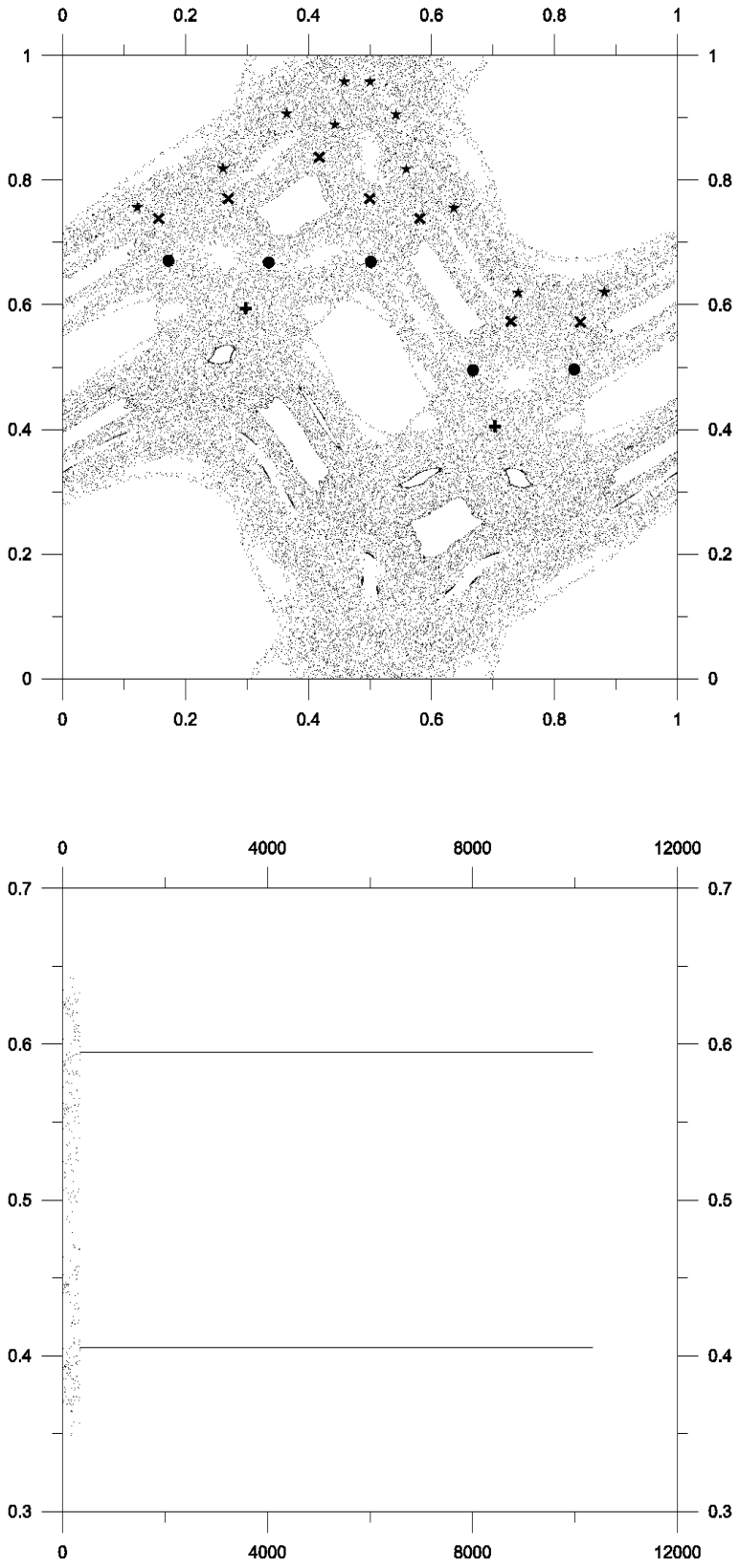

Figure 3.3: (a) **The Standard Map:** Top: A set of periodic orbits of the standard map selected for the control algorithm. $+$: period-2; $\bullet$: period-5; $\mathbf{x}$: period-7; $\star$: period-11 (horizontal axis: q, vertical axis: p). Bottom: period-2 controlled trajectory (vertical axis: p).

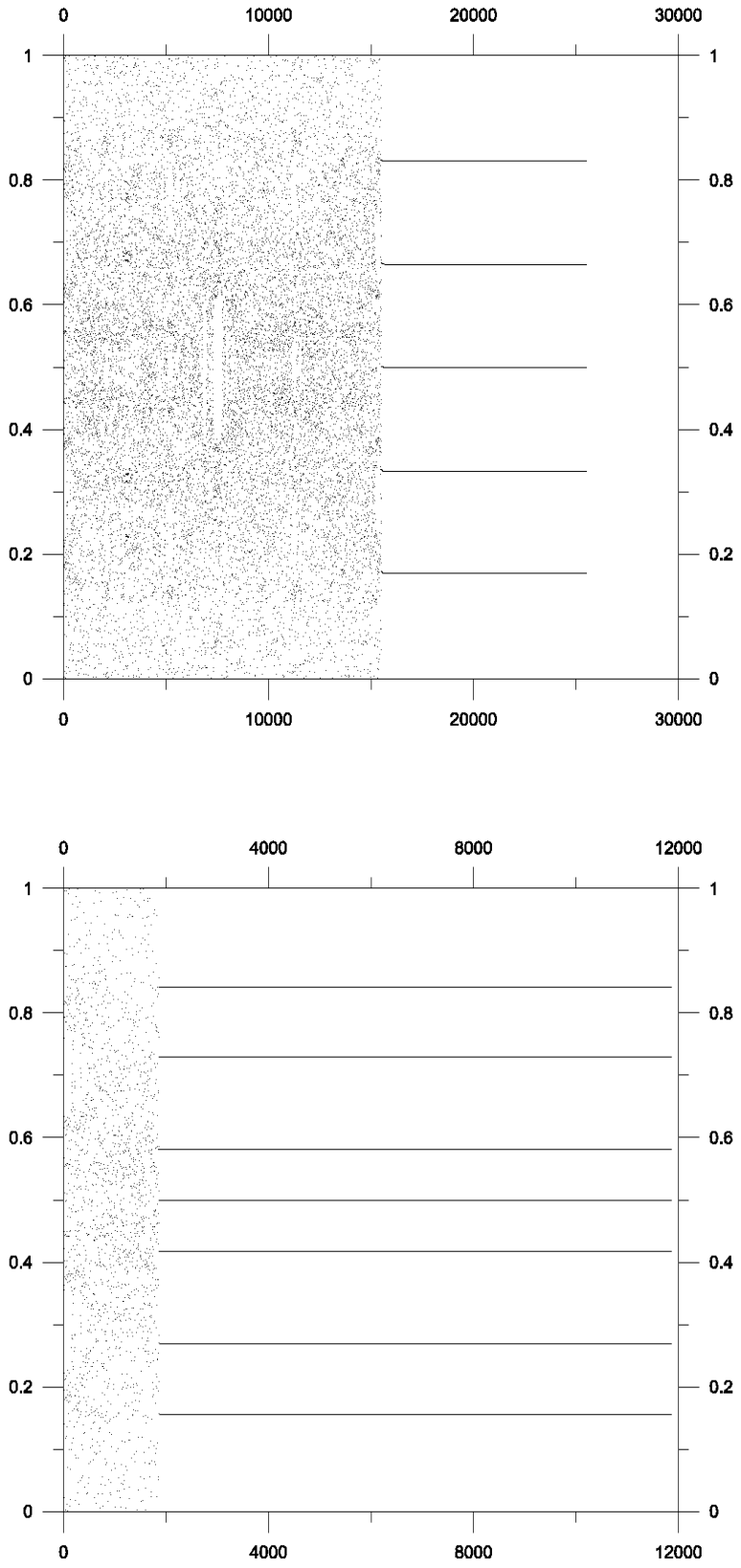

Figure 3.3: (b) **Controlled Trajectories for the Standard Map:** Top: period-5; Bottom: period-7 (horizontal axis: q, vertical axis: p).

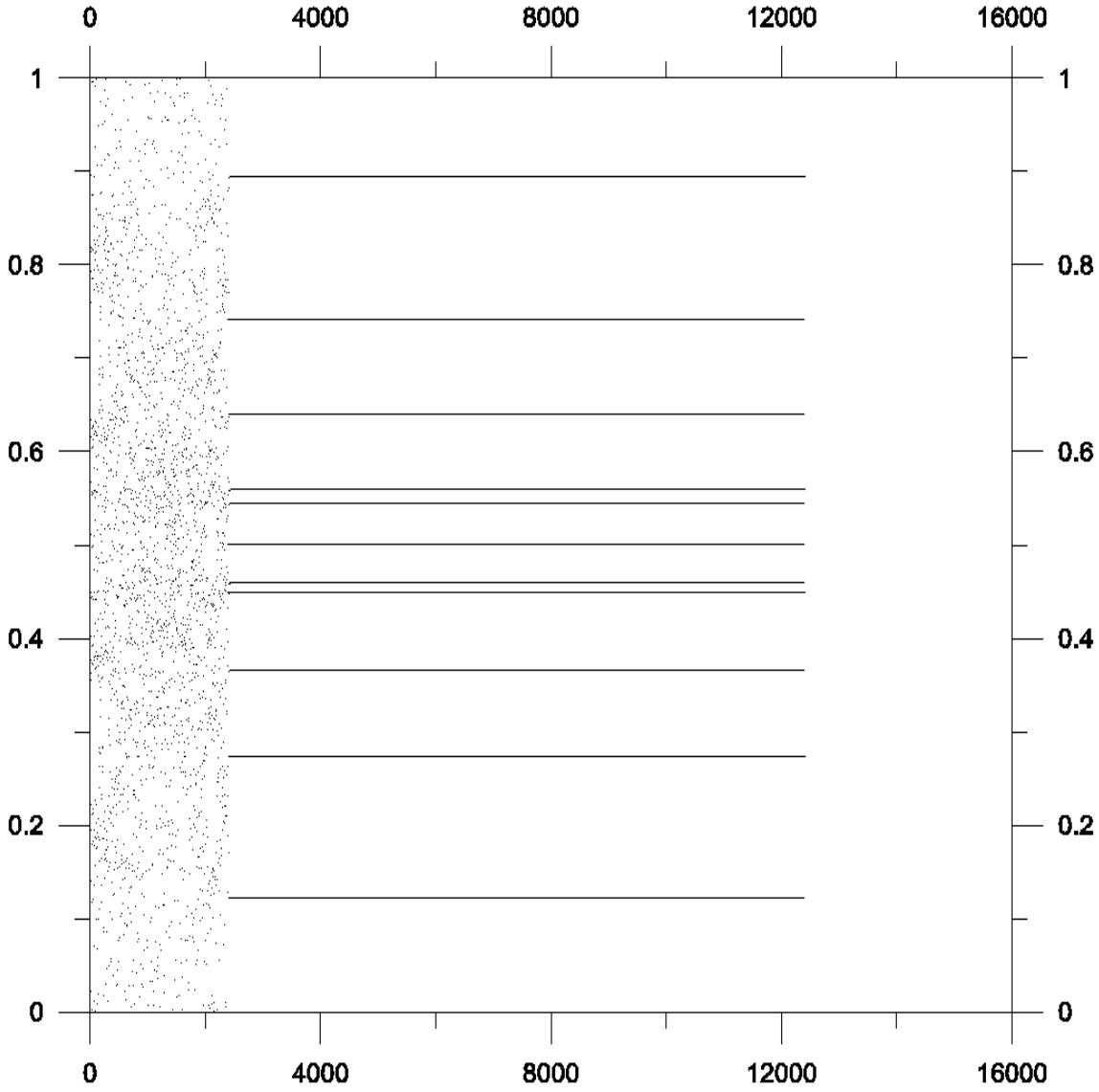

Figure 3.3: (c) **Controlled Trajectory for the Standard Map**: Period-11 (horizontal axis: q, vertical axis: p).

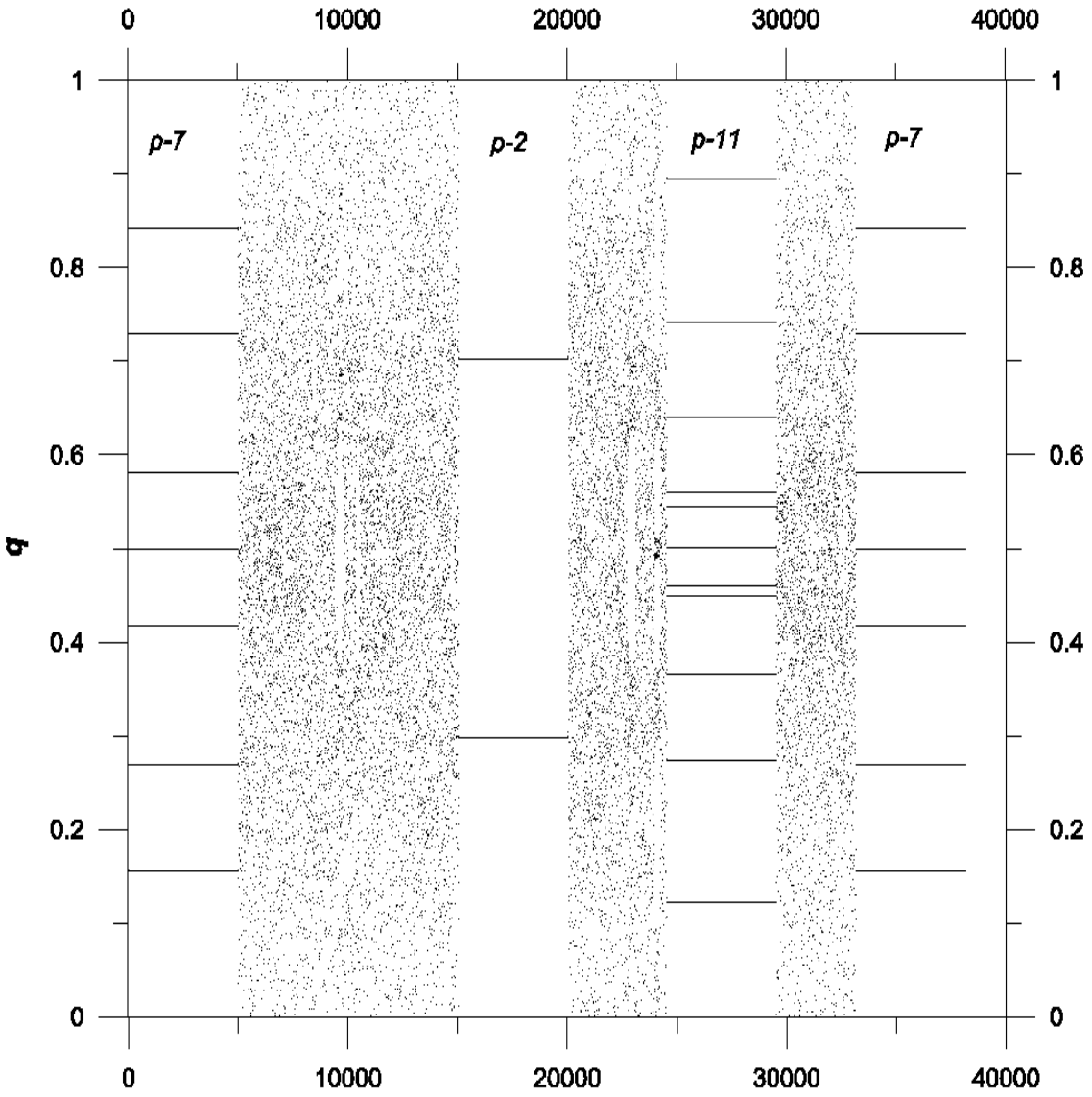

Figure 3.4: **Stabilization of the standard map around different periodic orbits**: A trajectory is stabilized around period-7, period-2, period-11 and period-7 cycles. At each step the trajectory is stabilized for 5000 iterates. The transient time intervals (number of iterations) from one periodic orbit to another are: 10041, 4495, 3626 respectively.

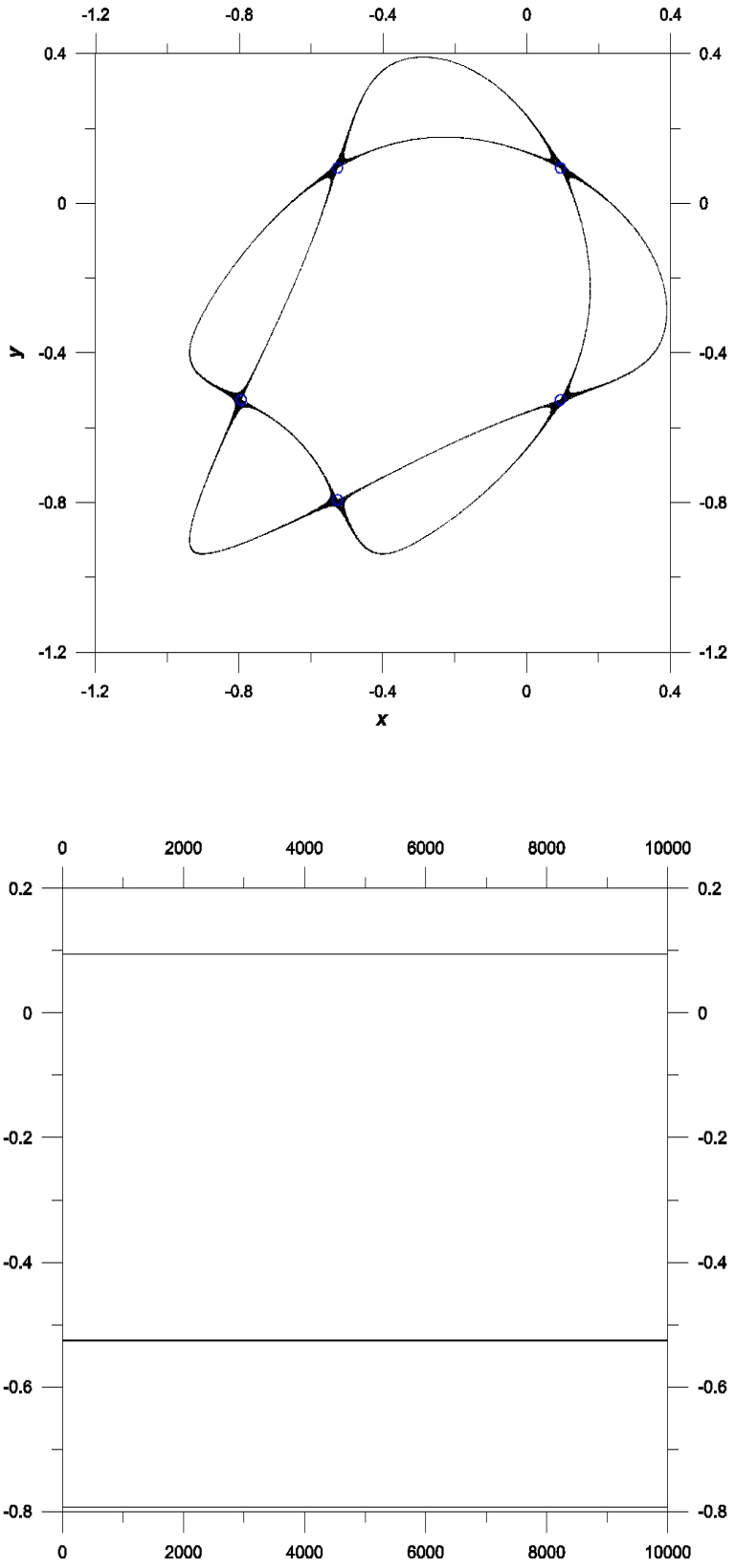

Figure 3.5: **The Crémona map:** A period - 5 orbit(top) and the controlled trajectory(bottom). Since the x(or y) coordinate of two pairs of points are identical, only three lines can be seen on the graph.

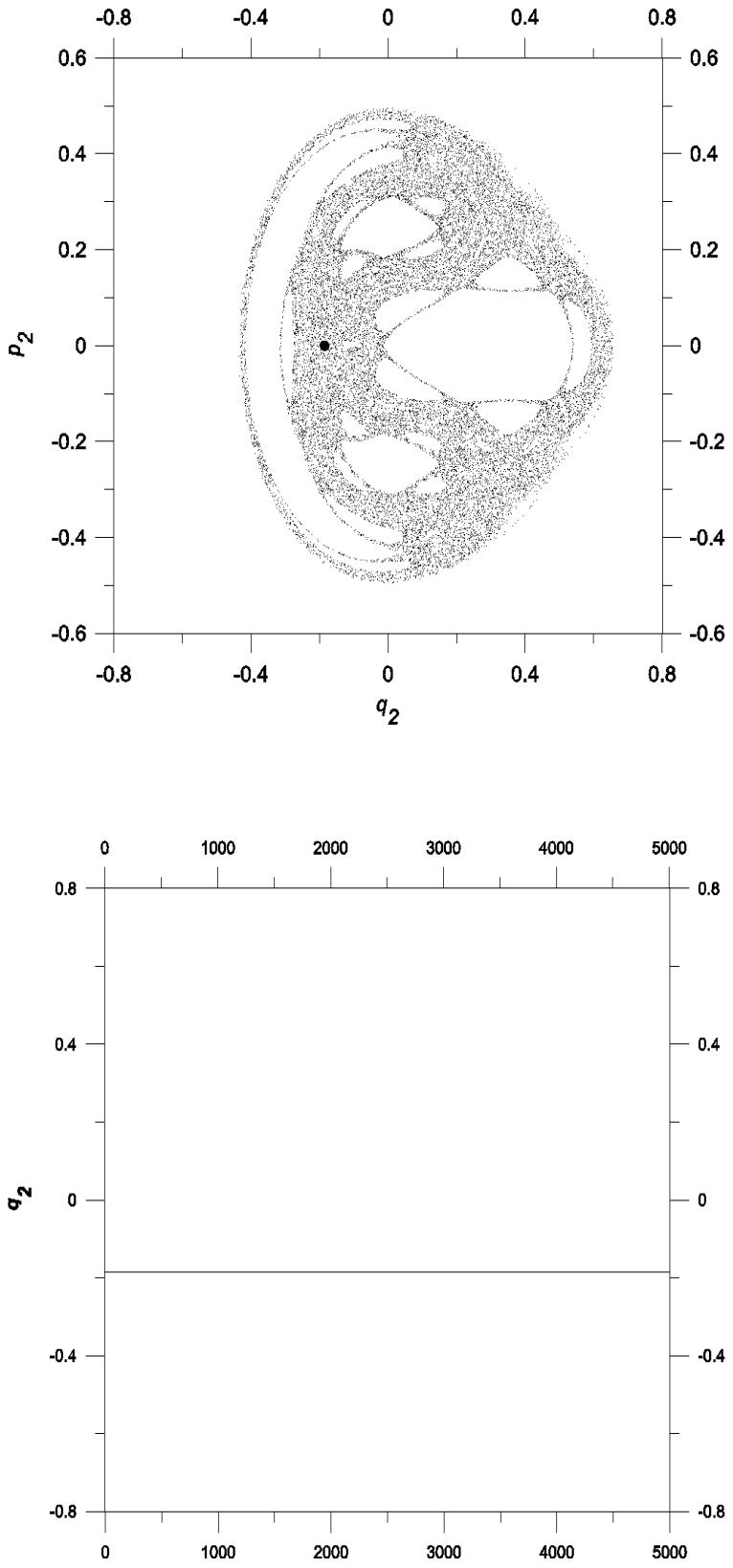

Figure 3.6: (a) **The Hénon - Heiles Hamiltonian:** Top: An unstable fixed point. Bottom: The controlled trajectory around the fixed point.

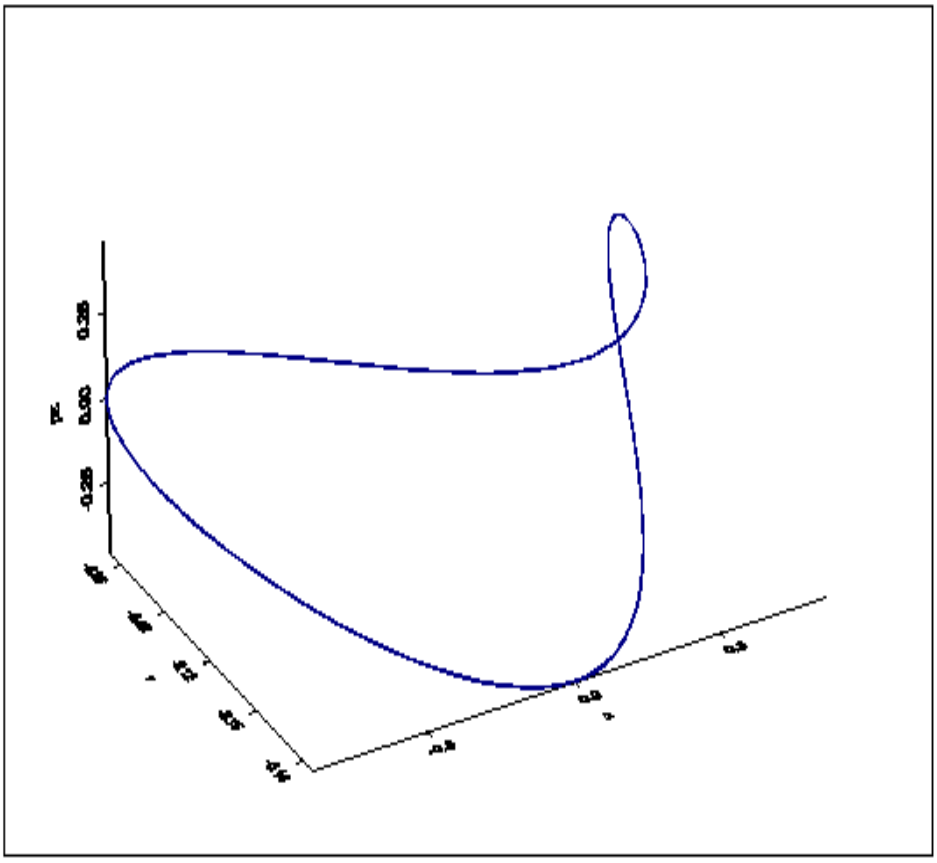

Figure 3.6: (b) **The Hénon - Heiles Hamiltonian:** The same period-1 controlled trajectory (3- dimensional: q_1, q_2, p_1).

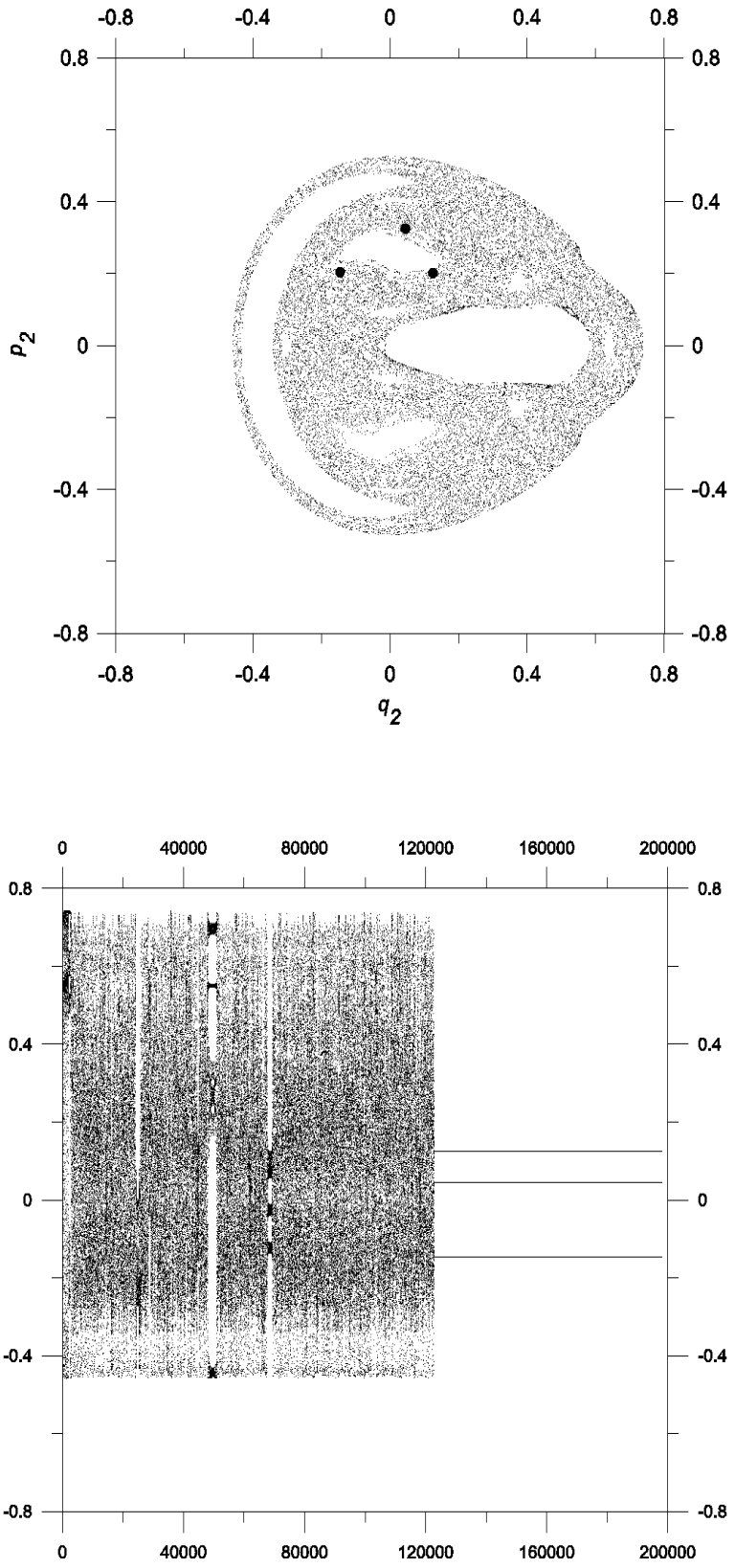

Figure 3.7: (a) **The Hénon - Heiles Hamiltonian:** Top: An unstable period-3 cycle. Bottom: The controlled trajectory around the period-3 cycle (vertical axis: q_2).

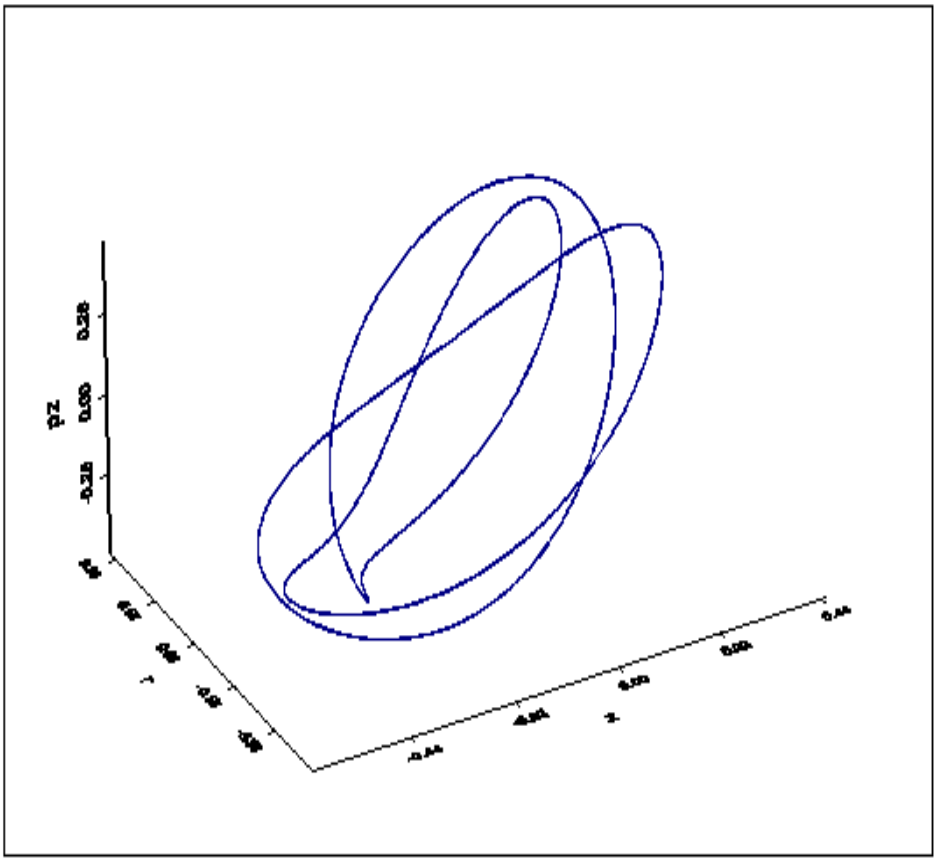

Figure 3.7: (b) **The Hénon - Heiles Hamiltonian:** The same period-3 controlled trajectory (3- dimensional: q_1, q_2, p_1).

control, because by changing the parameter value during control one might lose the target periodic orbits. Therefore one must choose those sets of periodic orbits which are more robust to parameter variation than the one shown in figure(3.8).

The data corresponding to the controlled trajectories presented in this chapter are summarized in table (3.2).

Figures(3.9), (3.10) and (3.11) show successful controls around period-1, period-2 and period-3 orbits respectively.

As mentionned previously, the system parameter may vary during the control process. Then the following question may arise: Is it possible to maintain control while the system parameter varies? In other words is it possible to update the position of periodic orbits as well as the related parameters, when the system parameter is changed? This important issue is addressed in the next chapter.

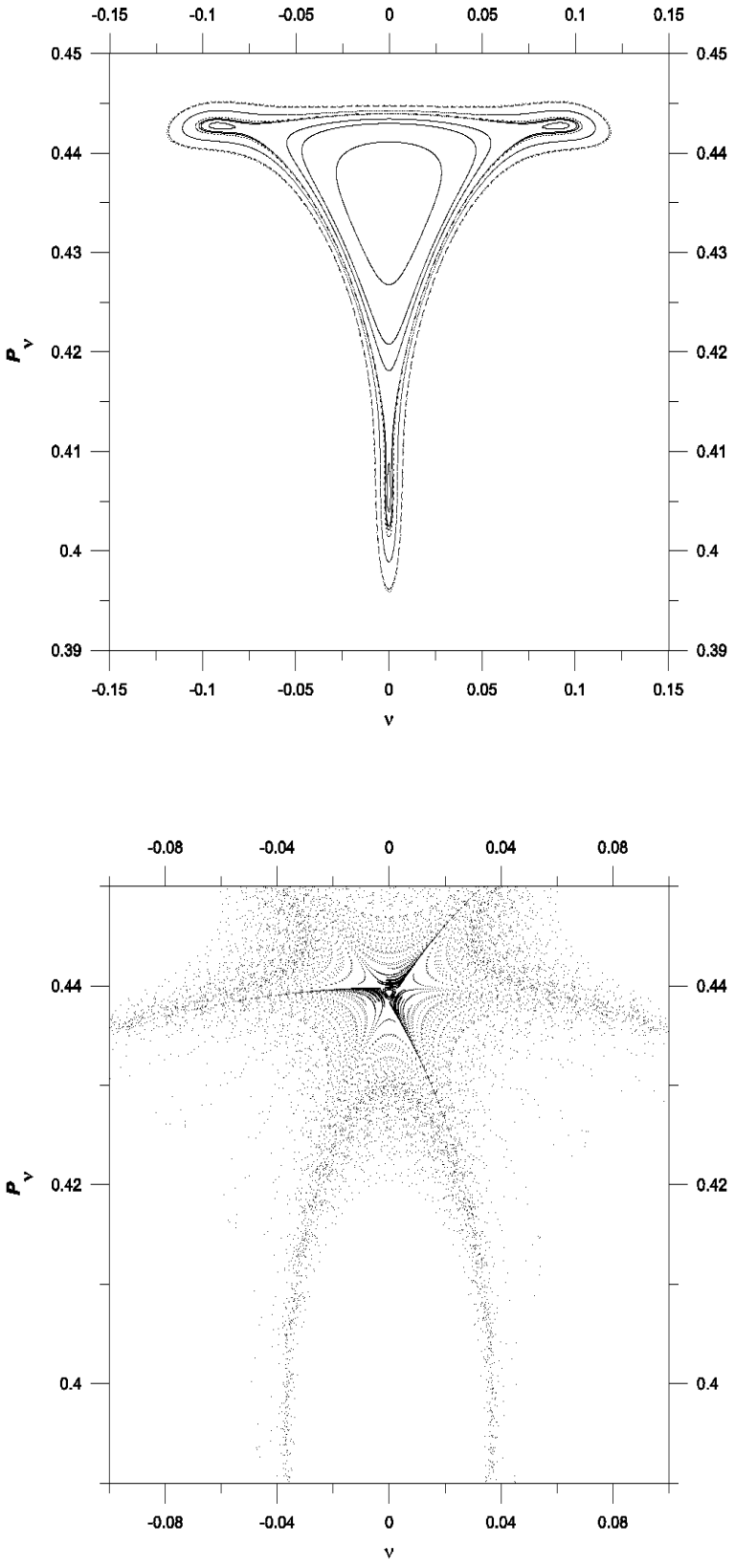

Figure 3.8: (a) **Poincaré section of the DKP for two different values of the scaled energy**: ϵ_1 = -0.31985 (top), ϵ_2 = -0.318478 (bottom). Even a small variation of the system parameter results in a dramatic change in the local geometry as well as the stability of the system.

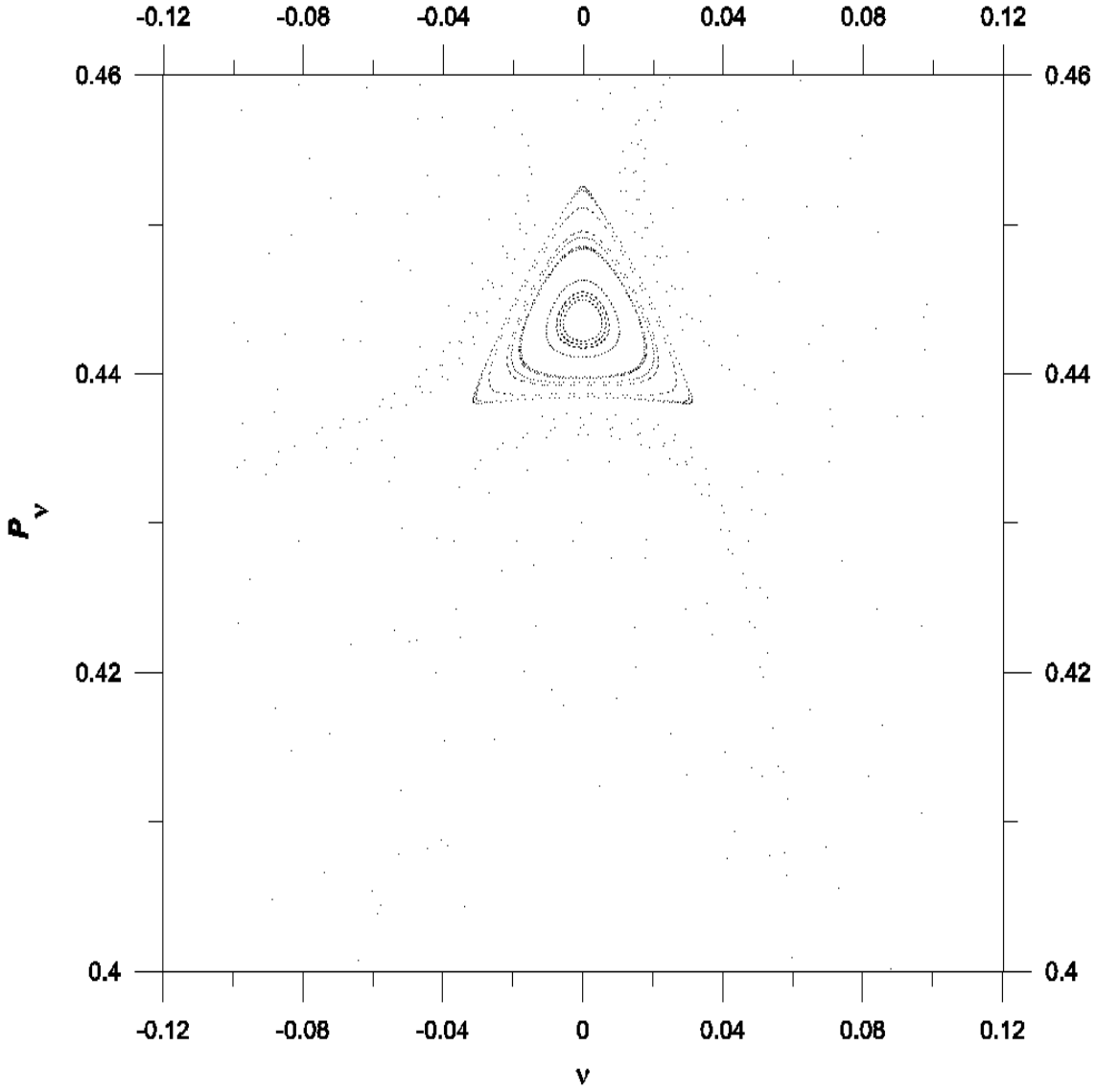

Figure 3.8: (b) **Poincaré section of the DKP** for ϵ_3 = -0.317.

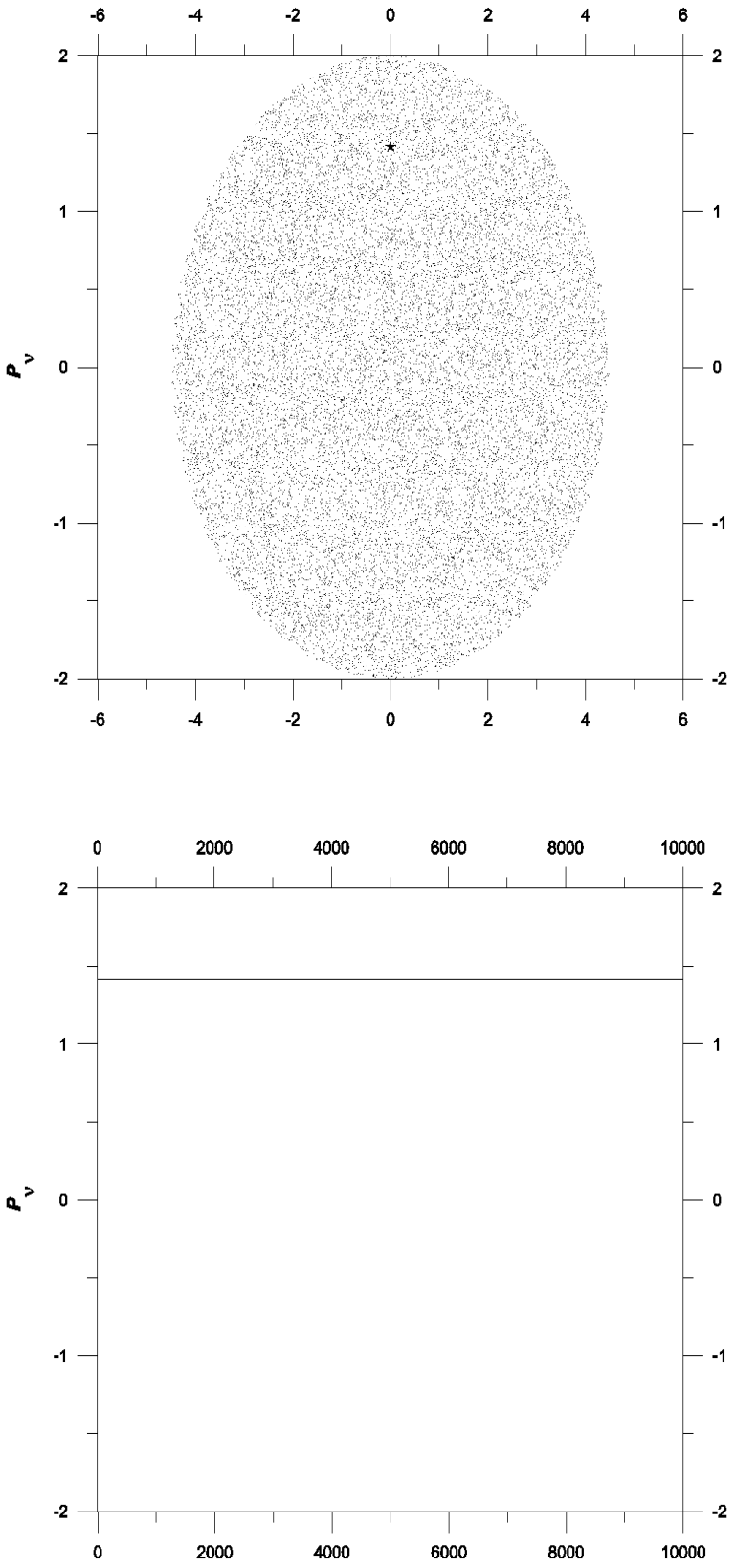

Figure 3.9: (a) **The DKP:** Top: An unstable fixed point ($\epsilon = -0.1$). Bottom: The controlled trajectory around the fixed point.

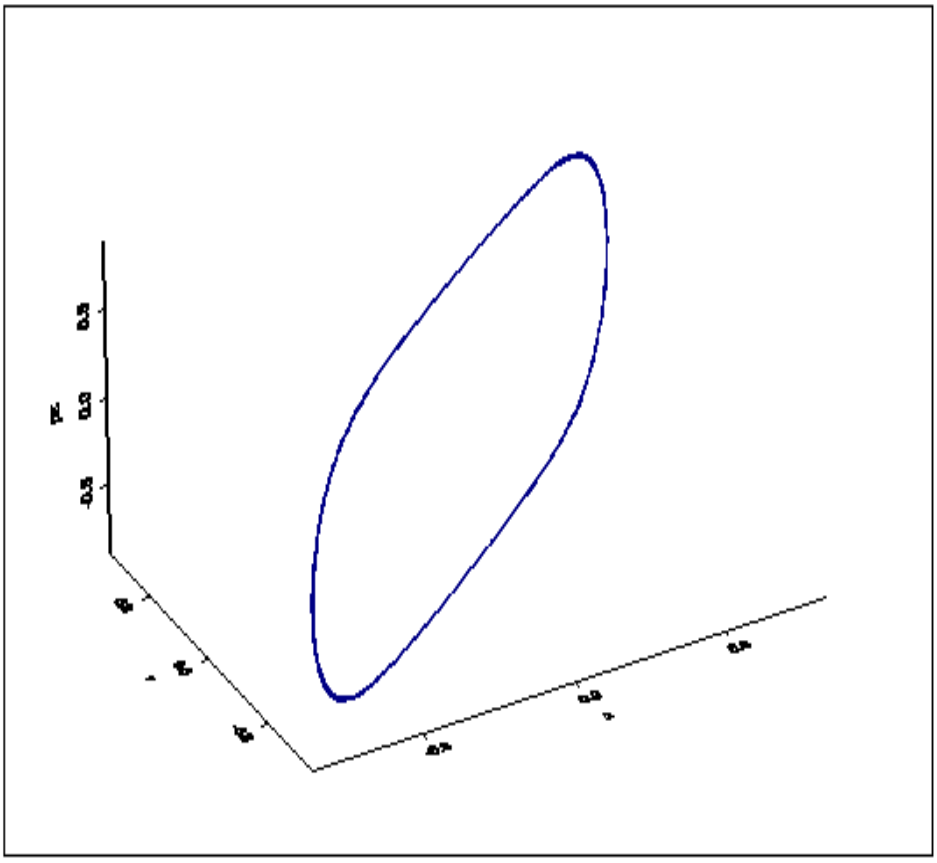

Figure 3.9: (b) **The DKP:** The same period-1 controlled trajectory (3- dimensional: μ, ν, p_μ).

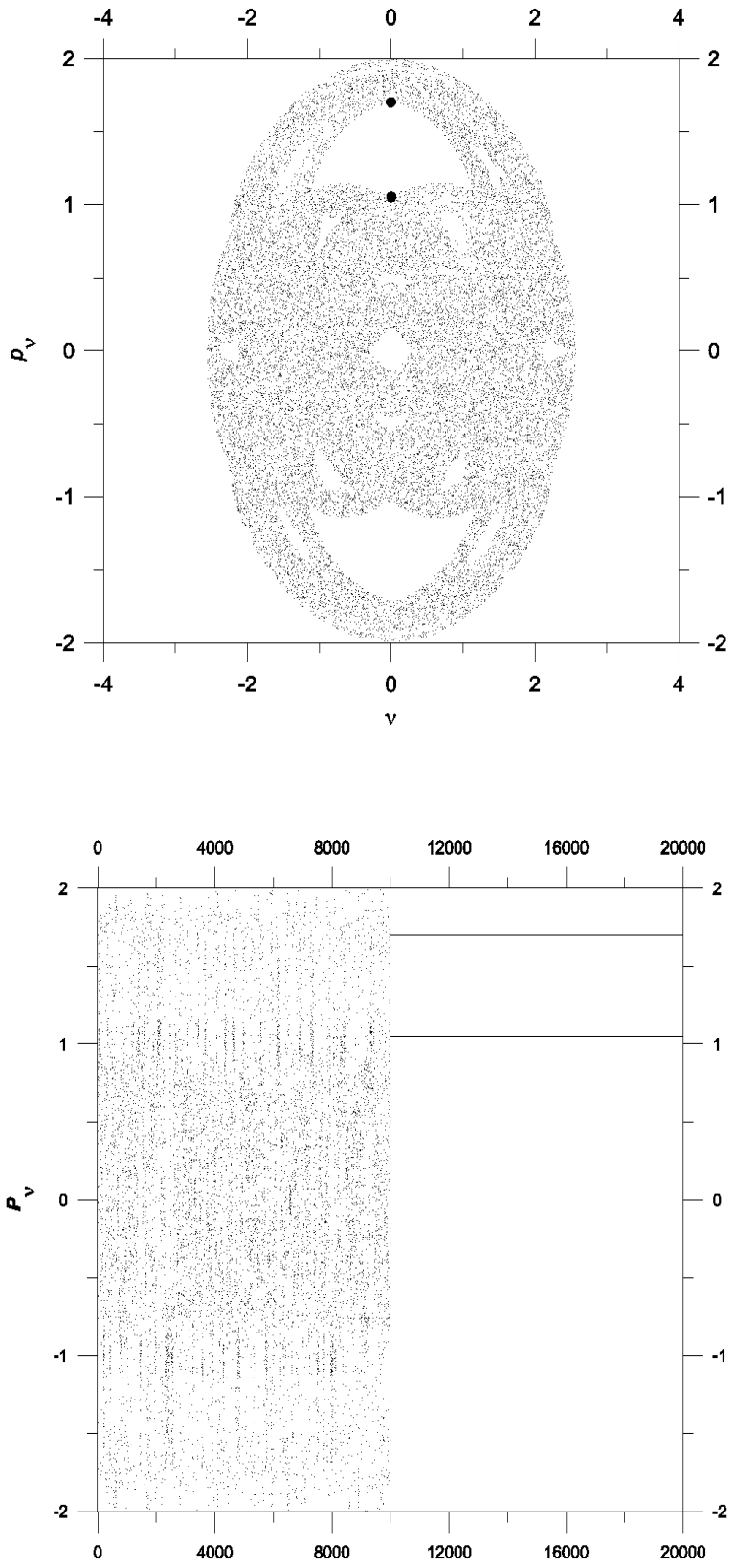

Figure 3.10: (a) **The DKP:** Top: An unstable period-2 orbit ($\epsilon = -0.3$). Bottom: The controlled trajectory around the period-2 orbit.

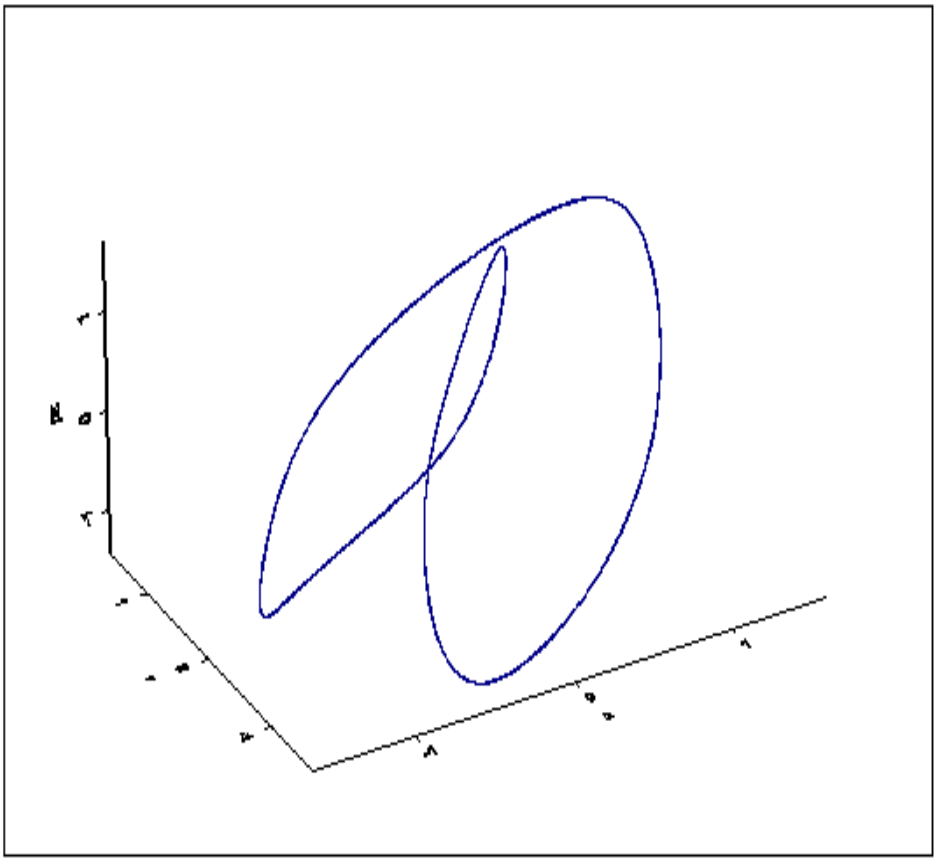

Figure 3.10: (b) **The DKP:** The same period-2 controlled trajectory (3- dimensional: μ, ν, p_μ).

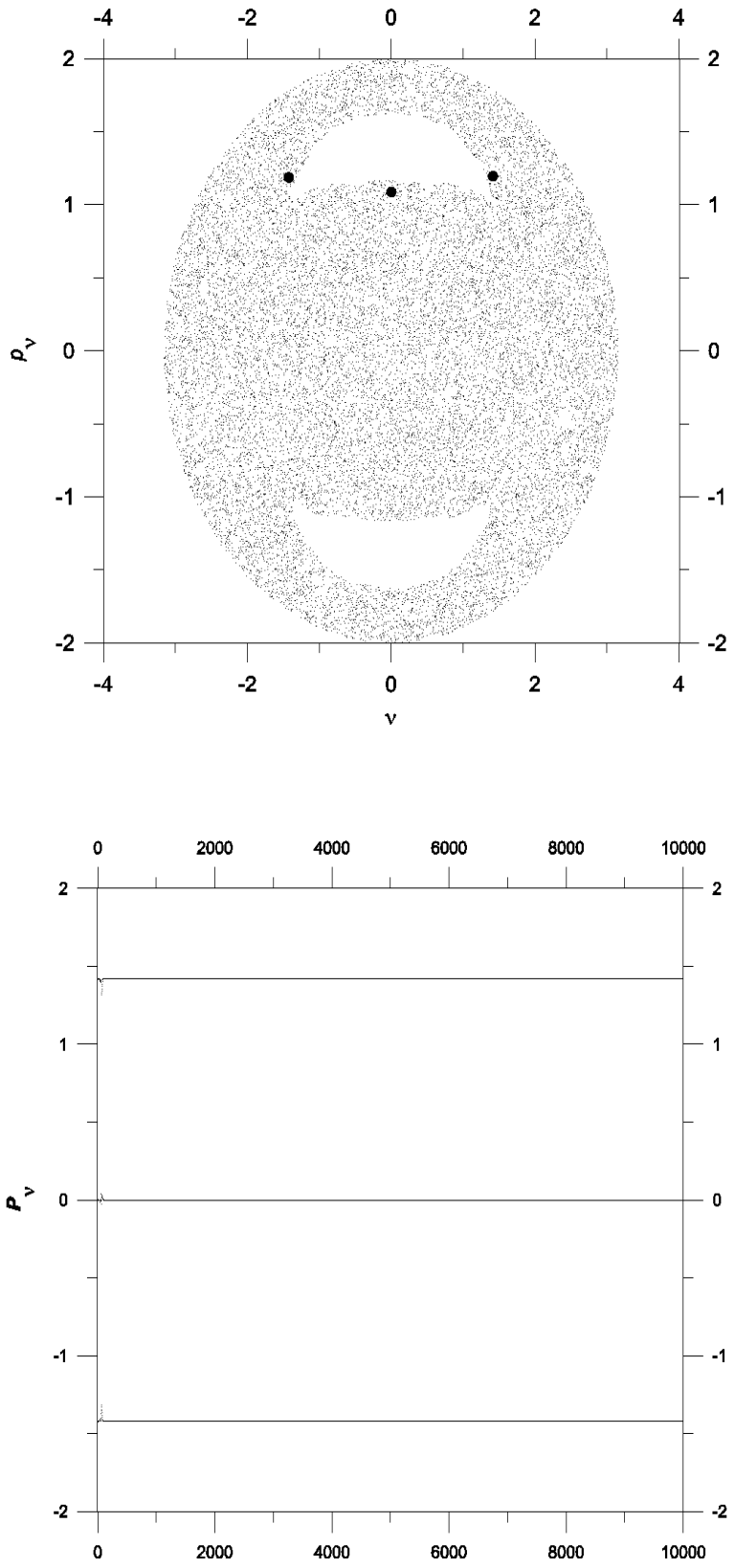

Figure 3.11: (a) **The DKP:** Top: An unstable period-3 orbit ($\epsilon = -0.2$). Bottom: The controlled trajectory around the period-3 orbit.

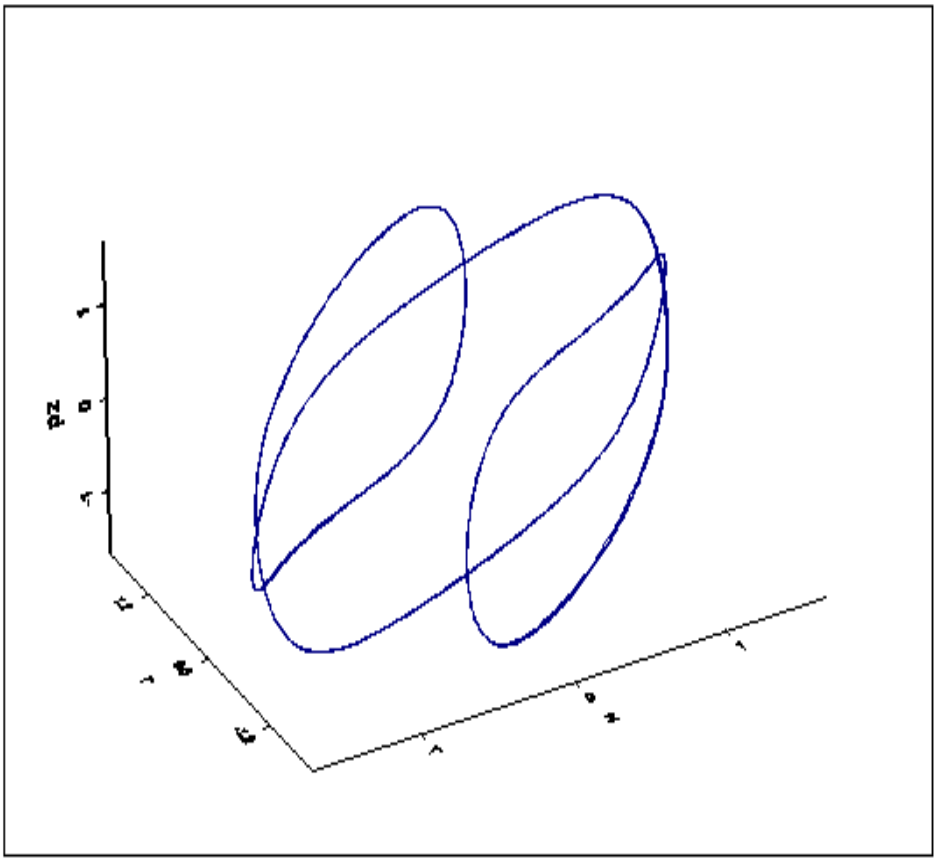

Figure 3.11: (b) **The DKP:** The same period-3 controlled trajectory (3- dimensional: μ, ν, p_μ)).

System		UPO Parameters					Control Parameters		
Map	Parameter	Period	δ_1	δ_2	N_{ic}	r	ϵ_c	δp_g	δp
DHM	$\mu = 1.4$	1	10^{-17}	0.0006	1681	0.01	0.05	0.005	$--^*$
DHM	$\mu = 1.4$	2	10^{-14}	0.0005	1681	0.01	0.05	0.005	$--^*$
DHM	$\mu = 1.4$	7	10^{-10}	0.00065	1681	0.01	0.05	0.002	$--^*$
DHM	$\mu = 1.4$	11	10^{-9}	0.00061	1681	0.01	0.05	0.001	$--^*$
Crémona	$\mu = -0.4224$	5	10^{-11}	0.0005	1681	0.01	0.05	0.001	$--^*$
Std	$K = 1.25$	2	10^{-17}	0.00041	1681	0.001	0.005	0.001	$--^*$
Std	$K = 1.25$	2	10^{-14}	0.00023	1681	0.001	0.005	0.001	$--^*$
Std	$K = 1.25$	2	10^{-14}	0.00055	1681	0.001	0.005	0.001	$--^*$
Std	$K = 1.25$	2	10^{-11}	0.00054	1681	0.001	0.005	0.001	$--^*$
Std	$K = 12$	2	10^{-9}	0.0021	1681	0.001	0.005	0.001	$--^*$
H-H	$E = 0.125$	1	10^{-4}	0.001	1000	0.001	0.001	0.001	$--^*$
H-H	$E = 0.14$	3	10^{-4}	0.0006	1000	0.001	0.001	0.001	$--^*$
DKP	$\epsilon = -0.3$	2	10^{-5}	0.001	1000	0.0005	0.001	0.001	$--^*$
DKP	$\epsilon = -0.2$	3	8×10^{-5}	0.002	1000	0.0002	0.001	0.0001	0.07
DKP	$\epsilon = -0.1$	1	10^{-9}	0.003	1000	0.0005	0.001	0.001	0.04

Table 3.2: **Data corresponding to the controlled trajectories for different maps.**

* In these cases the size of perturbation required for control is so small that there is no need to fix an upper limit for δp.

1. δ_1 : error in the position of periodic points
2. δ_2 : maximum error in the value of the Jacobian calculated at the periodic points
3. N_{ic} : number of initial conditions used
4. r : size of neighbourhood where the N_{ic} points are chosen
5. ϵ_c : size of neighbourhood where control mechanism is switched on
6. δp_g : change in p to calculate $\mathbf{g}_n$
7. δp : maximum absolute value allowed for parameter variation
8. H-H : the Hénon -Heiles Hamiltonian
9. Std : the standard map

Chapter 4

Tracking Hamiltonian Systems

A violent order is disorder; and
A great disorder is an order.
These two things are one.
Wallace Stevens
(Connaisseur of Chaos)

In this chapter we will develop a tracking algorithm which enables us to update the position of unstable periodic orbits belonging to a chaotic system while one of its parameters is changing, therefore maintaining control in the presence of parameter variation. We will present the tracking of a number of periodic orbits for the dissipative Hénon map, the standard map, and the diamagnetic Kepler problem (DKP).

A general question that appears constantly in both theory and experiment is, what happens to the solutions of a nonlinear system under study when a parameter is changed? This is known in the mathematical literature as continuation, and there is a wealth of information on how to construct the solutions as functions of parameters when one has a mathematical model in hand [Rheinboldt, 1986]. In nonlinear dynamical systems, bifurcation occurs as a result of the onset of instability as one or more parameters are changed. In typical dynamics experiments, only attractors are observed as parame-

ters are changed. In effect, only stable objects can be seen in the absence of outside intervention and unstable objects are shortly seen as transients. However, one of the underlying principles of the theory of nonlinear dynamical systems is that the dynamics observed over a large range of parameters is governed by the unstable states of the system. Examples of phenomena such as instability, chaos, crises, multiple attractors with fractal basin boundaries, and turbulence are the results of the rôle of one or more unstable states [Grebogi, Ott and Yorke, 1983; Brandstater and Swinney, 1987; Kreisberg, McCormick and Swinney, 1991; Schwartz, 1988a, 1988b]. Therefore one of the goals in trying to merge modelling and experimental efforts in nonlinear dynamics is to locate the governing unstable states both numerically and experimentally, and to investigate the properties of these states as parameters are changed.

In this chapter we will use the principles of continuation to motivate the location of unstable periodic orbits in physical experiments as a function of a parameter. The procedure of continuing an unstable state in a physical experiment is known as *tracking*. The initial paper which presented the original method applicable to experiments was done by Carroll, Schwartz, Triandaf and Pecora [1992], Triandaf and Schwartz [1993] and Schwartz, Carr and Triandaf [1997]. A sample of papers that have appeared since making use of tracking methods in experiments are: [Carroll *et al.*, 1992] in electronic circuits , [Gills, 1992; Bielawski *et al.*, 1994] in nonlinear optics, [Dressler *et al.*, 1995; In, Ditto and Spano, 1995] in mechanical systems, and [Petrov *et al.*, 1994] in chemistry. Other researchers have shown that tracking can be achieved in theoretical models: [Schwartz and Tsang, 1994], [Christini and Collins, 1995, 1996], [Rulkov, Tsimring and Abarbanel, 1994], [Volaseca, Kulminski and Corbalan, 1996], [Martin *et al.*, 1996].

We investigate the possibility of extending the application proposed by Schwartz and Triandaf to area-preserving mappings. We report the successful tracking of a modified version of this method on the standard map and the DKP.

4.1 Theoretical Foundations

The goal of tracking is to maintain control of the system as the system parameter is modified. This may be due to a change in the desired control point or due to the drift in the system over time. We consider the following dynamical system:

$$\mathbf{x}_{n+1} = \mathbf{F}(\mathbf{x}_n, P), \tag{4.1}$$

where $\mathbf{x}_n \in \mathcal{R}^{\mathcal{N}}$, $P \in \mathcal{R}$. The fixed points of the map satisfy

$$\mathbf{x}_f = \mathbf{F}(\mathbf{x}_f, P_f). \tag{4.2}$$

When bifurcation experiments are done in dynamics, curves of attractors are mapped as a function of an experimentally accessible parameter. Only stable states may be mapped out by this approach and one obtains the bifurcation diagram. Therefore to continue a branch of unstable orbits in an experiment, outside intervention is required to maintain (stabilize) an unstable state at a given parameter value. Therefore one must investigate the existence of the curve of unstable states: Let $\mathbf{G}$ be mapping from $(\mathcal{R}^{\mathcal{N}} \times \mathcal{R})$ to $\mathcal{R}^{\mathcal{N}}$ such that

$$\mathbf{G}(\mathbf{x}, P) = 0. \tag{4.3}$$

In the fixed point case, $\mathbf{G}(\mathbf{x}, P) = \mathbf{x} - \mathbf{F}(\mathbf{x}, P)$. Assuming $D_{\mathbf{x}}\mathbf{G}(\mathbf{x}, P)$ to be continuous in an open set $D \subset \mathcal{R}^{\mathcal{N}}$ containing $\mathbf{x}_f$ and nonsingular, the implicit function theorem implies the existence of open sets $S_1 \subset \mathcal{R}^{\mathcal{N}}$, $S_2 \subset \mathcal{R}$ such that for every $P \in S_2$, $G(\mathbf{x}, P) = 0$. Furthermore, there exists a unique function,

$$\mathbf{x} = \mathbf{W}(P), \tag{4.4}$$

such that $\mathbf{W}$ is a continuous mapping from S_2 to $\mathcal{R}^{\mathcal{N}}$. Using the assumption of non-singularity, differentiation of equation (4.3) and (4.4) yields the following:

$$\mathbf{W}'(P_f) = -[D_{\mathbf{x}}\mathbf{G}(\mathbf{x}_f, P_f)]^{-1} D_P \mathbf{G}(\mathbf{x}_f, P_f). \tag{4.5}$$

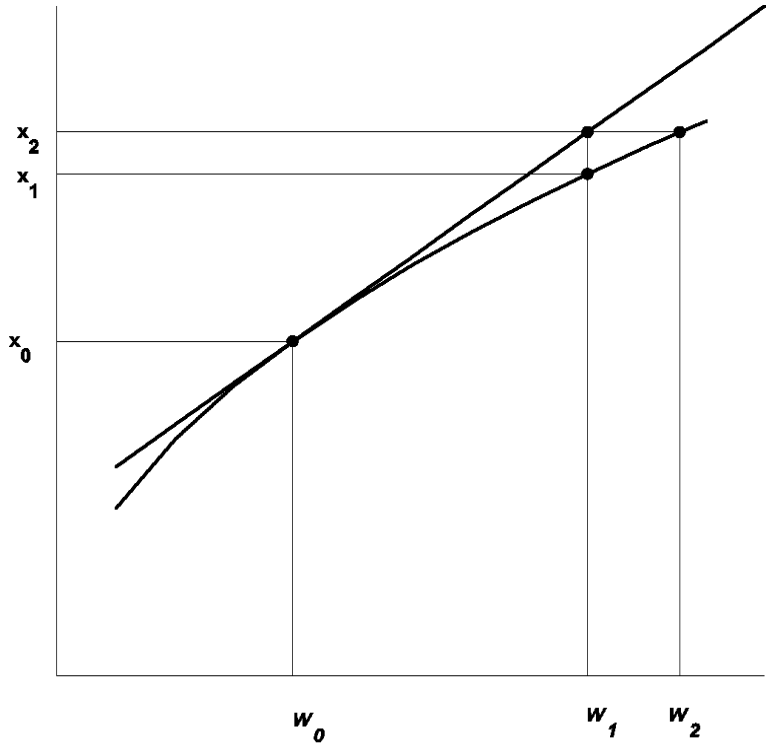

Figure 4.1: Curve of fixed points $\mathbf{x} = \mathbf{W}(P)$.

Equation (4.5) is quite general, and reveals a constructive method of creating a curve of fixed points. Substituting (4.4) into (4.3) and differentiating with respect to the parameter, we have as an initial value problem

$$\begin{aligned} \frac{d\mathbf{x}}{dP} &= -[D_{\mathbf{x}}\mathbf{G}(\mathbf{x}, P)]^{-1} D_P \mathbf{G}(\mathbf{x}, P), \\ \mathbf{x}(P_f) &= \mathbf{x}_f. \end{aligned} \tag{4.6}$$

Under the above hypotheses, equation (4.6) possesses a unique solution passing through the initial point. Therefore to perform tracking, one can initially make a prediction from some known fixed point $(\mathbf{x}_0, P_0)$, to a new point$(\mathbf{x}_2, P_0 + h)$ given by

$$\mathbf{x}_2 = \mathbf{x}_0 - h[D_{\mathbf{x}}\mathbf{G}(\mathbf{x}_0, P_0)]^{-1} D_P \mathbf{G}(\mathbf{x}_0, P_0). \tag{4.7}$$

This is shown schematically in figure (4.1) with $P_1 = P_0 + h$. By making such an approximation, an error from the graph $(\mathbf{W}(P), P)$ is made and is a function of the step size h. If we had a model for $\mathbf{G}$ at our disposal, we could make a correction by

solving

$$\mathbf{G}(\mathbf{x}, P_0 + h) = 0 \tag{4.8}$$

iteratively. Equations (4.7) and (4.1) are the basis of the prediction-correction algorithm proposed by Carroll, Schwartz, Triandaf and Pecora [1992]. In this method a linear predictor is used to make the prediction. Using a higher order predictor will of course yield a predicted point closer to the true curve. We have modified this method by replacing the linear predictor with a *rational function extrapolating algorithm* [Press *et al.*, 1992]. Upon a suitable choice of the parameters in this algorithm, we will show that the prediction remains close to the true curve over a long range of system parameter shift and this without the need of making any corrections. We discuss this algorithm in some details.

4.2 Rational Function Extrapolation

It is known that through any two points there is a unique line, through any three points a unique quadratic, and so on. The interpolating polynomial of degree $N-1$ through the N points $y_1 = f(x_1)$, $y_2 = f(x_2)$,$\cdots$, $y_N = f(x_N)$ is given explicitly by Lagrange's classical formula,

$$\begin{aligned} P(x) = \frac{(x-x_2)(x-x_3)\cdots(x-x_N}{(x_1-x_2)(x_1-x_3)\cdots(x_1-x_N)}y_1 + \frac{(x-x_1)(x-x_3)\cdots(x-x_N}{(x_2-x_1)(x_2-x_3)\cdots(x_2-x_N)}y_2 \\ + \cdots + \frac{(x-x_1)(x-x_2)\cdots(x-x_{N-1}}{(x_N-x_1)(x_N-x_2)\cdots(x_N-x_{N-1})}y_N \end{aligned} \tag{4.9}$$

Although the Lagrange's formula can be implemented straightforwardly, it is better to use the much more efficient *Neville's algorithm*. Let P_1 be the value at x of the unique polynomial of degree zero passing through the point (x_1, y_1); so $P_1 = y_1$. In the same way we define $P_2, P_3, \cdots, P_N$. Now, let P_{12} be the value at x of the unique polynomial of degree one passing through both (x_1, y_1) and (x_2, y_2). Likewise $P_{23}, P_{34}, \cdots, P_{(N-1)}N$. Similarly, for higher order polynomials, up to $P_{123\cdots N}$, which is the value of the unique

$x_1:$	$y_1 = P_1$			
		P_{12}		
$x_2:$	$y_2 = P_2$		P_{123}	
		P_{23}		P_{1234}
$x_3:$	$y_3 = P_3$		P_{234}	
		P_{34}		
x_4:	$y_4 = P_4$			

Table 4.1: Neville's algorithm ($N = 4$)

polynomial through all N points, i.e. the desired answer. This construction results in a *tableau* with *ancestors* on the left leading to a single *descendant* at the extreme right. Table (4.1) shows the tableau for $N = 4$.

A further improvement can be made by replacing the polynomial with a rational function. We denote by $R_{i(i+1)\cdots(i+m)}$ a rational function passing through the $m+1$ points $(x_i, y_i)\cdots(x_{i+m}, y_{i+m})$. More explicitly

$$R_{i(i+1)\cdots(i+m)} = \frac{P_\mu(x)}{Q_\nu(x)} = \frac{p_0 + p_1 x + \cdots + p_\mu x^\mu}{q_0 + q_1 x + \cdots + q_\nu x^\nu} \quad . \tag{4.10}$$

Rational functions are sometimes superior to polynomials, because of their ability to model functions with poles. Stoer and Bulirsch [1980] found an algorithm of the Neville type which performs rational function extrapolation on tabulated data. A tableau like that of table(4.1) is constructed column by column, leading to a result and an error estimate. The Bulirsch-Stoer algorithm produces the so-called diagonal rational function, with the degrees of the numerator and denominator equal (if m is even) or with the degree of denominator larger by one (if m is odd). the algorithm is summarized by a the following recurrence relation:

$$R_{i(i+1)\cdots(i+m)} = R_{(i+1)\cdots(i+m)} + \frac{R_{(i+1)\cdots(i+m)} - R_{i\cdots(i+m-1)}}{\left(\frac{x - x_i}{x - x_{i+m}}\right)\left(1 - \frac{R_{(i+1)\cdots(i+m)} - R_{i\cdots(i+m-1)}}{R_{(i+1)\cdots(i+m)} - R_{(i+1)\cdots(i+m-1)}}\right) - 1} \quad . \tag{4.11}$$

This recurrence generates the rational functions through $m+1$ points from the ones

through m and $m-1$ points. It is started with $R_i = y_i$ and with

$$R \equiv [R_{i(i+1)\cdots(i+m)} \quad with \quad m = -1] = 0. \tag{4.12}$$

An improvement on the recurrence (4.11) is to keep track of the small *differences* between "parents" and "daughters", namely to define (for m = 1,2,$\cdots$, N-1),

$$\begin{aligned} C_{m,i} &\equiv P_{i\cdots(i+m)} - P_{i\cdots(i+m-1)} \\ D_{m,i} &\equiv P_{i\cdots(i+m)} - P_{(i+1)\cdots(i+m)} \end{aligned} \tag{4.13}$$

These terms, which satisfy the relation

$$C_{m+1,i} - D_{m+1,i} = C_{m,i+1} - D_{m,i} \tag{4.14}$$

have the following recurrences

$$\begin{pmatrix} D_{m+1,i} \\ \\ \\ C_{m+1,i} \end{pmatrix} = \begin{pmatrix} \dfrac{C_{m,i+1}(C_{m,i+1} - D_{m,i})}{\left(\dfrac{x - x_i}{x - x_{i+m+1}}\right) D_{m,i} - C_{m,i+1}} \\ \\ \dfrac{\left(\dfrac{x - x_i}{x - x_{i+m+1}}\right) D_{m,i}(C_{m,i+1} - D_{m,i})}{\left(\dfrac{x - x_i}{x - x_{i+m+1}}\right) D_{m,i} - C_{m,i+1}} \end{pmatrix} . \tag{4.15}$$

At each level m, the C's and D's are the corrections that make the extrapolation one order higher. The final answer $P_{1\cdots N}$ is equal to the sum of any y_i plus a set of C's and/or D's that form a path through the family tree to the rightmost daughter.

In order to use this algorithm, one must provide a set of M initial pairs (x_i, y_i) and also a value for x at which the function must be calculated. The algorithm returns a value for y as well as an estimated error δy.

Since we are interested in studying the variation of the location of a periodic orbit as a function of the system parameter, we must provide, as the input to the above algorithm, one of the coordinates of an unstable point belonging to a periodic orbit for n values of the system parameter which are chosen from a small interval on the parameter axis, i.e. $\{(x_1, p_1), (x_2, p_2), \cdots, (x_n, p_n)\}$. Then, for sufficiently small increment of the

parameter value, $\delta p \ll 1$, the above algorithm gives the predicted value, for x_{n+1}, the coordinate of that unstable point (at $p_{n+1} = p_n + \delta p$). Next, we drop the first pair from the set of initial points (seeds) and add the new pair to it, and repeat the process to obtain new pair (x_{n+2}, p_{n+2}) and so on. It turns out that if the number of seeds n, the initial distribution of the parameter value $(p_1, \cdots, p_n)$ and the small increment δp are chosen properly, one can accurately extrapolate the value of x a long distance on the p axis away. We call this procedure "**adiabatic tracking (AT)**", since for $\delta p \ll 1$, we are advancing slowly on the parameter axis. We also note that after n applications of the extrapolation, all the original seeds have been replaced by extrapolated values. In the next section, we show the application of this method to a number of mappings.

4.3 Numerical Results

We present the numerical results obtained from the application of the AT to the dissipative Hénon map (DHM), the standard map (SM) and the diamagnetic Kepler problem (DKP).

For the Hénon map, we extended the tracking to the same range of the parameter values as was used by Carroll, Triandaf, Schwartz and Pecora [1992]. It is important to remark that in their work one has to correct the result obtained from a linear prediction at each step, while in our method one gets the accurate predicted value with no need to implement any correction over a reasonably long range on the parameter axis. As mentionned earlier, it is very important to select the right value for δp, the number of seeds and the initial distribution of the parameter values. Our experiments show that if one chooses an even number of seeds, the algorithm fails to perform adequately (i.e. to predict properly).This may be due to the fact that the solution to diagonal rational functions are ill-conditioned, but we have not investigated this matter further.

In our case, five seeds gave the best performance in all cases. Figure (4.2) shows the successful tracking of an unstable period-2 point over a long range of variation of the parameter μ of the DHM ($\epsilon = -0.3$). We choose the following five seeds for μ: 1.29, 1.30, 1.31, 1.32, 1.33 and set $\delta\mu = 0.001$. The results are in complete agreement with the values obtained by the stability transform algorithm (STA)(introduced in the previous chapter). It is important to note that even for $\mu = 1.53$ the trajectory explodes towards the attractor at infinity only after 15 iterations, indicating a high instability of the system for this value of μ. Figure (4.3) shows the tracking of a period-1 orbit of the map. By choosing each of the extrapolated points and iterating that point several times we observed that the for a number of times the iterates overlap one onother, a sign which identifies the point as a period-1 orbit. This test guarantees the effectiveness of the AT. The combination of the control algorithm introduced in the previous chapter with the present tracking algorithm creates an interesting and useful application: controlling the system during the system parameter variations. Figure (4.4) shows the control of a period-1 orbit, while the parameter μ changed from 1.4 to 1.54.

As the second example we applied the AT to the standard map. Figure (4.5) shows the continuation for a period-2 point, as well as the plot of the location of the same point using STA. For the five seeds we set μ as 1.00, 1.01, 1.02, 1.03, 1.04, and $\delta\mu = 10^{-3}$. The graph confirms the complete agreement between the two methods. We also applied the tracking algorithm backward. By choosing the initial value for μ as: 3.35, 3.25, 3.15, 3.05 and 2.95, we found the same agreement between the two algorithms.

The last example is the application of adiabatic tracking to the DKP. For the DKP, a successful tracking is remarkably important, because for a value of the system parameter $\epsilon > 0$, it is very difficult to detect the unstable periodic orbits numerically. The problem can be seen if one looks at the typical form of the potential for $\epsilon < 0$ as well as for $\epsilon > 0$ (figure (4.6)). For $e < 0$ the potential is locally bounded and the trajectory always explores a small region of the phase space (figure (4.7)) which results in many

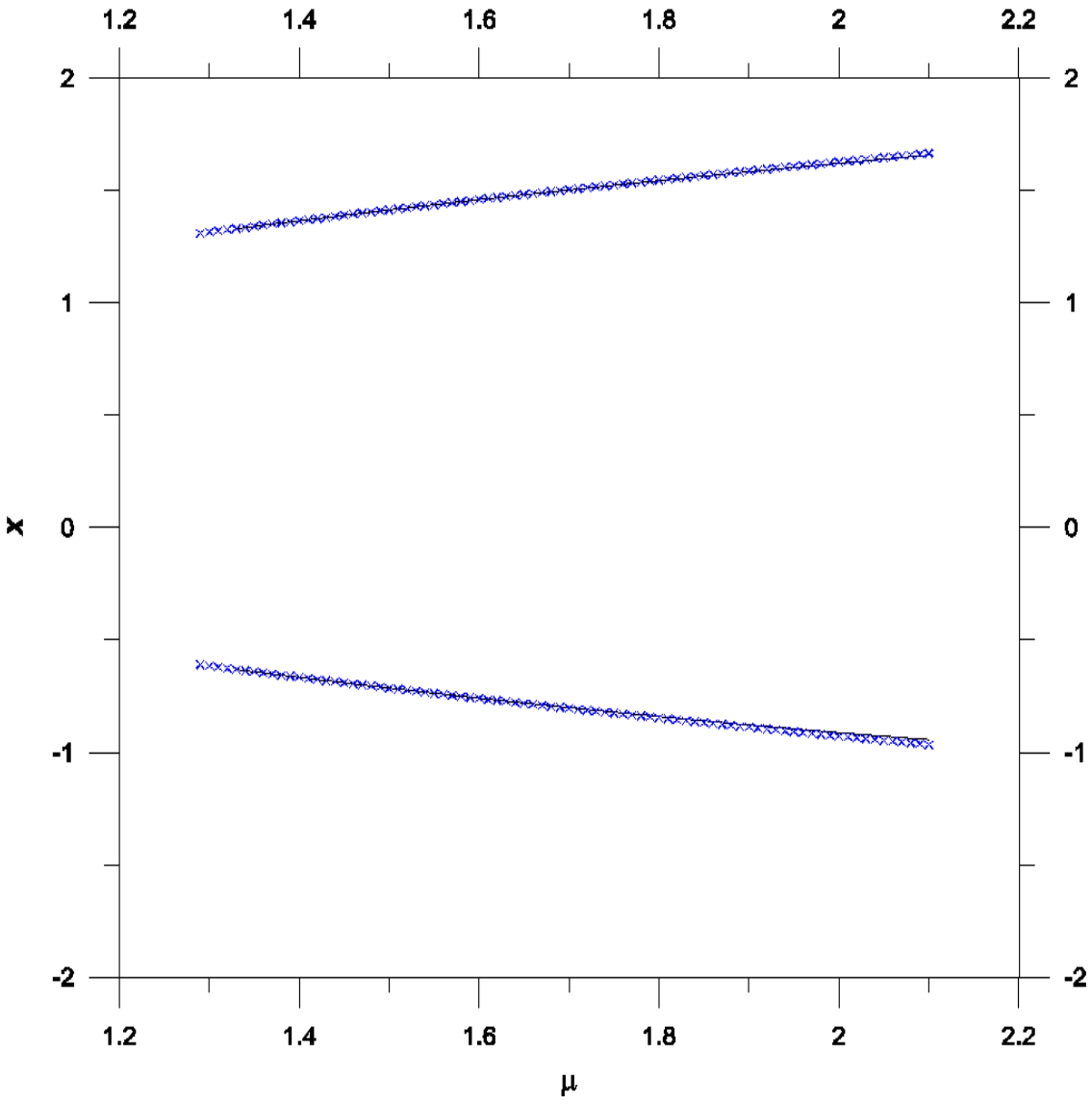

Figure 4.2: **Adiabatic tracking and the Hénon map: period-2.** Tracking an unstable period-2 point for 1.29$\leq \mu \leq$2.1. The results from "adiabatic tracking" (solid line) and the one from stability transform algorithm (x) are in complete agreement over a long range of parameter variation.

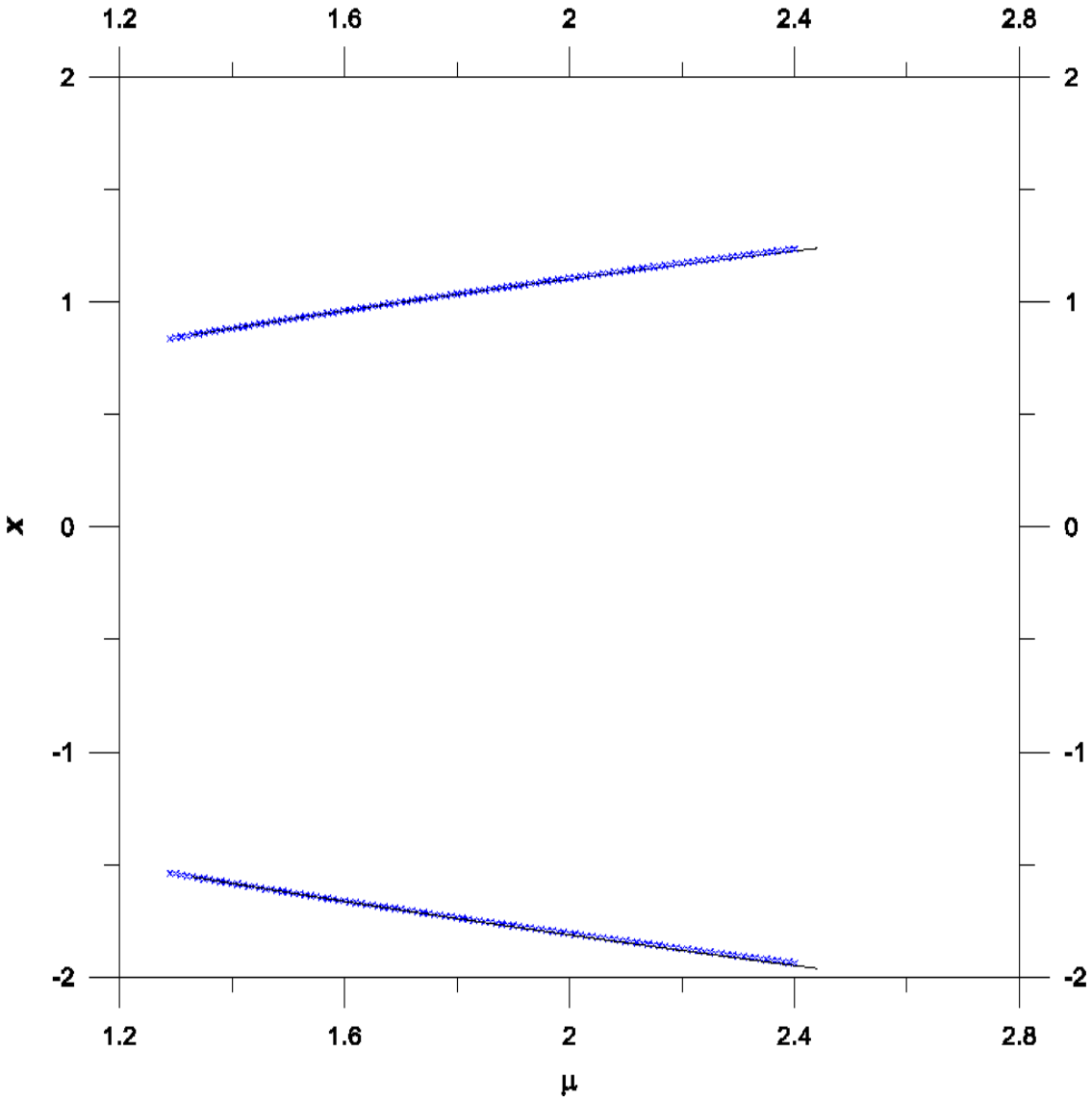

Figure 4.3: **Adiabatic tracking and the Hénon map: periods 1.** Tracking both fixed points (period-1) of Hénon map as a function of μ. Both curves are sketched on the same graph. For $\mu = 1.29$, the upper curve starts at $x^*_{1.29} = 0.838486$ and the lower curve starts at $x^*_{1.29} = -1.53849$.

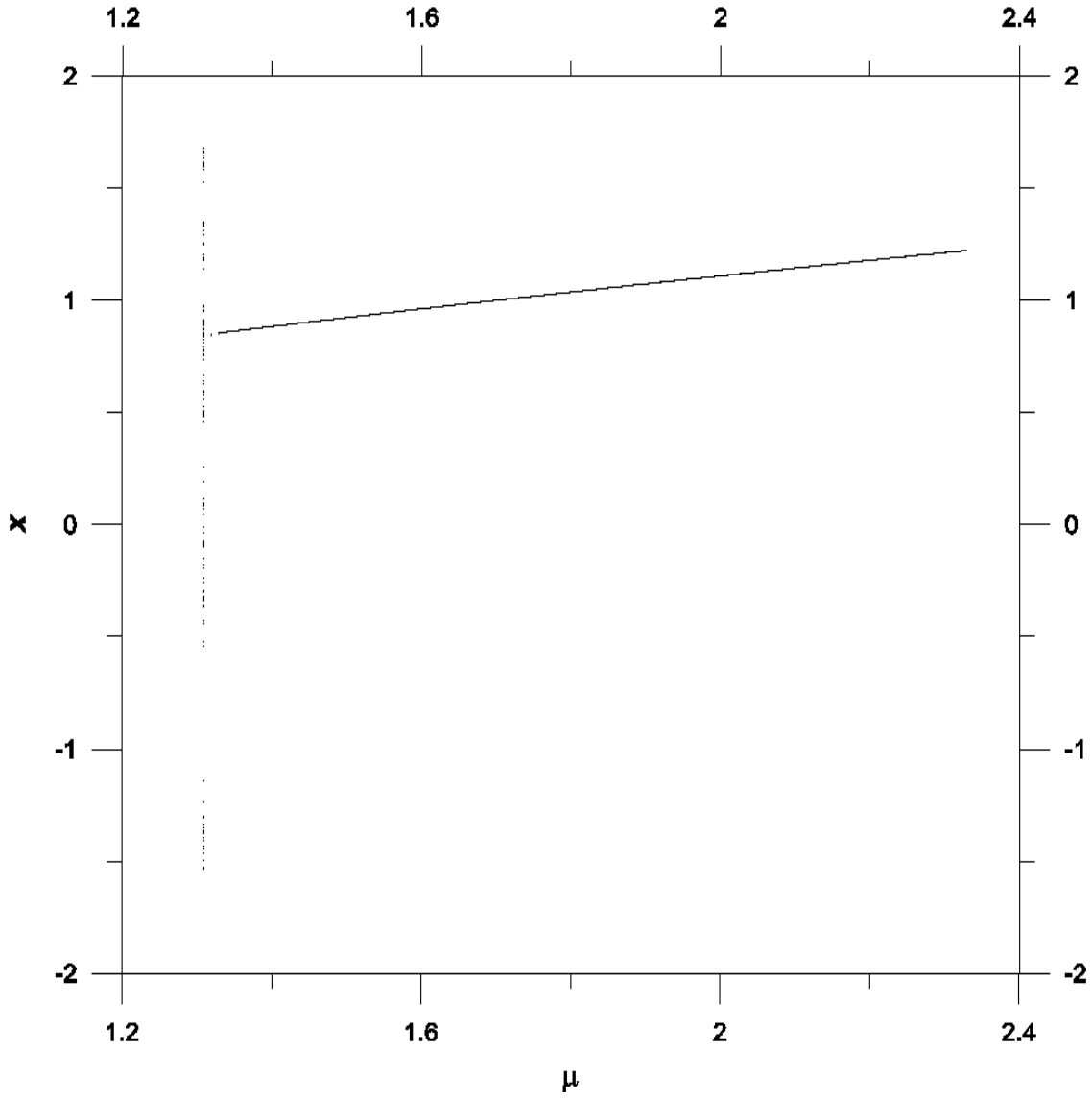

Figure 4.4: **Control and tracking in the Hénon map:** Controlling a period-1 orbit for $1.31 \leq \mu \leq 2.33$. We choose 3 seeds: $\mu = 1.29, 1.30$ and 1.31 and we increased μ at each step by 0.001. For each increment the trajectory is controlled for 100 iterations.

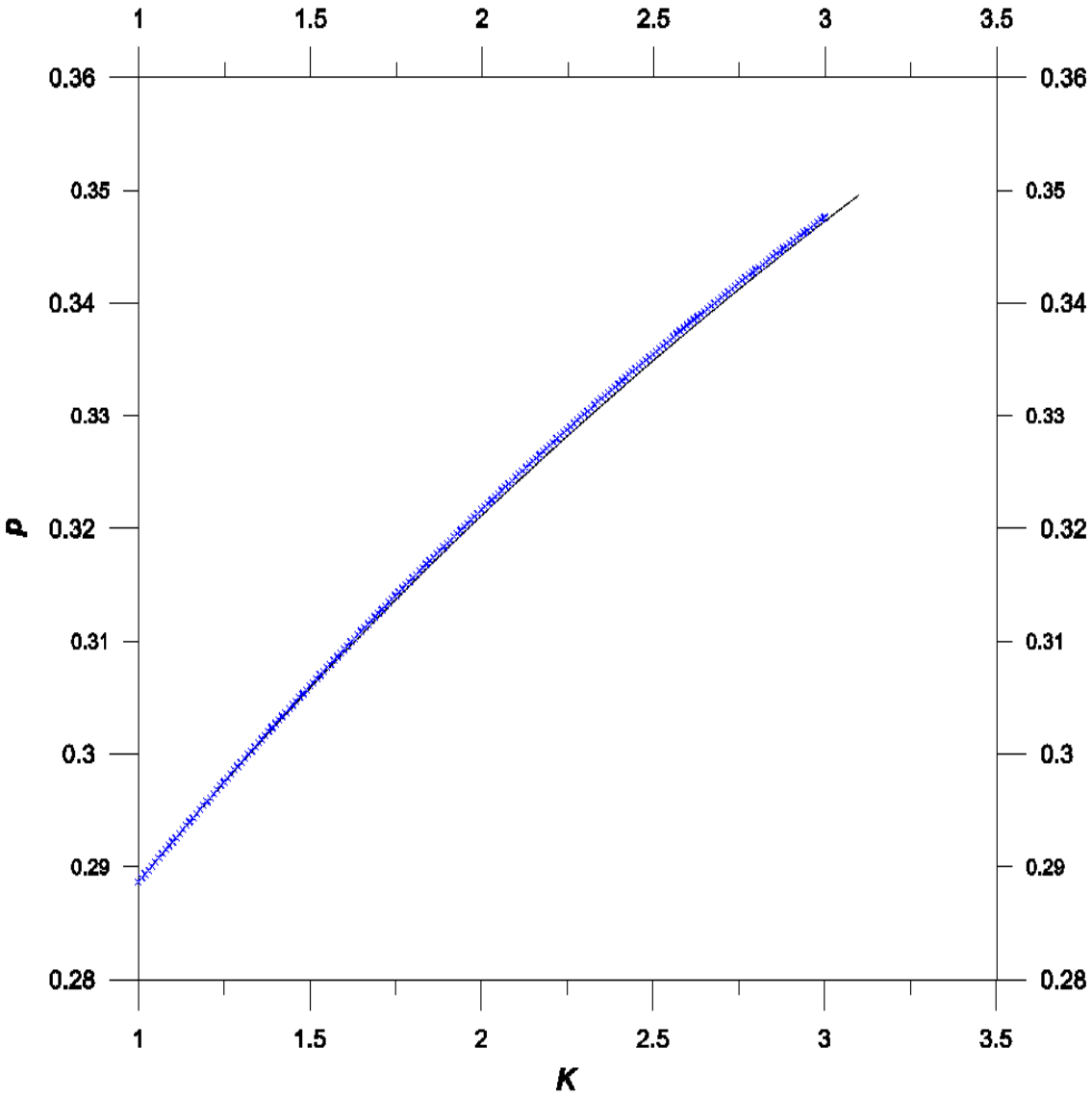

Figure 4.5: **Tracking and the standard map: period-2.** Tracking an unstable period-2 point for 1.0$\leq K \leq$3.0 (only one point shown). Number of seeds = 5 for K = 1.0, 1.01, 1.02, 1.03, 1.04 and $\delta\mu = 0.001$. Solid line: Adiabatic tracking, x: STA. For $K = 1.0$, $x_1^* = 0.288622$ and $y_1^* = 0.577246$.

intersections with the Poincaré section allowing us to determine the location of fixed points. By contrast for $\epsilon > 0$, the four branches of the potential well open up to infinity (figure (4.6b)), resulting in almost unbounded motion of the trajectory (figure (4.8)). Therefore when the trajectory falls into one of those branches, it spends a long time inside that branch, being reflected many times from the branch walls. Hence, it may take a very long time for the trajectory to come back to the central region and to hit the Poincaré section for the first time. After passing through the Poincaré section, the trajectory may fall into another branch and spend another long time in that branch before it comes back to the central region and hits the Poincaré section for the second time. It can be seen that as far as the calculation time is concerned, it is an extremely CPU intensive task to record only a few points on the Poincaré section. Therefore it would be very efficient and time saving if one finds the periodic orbits for $\epsilon < 0$ and then simply follow them using AT to predict their locations for $\epsilon > 0$. However, sudden disappearance of a periodic orbit is a natural barrier which sets a limit to AT. Figure (4.9) shows the tracking of a period-1 orbit for the DKP. We started from five seeds for ϵ: - 0.3, - 0.29, - 0.28, -0.27, -0.26 and set $\delta\mu = 0.001$. The results from the STA confirms the accuracy of the adiabatic tracking for $\epsilon < 0$. For $0 < \epsilon < \epsilon_c = 0.328782\cdots$, where the symbolic dynamic is not complete [Tanner, Hansen and Main, 1996], it is "almost impossible" to detect unstable orbits by existing algorithms (for $\epsilon > \epsilon_c$, there exists a complete symbolic description for unbounded chaotic motion). But even before reaching that point, the fixed point disappears at $\epsilon \simeq -0.075$. Figure (4.10) shows that the point obtained by AT up to that limit is indeed a period-1 orbit for $\epsilon = -0.075$.

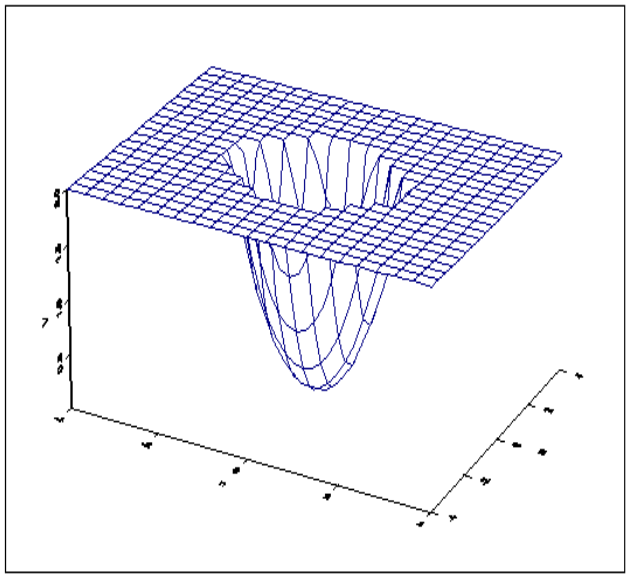

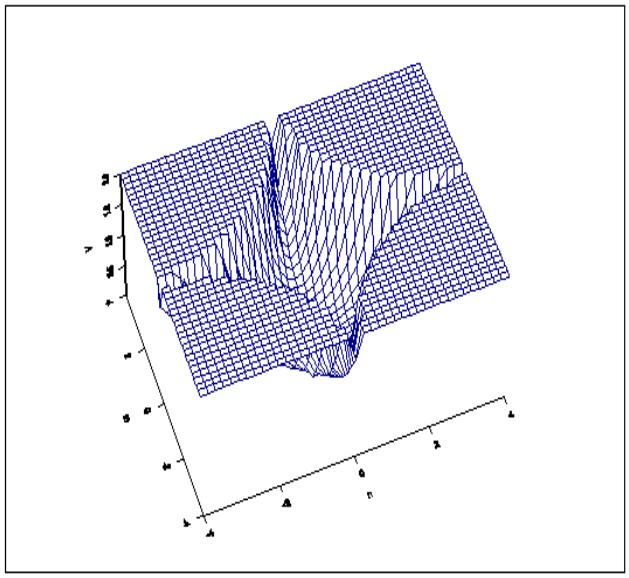

Figure 4.6: (a)**The DKP potential for negative values of ϵ:** Top: $\epsilon = -0.5$; Bottom: $\epsilon = -0.1$ (axes: μ, ν, V).

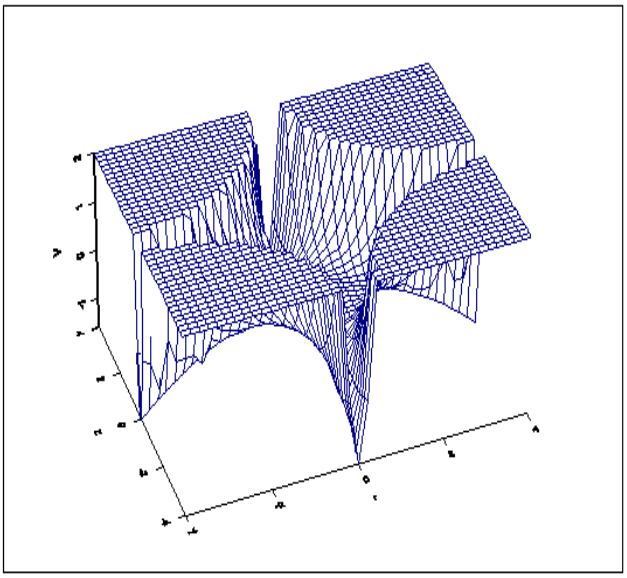

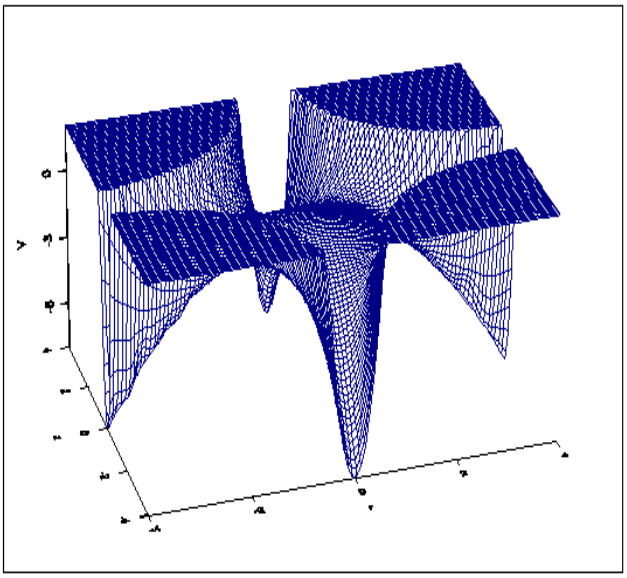

Figure 4.6: (b)**The DKP potential for positive values of ϵ:** Top: $\epsilon = 0.1$; Bottom: $\epsilon = 0.5$ (axes: μ, ν, V).

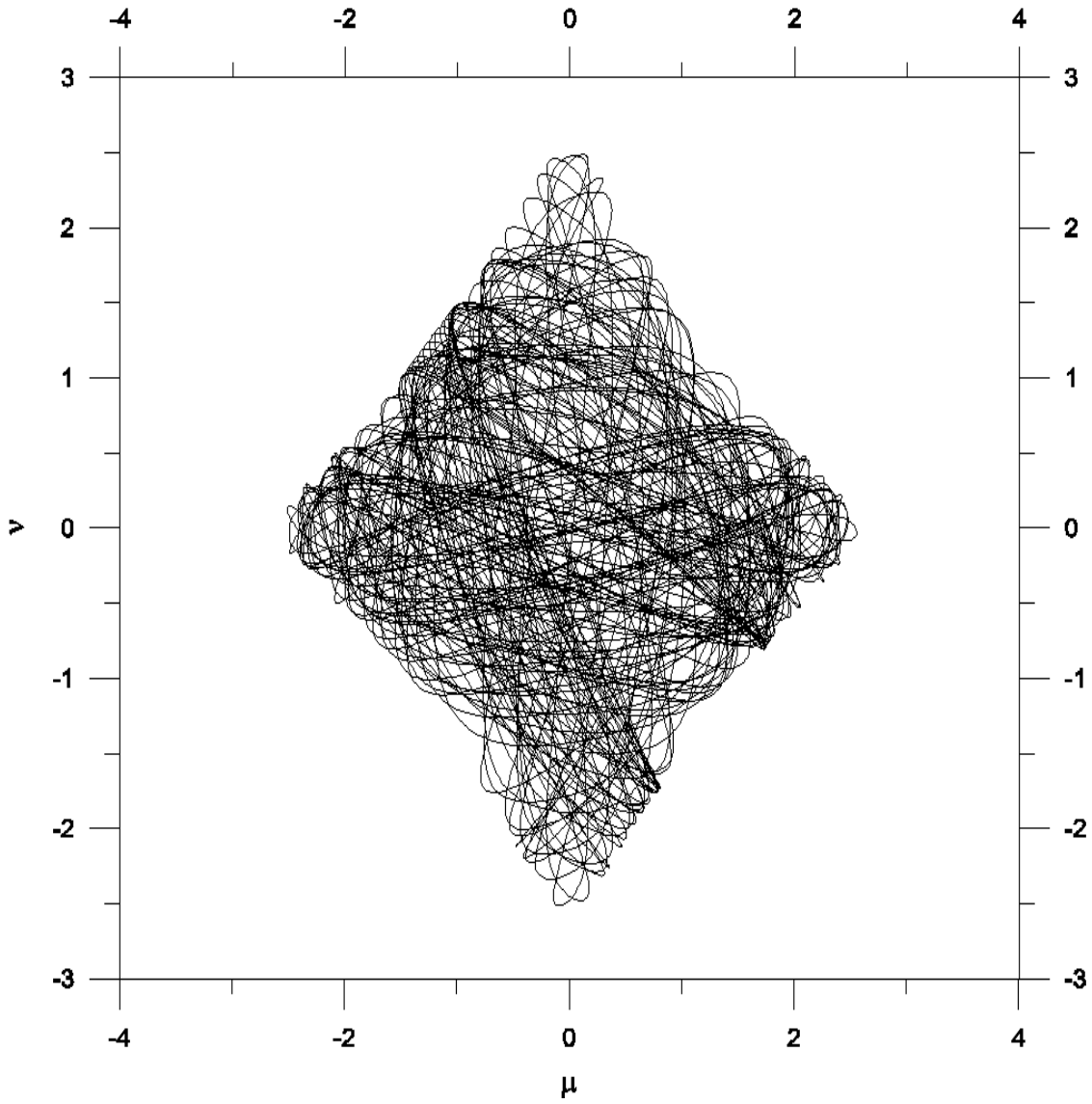

Figure 4.7: **A bounded trajectory for the DKP:** A typical trajectory for $\epsilon < 0$(ϵ = - 0.3).

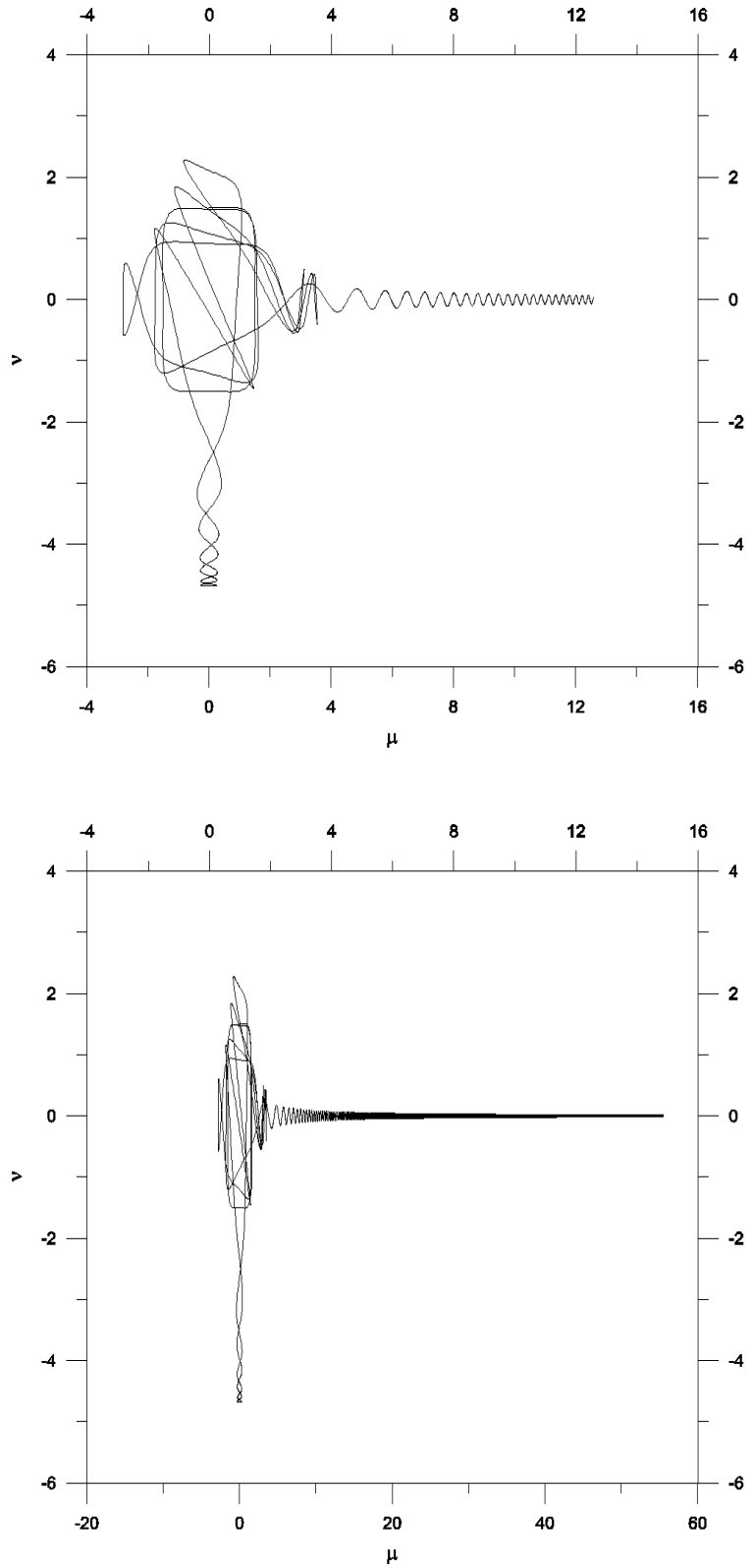

Figure 4.8: **An unbounded trajectory for the DKP:** A typical trajectory for $\epsilon > 0(\epsilon = 0.1)$. Top: number of points on the Poincaré section = 13, calculation time $\tau \ll 1sec.$(with a Pentium II, $400MHz$ processor) ; Bottom: The same trajectory. Number of points obtained on the Poincaré section: 14, calculation time $\tau = 7333$ *secs.*! . The curve only shows the first few seconds of the evolution of the trajectory.

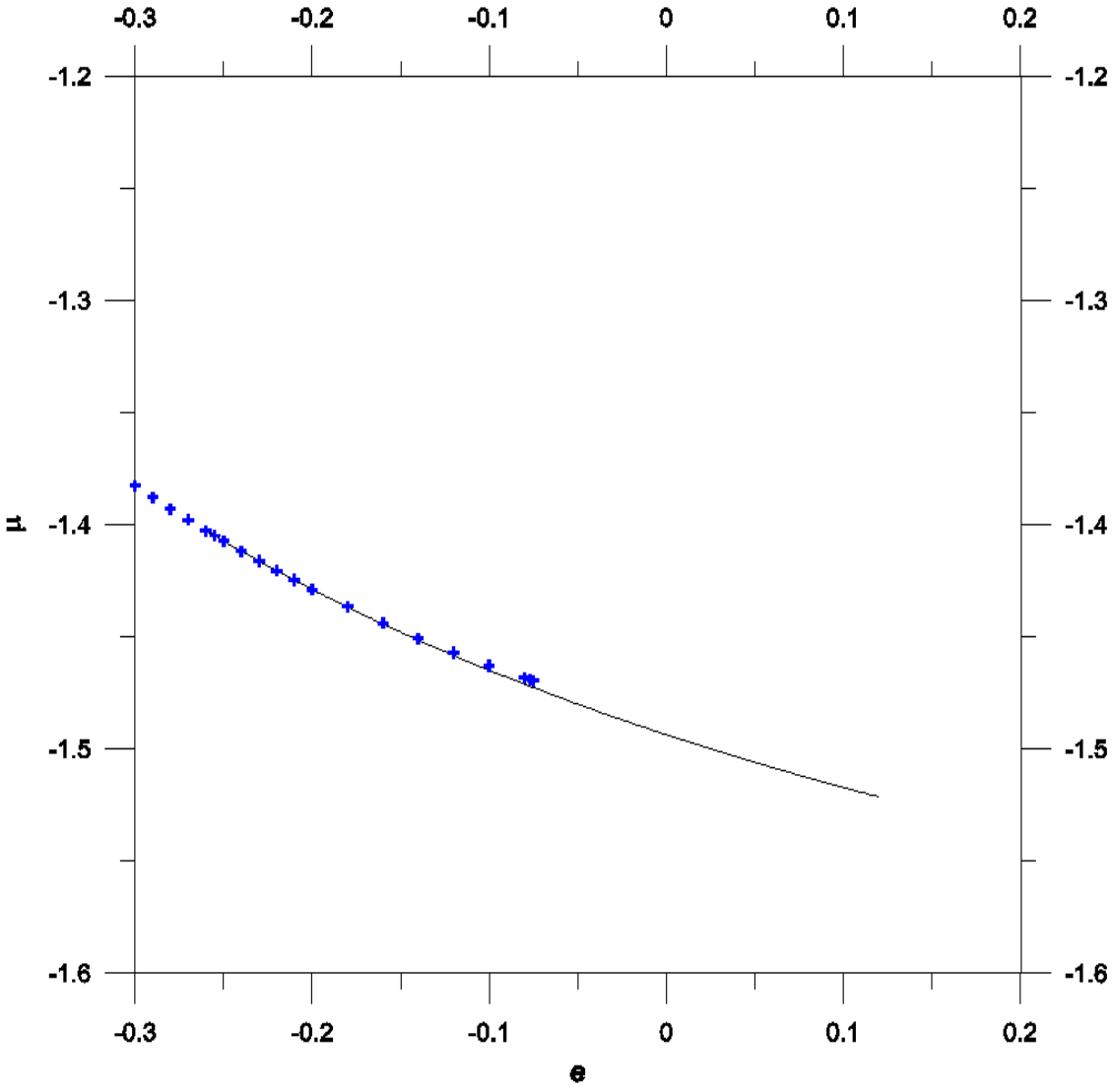

Figure 4.9: **Adiabatic tracking and the DKP:** Tracking an unstable period-1 point for - 0.3$\leq \epsilon \leq$- 0.075. Solid line: Adiabatic tracking. +: STA.

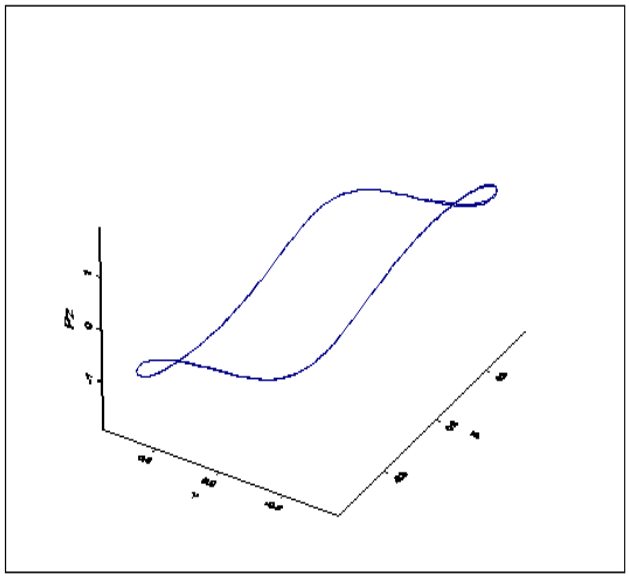

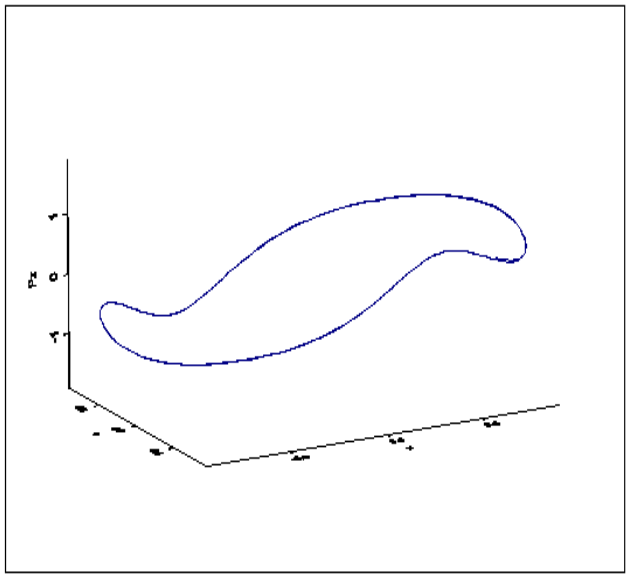

Figure 4.10: **A period-1 orbit of the DKP obtained by AT:** The initial condition of this trajectory is obtained by adiabatic tracking. ϵ = - 0.075, $\nu^* = -1.46942$ and $p_\nu^* = -0.000133596$(shown from two different angles).

Conclusion

CHAOS is the score on which the reality is written.
Henry Miller
(Black Spring)

The objective of this thesis was to study the probability of control and tracking in Hamiltonian systems. In particular, we were interested in stabilizing chaotic trajectories in an atomic system such as the Diamagnetic Kepler Problem.

In **chapter 1** we have discussed the theory of Hamiltonian dynamics and have presented the models used throughout this thesis. We have shown that, since the diamagnetic Kepler problem can exhibit chaos over a range of system parameters, it may be possible to transform the chaotic behaviour of an electron into regular motion.

In **chapter 2** we have introduced algorithms for detecting periodic orbits in chaotic systems. We have presented the recurrence algorithm as well as a recently developed algorithm proposed by *Schmelcher* and *Diakonos*. In particular, we have discussed the advantages and disadvantages of each method when applied to Hamiltonian systems. We have obtained a number of unstable periodic orbits for different systems for the further task of stabilizing chaotic trajectories around one of its unstable orbits.

In **chapter 3** we have introduced the OGY control algorithm and have reported for the first time the successful control of the chaotic behaviour of the Hénon -Heiles

Hamiltonian. We have also shown for the first time that the successful control can be applied to the chaotic motion of an electron in the presence of a magnetic field (the classical version of the DKP) and hencewith demonstrated the versatility of the OGY method and its possible application in atomic physics.

In **chapter 4** we have developed a tracking algorithm which enables us to update the position of unstable periodic orbits belonging to a chaotic system while one of its parameters is changing, therefore maintaining control in the presence of parameter variation. The tracking of a number of periodic orbits for the dissipative Hénon map, the standard map and the DKP has been presented.

The presence of chaos may be a great advantage for control in a variety of situations. In a nonchaotic system, small controls typically can only change the system dynamics slightly. Short of applying large controls or greatly modifying the system, we are stuck with whatever system performance already exists. In a chaotic system, on the other hand, we are free to choose between a rich variety of dynamical behaviours. Thus it may be advantageous to design chaos into systems, allowing such variety without requiring large controls or the design of separate systems for each desired behaviour. The general problem of controlling chaotic systems is very rich, and may help solve technologically important problems in widely diverse fields of study. The wealth of results already achieved encourage us to look forward to a fruitful future for the control of chaotic systems.

If there be nothing new, but that which is
Hath been before, how are our brains beguiled,
Which, laboring for invention, bear amiss
The second burden of a former child!
(Shakespeare, Sonnet 59)

Appendix

As discussed in *Chapter 1* the Hamiltonian of the DKP can be written as

$$H_{DK} = \frac{1}{2m_e}(p_\rho^2 + p_z^2) - \frac{e^2}{(\rho^2 + z^2)^{\frac{1}{2}}} + \frac{L_z^2}{2m_e\rho^2} + \lambda\rho^2 \tag{1}$$

where

$$\lambda \quad = \quad \frac{e^2B^2}{8m_ec^2} \quad = \quad \frac{1}{8}\frac{m_e^3e^8}{\hbar^6}\gamma_0^2 \tag{2}$$

We wish to perform a dimensional analysis in order to reduce the number of parameters (presently four of them (m_e, e, λ, L_z)) into non-dimensional groups. Let us introduce the dimensionless variables:

$$\hat{\rho} = \frac{\rho}{\alpha}\ , \quad \hat{p}_\rho = \frac{p_\rho}{\beta} \qquad \hat{z} = \frac{z}{\alpha}\ , \quad \hat{p}_z = \frac{p_z}{\beta} \qquad \hat{t} = \frac{t}{\gamma}, \tag{3}$$

Obviously, α, β and γ have the dimensions of length, momentum and time, respectively:

$$[\alpha] = L, \qquad [\beta] = MLT^{-1}, \qquad [\gamma] = T. \tag{4}$$

In order to find the parameters α, β and γ one can proceed as follows:

- **Calculation of** α:

We pose that α should be expressible as products of the available parameters raised to certain powers to be determined, i.e.

$$\alpha \propto m_e^a e^b \lambda^c L_z^d. \tag{5}$$

Therefore,

$$[\alpha] = M^a[ML^3T^{-2}]^{\frac{b}{2}}[MT^{-2}]^c[ML^2T^{-1}]^d. \tag{6}$$

Equating the exponents of each unit on both sides, we obtain:

$$\begin{aligned} a + \frac{b}{2} + c + d &= 0 \\ \frac{3}{2}b + 2d &= 1 \\ -b - 2c - d &= 0 \end{aligned} \tag{7}$$

The simplest solution is obtained by

$$d = 0 \longrightarrow b = \frac{2}{3} \longrightarrow c = -\frac{1}{3} \longrightarrow a = 0 \tag{8}$$

Therefore,

$$\alpha \propto \frac{e^{\frac{2}{3}}}{\lambda^{\frac{1}{3}}} \tag{9}$$

which is the same as the parameter introduced in equation (1.33) up to a constant factor.

- **Calculation of β**:

  Similarly for β, we write

$$\beta \propto m_e^a e^b \lambda^c L_z^d. \tag{10}$$

It follows that,

$$[\beta] = M^a[ML^3T^{-2}]^{\frac{b}{2}}[MT^{-2}]^c[ML^2T^{-1}]^d \tag{11}$$

Equating the exponents of each unit on both sides, we obtain:

$$\begin{aligned} a + \frac{b}{2} + c + d &= 1 \\ \frac{3}{2}b + 2d &= 1 \\ -b - 2c - d &= -1 \end{aligned} \tag{12}$$

Again one has

$$d = 0 \longrightarrow b = \frac{2}{3} \longrightarrow c = \frac{1}{6} \longrightarrow a = \frac{1}{2} \tag{13}$$

Therefore,

$$\beta \propto m_e^{\frac{1}{2}} e^{\frac{2}{3}} \lambda^{\frac{1}{6}} \tag{14}$$

in accord with equation (1.33).

- **Calculation of γ:**

Finally, for γ, we set again

$$\gamma \propto m_e^a e^b \lambda^c L_z^d \tag{15}$$

leading to

$$[\gamma] = M^a [ML^3T^{-2}]^{\frac{b}{2}} [MT^{-2}]^c [ML^2T^{-1}]^d \tag{16}$$

Equating the exponents of each unit on both sides, we obtain:

$$\begin{aligned} a + \frac{b}{2} + c + d &= 0 \\ \frac{3}{2}b + 2d &= 0 \\ -b - 2c - d &= 1 \end{aligned} \tag{17}$$

The simplest solution is obtained by

$$d = 0 \longrightarrow b = 0 \longrightarrow c = -\frac{1}{2} \longrightarrow a = \frac{1}{2} \tag{18}$$

such that

$$\gamma \propto \frac{e^{\frac{1}{2}}}{\lambda^{\frac{1}{2}}} \tag{19}$$

as in equation (1.33).

Consider the Hamiltonian

$$\hat{H}_{DK} = \frac{m_e}{\beta^2} H_{DK} = \frac{1}{2}(\hat{p}_\rho^2 + \hat{p}_z^2) - \frac{m_e e^2}{\alpha\beta^2} \frac{1}{(\hat{\rho}^2 + \hat{z}^2)^{\frac{1}{2}}} + \frac{1}{2} \frac{1}{\alpha^2\beta^2} \frac{L_z^2}{\hat{\rho}^2} + \lambda \frac{m_e \alpha^2}{\beta^2} \hat{\rho}^2. \tag{20}$$

One can rewrite it as

$$\hat{H}_{DK} = \frac{1}{2}(\hat{p}_\rho^2 + \hat{p}_z^2) - \frac{1}{(\hat{\rho}^2 + \hat{z}^2)^{\frac{1}{2}}} + \frac{\hat{L}^2}{2\hat{\rho}^2} + \frac{1}{8}\hat{\rho}^2. \tag{21}$$

with

$$\hat{L} = \left(\frac{8\lambda}{m_e^3 e^8}\right)^{\frac{1}{6}} L_z = \gamma_0^{\frac{1}{3}} \left(\frac{L_z}{\hbar}\right). \tag{22}$$

We have thereby reduced our original 4 parameter Hamiltonian to a 1 parameter Hamiltonian. Up to a multiplicative factor, one can also obtain a non-dimensional parameter out of (m_e, e, λ, L_z), namely, $\hat{L} \propto m_e^a e^b \lambda^c L_z^d$

$$\begin{aligned} a + \frac{b}{2} + c + d &= 0 \\ \frac{3}{2}b + 2d &= 0 \\ -b - 2c - d &= 0 \end{aligned} \tag{23}$$

which yields

$$[\hat{L}] = M^a [ML^3T^{-2}]^{\frac{b}{2}} [MT^{-2}]^c [ML^2T^{-1}]^d \tag{24}$$

A non-trivial solution may be obtained by choosing $d = 1$:

$$d = 1 \longrightarrow b = -\frac{4}{3} \longrightarrow c = -\frac{b+d}{2} = \frac{1}{6} \longrightarrow a = -(\frac{b}{2} + c + d) = -\frac{1}{2}. \tag{25}$$

Therefore,

$$\hat{L} \quad \propto \quad m_e^{-\frac{1}{2}} e^{-\frac{4}{3}} \lambda^{\frac{1}{6}} L_z \quad \propto \quad \left(\frac{\lambda}{m_e^3 e^8}\right) L_z, \tag{26}$$

as expected.

Bibliography

[1] P. M. Alsing, A. Gavrielides, and V. Kovanis, *History-dependent control of unstable periodic orbits*, Physical Review E, **50** (1994), pp. 1968–77.

[2] ——, *Using neural networks for controlling chaos*, Physical Review E, **49** (1994), pp. 1225–31.

[3] V. I. Arnol'd, *Small denominators and problems of stability of motion in classical and celestial mechanics*, Russian Mathematical Surveys, **18:6** (1963), pp. 85–191.

[4] D. Auerbach et al., *Exploring chaotic motion through periodic orbits*, Physical Review Letters, **58** (1987), pp. 2387–9.

[5] D. Auerbach, C. Grebogi, E. Ott, and J. A. Yorke, *Controlling chaos in high dimensional systems*, Physical Review Letters, **69** (1992), pp. 3479–82.

[6] M. V. Berry, *Regular and irregular motion*, AIP Conference Proceedings, **46** (1978), pp. 16–120.

[7] S. Bielawski, D. Derozier, and P. Glorieux, *Controlling unstable periodic orbits by a delayed continuous feedback*, Physical Review E, **49** (1994), pp. R971–4.

[8] Y. l. Bolotin et al., *Control of unstable high-period orbits in complex systems*, Physical Review Letters, **82** (1999), pp. 2504–7.

[9] E. M. Bolt and J. D. Meiss, *Controlling chaotic transport through recurrence*, Physica D, **81** (1995), pp. 280–94.

[10] A. Brandstater and H. L. Swinney, *Strange attractors in weakly turbulent Couette-Taylor flow*, Physical Review A, **35** (1987), pp. 2207–20.

[11] T. L. Carroll, I. Triandaf, I. Schwartz, and L. Pecora, *Tracking unstable orbits in an experiment*, Physical Review A, **46** (1992), pp. 6189–92.

[12] L. Casetti, *Efficient symplectic algorithms for numerical simulations of Hamiltonian flows*, Physica Scripta, **51** (1995), pp. 29–34.

[13] P. J. Channell and C. Scovel, *Symplectic integration of Hamiltonian systems*, Nonlinearity, **3** (1990), pp. 231–59.

[14] N. P. Chau, *Controlling continuous chaotic dynamics by periodic proportional pulses*, Physical Review E, **57** (1998), pp. 378–80.

[15] B. V. Chirikov, *Resonance processes in magnetic traps*, Journal of Nuclear Energy C, **1** (1960), pp. 253–60.

[16] D. J. Christini and J. J. Collins, *Using noise and chaos control to control nonchaotic systems*, Physical Review E, **52** (1995), pp. 5806–9.

[17] ——, *Using chaos control and tracking to suppress a pathological nonchaotic rhythm in a cardiac model*, Physical Review E, **53** (1996), pp. R49–52.

[18] J. B. Delos et al., *Atomic electrons in strong magnetic fields: Transition from elliptical to helical behavior*, Physical Review A, **37** (1988), pp. 4582–98.

[19] J. B. Delos, S. K. Knudson, and D. W. Noid, *High Rydberg states of an atom in a strong magnetic field*, Physical Review Letters, **50** (1983), pp. 579–83.

[20] ——, *Highly excited states of a hydrogen atom in a strong magnetic field*, Physical Review A, **28** (1983), pp. 7–21.

[21] ——, *Trajectories of an atomic electron in a magnetic field*, Physical Review A, **30** (1984), pp. 1208–18.

[22] F. K. Diakonos, P. Schmelcher, and O. Biham, *Systematic computation of the least unstable periodic orbits in chaotic attractors*, Physical Review Letters, **81** (1998), pp. 4349–52.

[23] M. Ding et al., *Control and synchronization of chaos in high dimensional systems: Review of some recent results*, Chaos, **7(4)** (1997), pp. 644–52.

[24] W. L. Ditto, S. N. Rauseo, and M. L. Spano, *Experimental control of chaos*, Physical Review Letters, **65** (1990), pp. 3211–4.

[25] W. L. Ditto, M. L. Spano, and J. F. Lindher, *Techniques for the control of chaos*, Physica D, **86** (1995), pp. 198–211.

[26] B. G. S. Doman, *Relativistic energy levels of hydrogen in strong magnetic fields*, Journal of Physics B, **13** (1980), pp. 3335–40.

[27] U. Dressler et al., *Tracking unstable periodic orbits in a bronze ribbon experiment*, Physical Review E, **51** (1995), pp. 1845–8.

[28] J. P. Eckmann and D. Ruelle, *Ergodic theory of chaos and strange attractors*, Reviews of Modern Physics, **57** (1985), pp. 617–56.

[29] B. I. Epureanu and E. H. Dowell, *On the optimality of the Ott-Grebogi-Yorke control scheme*, Physica D, **116** (1998), pp. 1–7.

[30] U. Feudel and C. Grebogi, *Multistability and the control of complexity*, Chaos, **7(4)** (1997), pp. 597–604.

[31] A. Fouladi and J. A. Valdivia, *Period control of chaotic systems by optimization*, Physical Review E, **55** (1997), pp. 1315–20.

[32] H. Friedrich and D. Wintgen, *The hydrogen atom in a uniform magnetic field - an example of chaos*, Physics Reports, **183** (1989), pp. 37–79.

[33] R. H. Garstang, *Atoms in high magnetic fields*, Reports on Progress in Physics, **40** (1977), pp. 105–54.

[34] Z. Gills et al., *Tracking unstable steady states: Extending the stability regime of a multimode laser*, Physical Review Letters, **69** (1992), pp. 3169–72.

[35] H. Goldstein, *Classical Mechanics*, Addison - Wesley, 2^{nd} ed., (1980).

[36] P. Góra and A. Boyarsky, *A new approach to controlling chaotic systems*, Physica D, **111** (1998), pp. 1–15.

[37] C. Grebogi, E. Ott, and J. A. Yorke, *Crises, sudden changes in chaotic attractors, and transient chaos*, Physica D, (1983), pp. 181–200.

[38] J. M. Greene, *A method for determining a stochastic transition*, Journal of Mathematical Physics, **20** (1979), pp. 1183–201.

[39] M. C. Gutzwiller, *Chaos in Classical and Quantum Mechanics*, Springer - Verlag, (1990).

[40] ——, *Moon-Earth-Sun: The oldest three-body problem*, Reviews of Modern Physics, **70** (1998), pp. 589–639.

[41] K. T. Hansen, *Bifurcations and complete chaos for the diamagnetic Kepler problem*, Physical Review A, **51** (1994), pp. 1838–44.

[42] M. Hénon, *Numerical study of area-preserving mappings*, Quarterly of Applied Mathematics, **27** (1969), p. 291.

[43] M. Hénon, *A two-dimensional mapping with a strange attractor*, Communications in Mathematical Physics, **50** (1976), pp. 69–77.

[44] ——, *Numerical Exploration of Hamiltonian Systems*, North-Holland, (1983). (appeared in *Chaotic Behaviour of Deterministic Systems* (pp. 55-170) edited by: G.Iooss, R.Helleman and R.Stora).

[45] M. Hénon and C. Heiles, *The applicability of the third integral of motion: Some numerical experiments*, The Astronomical Journal, **69** (1964), pp. 73–79.

[46] H. Herold, H. Ruder, and G. Wunner, *The two-body problem in the presence of a homogeneous magnetic field*, Journal of Physics B, **14** (1981), pp. 751–64.

[47] A. Hübler et al., *Resonant simulation of nonlinear damped oscillators by Poincaré maps*, Helv. Phys. Acta, **61** (1988), pp. 897–900.

[48] E. R. Hunt, *Stabilizing high-period orbits in a chaotic system: The diode resonator*, Physical Review Letters, **67** (1991), pp. 1953–5.

[49] V. In, W. L. Ditto, and M. Spano, *Adaptive control and tracking of chaos in a magnetoelastic ribbon*, Physical Review E, **51** (1995), pp. R2689–92.

[50] E. A. Jackson, *Perspectives of Nonlinear Dynamics*, Cambridge University Press, (1989).

[51] ——, *The OPCL control method for entrainment, model-resonance, and migration actions on multiple attractor systems*, Chaos, **7(4)** (1997), pp. 550–9.

[52] W. Just et al., *Delayed feedback control of periodic orbits in autonomous systems*, Physical Review Letters, **81** (1998), pp. 562–5.

[53] A. Kittel, K. Pyragas, and R. Richter, *Prerecorded history of a system as an experimental tool to control chaos*, Physical Review E, **50** (1994), pp. 262–8.

[54] N. Kreisberg, W. D. McCormick, and H. L. Swinney, *Experimental demonstrations of subtleties in subharmonic intermittency*, Physica D, **50** (1991), pp. 463–77.

[55] Y. C. Lai, M. Ding, and C. Grebogi, *Controlling Hamiltonian chaos*, Physical Review E, **47** (1993), pp. 86–92.

[56] Y. C. Lai, C. Grebogi, J. A. Yorke, and I. Kan, *How often are chaotic saddles nonhyperbolic?*, Nonlinearity, **6** (1993), pp. 779–97.

[57] P. S. Laplace, *A Philosophical Essay on Probabilities*, Trans. by F.W.Truscott and F.L.Emory,Dover Pub., New York, (1951).

[58] M. Löcher, G. A. Johnson, and E. R. Hunt, *Stability analysis of fixed points via chaos control*, Chaos, **7(4)** (1997), pp. 590–6.

[59] E. Lorenz, *Atmospheric predictability as revealed by naturally occuring analogies*, Journal of Atmospheric Science, **26** (1969), p. 636.

[60] R. S. MacKay, *A renormalisation approach to invariant circles in area-preserving maps*, Physica D, **7** (1983), pp. 283–300.

[61] ——, *Stability of equilibria of Hamiltonian systems*, Nonlinear Phenomena and Chaos, (1986), pp. 254–70.

[62] R. S. MacKay and J. D. Meiss, *Hamiltonian Dynamical Systems*, Adam Hilger, Bristol, (1987).

[63] R. S. MacKay, J. D. Meiss, and I. C. Percival, *Transport in Hamiltonian systems*, Physica D, **13** (1984), pp. 55–81.

[64] J. M. Mao and J. B. Delos, *Hamiltonian bifurcation theory of closed orbits in the diamagnetic Kepler problem*, Physical Review A, **45** (1992), p. 1746.

[65] R. Martin, A. J. Scroggie, G. L. Oppo, and W. J. Firth, *Stabilization, selection and tracking of unstable patterns by Fourier space techniques*, Physical Review Letters, **77** (1996), pp. 4007–10.

[66] S. Mascolo and G. Grassi, *Controlling chaos via backstepping design*, Physical Review E, **56** (1997), pp. 6166–9.

[67] J. D. Meiss, *Symplectic maps, variational principles, and transport*, Reviews of Modern Physics, **64** (1992), pp. 795–848.

[68] J. K. Moser, *Lectures on Hamiltonian systems*, Memoirs of the American Mathematical Society, **81** (1968), pp. 1–60.

[69] ——, *Is the solar system stable?*, Mathematical Intelligencer, **1** (1978), pp. 65–71.

[70] G. V. Osipov, A. K. Kozlov, and V. D. Shalfeev, *Impulse control of chaos in continuous systems*, Physics Letters A, **247** (1998), pp. 119–28.

[71] E. Ott, *Chaos in Dynamical Systems*, Cambridge University Press, (1993).

[72] E. Ott, C. Grebogi, and J. A. Yorke, *Controlling chaos*, Physical Review Letters, **64** (1990), pp. 1196–9.

[73] E. Ott, T. Sauer, and J. A. Yorke, *Coping With Chaos*, John Wiley & Sons Inc., (1994).

[74] V. Petrov, M. Crowley, and K. Showalter, *Tracking unstable periodic orbits in the Belouzov-Zhabotinsky reaction*, Physical Review Letters, **72** (1994), pp. 2955–8.

[75] V. Petrov, V. Gáspár, J. Masere, and K. Showalter, *Controlling chaos in the Belousov-Zhabotinsky reaction*, Nature (London), **361** (1993), pp. 240–3.

[76] A. N. Pisarchik, B. F. Kuntsevich, and R. Corbalán, *Stabilizing unstable orbits by slow modulation of a control parameter in a dissipative dynamic system*, Physical Review E, **57** (1998), pp. 4046–53.

[77] R. Poulin, *Intégration symplectique et étude dynamique de systèmes Hamiltoniens*, PhD thesis, Université Laval, Québec, Canada, Décembre 1997.

[78] W. H. Press, S. A. Teukolsky, W. T. Vetterling, and B. P. Flannery, *Numerical Recipes in C*, Cambridge University Press, 2^{nd} ed., (1992).

[79] K. Pyragas, *Continuous control of chaos by self-controlling feedback*, Physics Letters A, **170** (1992), pp. 421–8.

[80] L. E. Reichl, *The Transition to Chaos*, Springer - Verlag, (1992).

[81] W. C. Rheinboldt, *Numerical Analysis of Parametrized Nonlinear Equations*, Wiley, New York, (1986).

[82] R. W. Rollins, P. Parmanada, and P. Sherard, *Controlling chaos in highly dissipative systems: A simple recursive algorithm*, Physical Review E, **47** (1993), pp. R780–3.

[83] R. Roy et al., *Dynamical control of a chaotic laser: Experimental stabilization of a globally coupled system*, Physical Review Letters, **68** (1992), pp. 1259–62.

[84] N. F. Rulkov, L. S. Tsimring, and H. D. Abarbanel, *Tracking unstable orbits in chaos using dissipative feedback-control*, Physical Review E, **50** (1994), pp. 314–24.

[85] P. Schmelcher and F. K. Diakonos, *Detecting unstable periodic orbits of chaotic dynamical systems*, Physical Review Letters, **78** (1997), pp. 4733–6.

[86] ——, *A turning point analysis of the ergodic dynamics of iterative maps*, International Journal of Bifurcation and Chaos, **7** (1997), pp. 2459–74.

[87] ——, *General approach to the localization of unstable periodic orbits in chaotic dynamical systems*, Physical Review E, **57** (1998), pp. 2739–46.

[88] C. G. Schroer and E. Ott, *Targeting in Hamiltonian systems that have mixed regular/chaotic phase spaces*, Chaos, **7(4)** (1997), pp. 512–9.

[89] H. G. Schuster and M. B. Stemmler, *Control of chaos by oscillating feedback*, Physical Review E, **56** (1997), pp. 6410–7.

[90] I. B. Schwartz, *Infinite primary saddle-node bifurcation in periodically forced systems*, Physics Letters A, **126** (1988), pp. 411–8.

[91] ——, *Sequential horse-shoe formation in the birth and death of chaotic attractors*, Physical Review Letters, **60** (1988), pp. 1359–62.

[92] I. B. Schwartz, T. W. Carr, and I. Triandaf, *Tracking controlled chaos: Theoretical foundations and applications*, Chaos, **7** (1997), pp. 664–79.

[93] I. B. Schwartz and K. Y. Tsang, *Antiphase switching in Josephson junction arrays*, Physical Review Letters, **73** (1994), pp. 2797–2800.

[94] T. Shinbrot, C. Grebogi, E. Ott, and J. A. Yorke, *Using small perturbations to control chaos*, Nature, **363** (1993), pp. 411–7.

[95] J. Singer, Y. Z. Wang, and H. H. Bau, *Controlling a chaotic system*, Physical Review Letters, **66** (1991), pp. 1123–25.

[96] S. Sinha and N. Gupte, *Adaptive control of spatially extended systems: Targeting spatiotemporal patterns and chaos*, Physical Review E, **58** (1998), pp. R5221–4.

[97] P. So et al., *Extracting unstable periodic orbits from chaotic time series data*, Physical Review E, **55** (1997), pp. 5398–417.

[98] J. Stoer and R. Bulirsch, *Introduction to Numerical Analysis*, Springer-Verlag, New York, (1980).

[99] S. H. Strogatz, *Nonlinear Dynamics and Chaos*, Addison Wesley, (1994).

[100] M. Tabor, *Chaos and Integrability in Nonlinear Dynamics*, John Wiley & Sons, (1989).

[101] G. Tanner, K. T. Hansen, and J. Main, *The semiclassical resonance spectrum of hydrogen in a constant magnetic field*, Nonlinearity, **9** (1996), pp. 1641–70.

[102] I. Triandaf and I. B. Schwartz, *Stochastic tracking in nonlinear dynamical systems*, Physical Review E, **48** (1993), pp. 718–22.

[103] T. Ushio and S. Yamamoto, *Delayed feedback control with nonlinear estimation in chaotic discrete-time systems*, Physics Letters A, **247** (1998), pp. 112–8.

[104] M. Vincke and D. Baye, *Centre-of-mass effects on the hydrogen atom in a magnetic field*, Journal of Physics B, **21** (1988), pp. 2407–24.

[105] R. Volaseca, A. Kulminski, and R. Corbalan, *Tracking unstable steady states by large periodic modulation of a control parameter in a nonlinear system*, Physical Review E, **54** (1996), pp. 82–5.

[106] R. L. Waterland, J. B. Delos, and M. L. Du, *High Rydberg states of an atom in parallel electric and magnetic fields*, Physical Review A, **35** (1987), pp. 5064–80.

[107] K. Yagasaki and T. Uozumi, *Controlling chaos using nonlinear approximations and delay coordinate embedding*, Physics Letters A, **247** (1998), pp. 129–39.

[108] ——, *A new approach for controlling chaotic dynamical systems*, Physics Letters A, **238** (1998), pp. 349–57.

[109] T. Yang, L. B. Yang, and C. M. Yang, *Theory of control of chaos using sampled data*, Physics Letters A, **246** (1998), pp. 284–8.